

University of Nevada, Reno

**Reliability-based Approaches to Quantify Maximum Permissible Penetration Level
of Electric Vehicles in Power Systems**

A dissertation submitted in partial fulfillment of the
Requirements for the degree of Doctor of Philosophy in
Electrical Engineering

By

MD Kamruzzaman

Dr. Mohammed Ben-Idris/Dissertation Advisor

December 2020



THE GRADUATE SCHOOL

We recommend that the dissertation
prepared under our supervision by

MD KAMRUZZAMAN

Entitled

**Reliability-based Approaches to Quantify Maximum Permissible Penetration Level
of Electric Vehicles in Power Systems**

be accepted in partial fulfillment of the requirements for
the degree of

Doctor of Philosophy

Mohammed Ben-Idris, Ph.D., Advisor

Mehdi Etezadi-Amoli, Ph.D., Committee member

Hanif Livani, Ph.D., Committee member

Engin Arslan, Ph.D., Committee member

Christopher Barile, Ph.D., Graduate School Representative

David W. Zeh, Ph.D., Dean, Graduate School

December 2020

ABSTRACT

The growing concern for environmental and pollution-related problems has led to increase the penetration of sustainable resources in both power and transportation systems. Although transitioning from fossil fuel-based vehicles to electric vehicles (EVs) in transportation systems helps in alleviating many environmental and pollution-related concerns associated with conventional cars, the inclusion of EVs represents a new type of electric load that requires allocating appropriate resources to maintain/improve power system reliability. Therefore, it is important to analyze the reliability of power systems with EVs for operation and planning perspectives.

In order to maintain the reliability of a power system, load demand should be satisfied. If all or part of the load cannot be satisfied, load curtailments are needed to maintain system stability. The number of EVs is expected to exponentially increase in the coming years. This high-expected growth in the number of EVs will increase the probability of load curtailments of power systems. However, load curtailments can be avoided by incorporating demand response (DR) programs and optimum energy management systems. Existing methods to investigate the effect of DR programs on power system reliability do not include penalty terms, which is an important factor for effective participation of customers in DR programs. Thus, in addition to the existing economic models, a load curtailment model to emulate customers' active participation in DR programs needs to be developed to improve the reliability of power systems. In addition, it is obvious that the continuous increase of EVs produce several challenges related to the variability of charging time, duration, and location for planning of future power system. Determining the amount of controlled charging of EV loads that can be incorporated in existing power systems is a promising factor in addressing these challenges.

One of the promising solutions to deal with the challenges of accommodating EVs in power systems is that, with knowledge of load profiles of EVs, or behavior and preferences of EV drivers to charge their vehicles, and load profiles of conventional electric loads, the DR programs can reduce or even avoid the negative impacts of EVs on power system reliability.

The work presented in this dissertation tabulates load profile of EVs in forms of hourly, daily, and weekly loads in percent of their maximum load. This load model considers drivers' behavior and preferences, which include weekdays/weekends and seasonal charging patterns. Also, this work introduces two new metrics to measure the capability of a power system to accommodate EV loads without deteriorating its reliability. Moreover, this work proposes methods to increase or maximize the number of EVs that can be incorporated in power systems. The conducted work of this dissertation can be divided into three parts. Part I presents the concept of developing load profiles for the EVs. This part also describes the proposed methods to quantify EV loads in existing power systems under both controlled and uncontrolled charging. Moreover, this part provides algorithms to determine permissible penetration level of EVs at different regions (buses) of power systems. Part II of this dissertation describes several proposed smart charging/discharging strategies for EVs to increase their penetration level in power systems with existing resources. Part III presents a DR-based method to maximize the penetration level of EVs in power systems under uncontrolled charging scenario.

In summary, the thesis presented here is that, with accurate modeling of EV load profiles based on drivers' behavior and preferences, demand response (DR) programs and smart charging/discharging strategy will reduce negative impacts of EVs on power systems and defer expansion plans.

Acknowledgements

I would like to express my sincere and deepest appreciation to my advisor, Dr. Mohammad Ben-Idris for his unconditional assistance, guidance, invaluable comments, support and direction to accomplish this dissertation. It has been an honor to be one of his Ph.D. students. I would also like to thank Prof. Mehdi Etezadi-Amoli, Dr. Hanif Livani, Dr. Engin Arslan, and Dr. Christopher Barile for serving on my committee and their valuable suggestions and comments.

I sincerely acknowledge the funding sources that helped me to complete my Ph.D. work, which include University of Nevada, Reno and the US National Science Foundation.

I offer my special thanks to my friends at the University of Nevada, Reno and the research group at the E-RESILIENCY lab. The group has been a good advice and collaboration. In particular, I would like to acknowledge Michael Abdelmalek and Narayan Bhusal for their valuable comments, suggestions, and collaboration.

Finally, it is an honor for me to acknowledge the support and encouragement of my family specially my father, my mother, my wife, my brothers, and sisters. All of your love and support encourage me to overcome all the challenges that I have faced.

From the bottom of my heart, thank you all.

Table of Contents

Chapter 1.	Introduction.....	1
1.1	Background.....	2
1.2	Contribution.....	7
1.3	Dissertation Organization	8
Chapter 2.	Reliability-based Metrics to Quantify the Maximum Permissible Load Demand of EVs	10
2.1	Extra Effective Available Energy to Accommodate EVs	11
2.1.1	Hourly Generation Capacity	11
2.1.2	Calculation of the Daily Required Energy to Charge EVs	13
2.1.3	Load Profiles of EVs.....	14
2.1.4	Calculation of the EEAE-EVs.....	17
2.2	Extra Effective Required Generation to Accommodate EVs.....	21
2.3	Calculation of the Reliability Indices.....	23
2.3.1	Calculation of the LOLP Index.....	23
2.3.2	Calculation of the EDNS Index	24
2.3.3	Calculation of Frequency of Failure Index:	24
2.4	Simulation Results	25
2.4.1	Case I: IEEE-RTS Base Case.....	26
2.4.2	Case II: Analyzing the Effects of EVs.....	26
2.4.3	Case III. Calculation of EEAE-EVs:.....	27
2.4.1	Case IV. Calculation of EERG-EVs:	29
2.5	Discussion	30
Chapter 3.	Maximum Permissible Load Demand for EVs at Power System Buses.....	32
3.1	Extra Accessible Loading Capacity	32
3.1.1	Maximum Permissible Number of EVs at System Buses.....	32
3.1.2	Calculation of EALCB.....	34
3.1.3	Load Profiles of EVs.....	36
3.2	Network Modeling.....	36
3.3	Case Studies.....	38
3.3.1	Case I:	38
3.3.2	Case II:	39
3.3.3	Case III:.....	39
3.3.4	Case IV:	40
3.4	Results and Discussion	40

Chapter 4.	Determining Maximum Hosting Capacity of Electric Distribution Systems to EVs	43
4.1	Maximum Hosting Capacity of DSs to EVs	43
4.1.1	Maximum Hosting Capacity of DSs under Uncontrolled Charging Scenario	44
4.1.2	Maximum Hosting Capacity of DSs under Fully Controlled Charging Scenario..	45
4.2	Construction of Load Profiles for EVs and Calculation of HEAP.....	47
4.2.1	Hourly Load Demand to Charge EVs	47
4.2.2	Calculation of HEAP	51
4.3	Case Studies	52
4.3.1	Case I: Maximum Hosting Capacity for All Nodes under Uncontrolled Charging	53
4.3.2	Case II: Maximum Hosting Capacity for All Nodes under Fully Controlled Charging Scenario.....	54
4.3.3	Case III: Maximum Hosting Capacity for Selected Nodes under Uncontrolled Charging	55
4.3.4	Case IV: Maximum Hosting Capacity for Selected Nodes under Fully Controlled Charging	56
4.4	Results and Discussion	56
Chapter 5.	A Method to Evaluate the Maximum Hosting Capacity of Power Systems to EVs	58
5.1	Smart Charging/Discharging Strategy to Maximize the Hosting Capacity	58
5.1.1	System Architecture.....	58
5.1.2	Objective Function.....	61
5.1.3	Network Constraints	61
5.2	Calculation of the EMHC	64
5.3	Numerical Examples	67
Chapter 6.	Demand Response-based Power System Reliability Enhancement.....	70
6.1	Modeling of Demand Response Considering Interruptible/Curtailable Loads	70
6.1.1	Interruptible/Curtailable Load Modeling Approach	70
6.1.2	Interruptible/Curtailable Load Modeling Approach	72
6.2	Simulation Results	74
6.2.1	Case Study I.....	75
6.2.2	Case Study II.....	76
Chapter 7.	A Reliability-constrained Demand Response-based Method to Increase the Hosting Capacity of Power Systems to EVs.....	78
7.1	Maximizing Permissible Penetration Level of EVs in Power Systems	79
7.1.1	Restructuring Bus Load Profiles	79

7.1.1	Constructing Load Profiles for EVs.....	79
7.1.2	Calculation of I/C Loads based on DR Program.....	82
7.2	Calculation of Maximum Permissible Penetration	83
7.3	Reliability Evaluation Using the MC.....	85
7.3.1	Sampling System States	85
7.3.2	Classifying System States	86
7.3.3	Convergence Criterion	88
7.4	Numerical Examples	89
7.4.1	Case Studies for the RBTS.....	90
7.4.2	Case Studies for the IEEE-RTS	94
7.4.3	Case Studies for the IEEE 33-bus Distribution System	96
7.5	Results and Discussion	99
Chapter 8.	Conclusions and Future Work.....	104
References.....		107

List of Tables

Table 1. Hourly Peak Loads in Percent of Daily Peak Loads.....	15
Table 2. Daily Peak Loads in Percent of Weekly Peak Loads.....	16
Table 3. Weekly Peak Loads in Percent of Annual Peak Loads.....	17
Table 4. Calculated Reliability Indices for the IEEE-RTS	27
Table 5. Required Generation to Maintain LOLP and EDNS with EVs	30
Table 6. Maximum EVs Load Allocation at Load Buses of the IEEE-RTS.....	39
Table 7. Maximum EVs Load Allocation at Selected Load Buses of the IEEE-RTS	40
Table 8. Maximum Hosting Capacity for All the Nodes	54
Table 9. Maximum Hosting Capacity for the Selected Nodes.....	56
Table 10. Ratings of Generators of the Modified IEEE 33-Bus	68
Table 11. Self-Cross Elasticities	75
Table 12. Load Curtailment with Different Penalties and Incentives for Case Study I.....	76
Table 13. Annual Reliability Indices of the IEEE-RTS with and without I/C Loads Program for Case Study I.....	77
Table 14. Load Curtailment with Different Penalties and Incentives for Case Study II.....	77
Table 15. Annual Reliability Indices of the IEEE-RTS with and without I/C Loads Program for Case Study II.....	77
Table 16. Reliability Indices of Cases for the RBTS	91
Table 17. Bus EDNS of Cases for the RBTS.....	91
Table 18. Reliability Indices of Cases for the IEEE-RTS.....	95
Table 19. Bus EDNS of Cases for the IEEE-RTS.	96
Table 20. Reliability Indices of Cases for the IEEE 33-Bus.....	97
Table 21. Bus EDNS of Cases for the IEEE 33-Bus	98

Table of Figures

Figure 1. Relationship between generation capacity, system reserve, load profile, HEAG, and EEAE of a power system.	19
Figure 2. Flowchart to calculate the EEAE-EVs under fully controlled charging.	20
Figure 3. Flowchart to calculate the EERG-EVs.	21
Figure 4. Calculation of the required generation based on the EERG-EVs concept.	22
Figure 5. EV loads based on the EEAE-EVs concept for IEEE-RTS.	27
Figure 6. Required generation to avoid effects of EVs on LOLP.	29
Figure 7. Required generation to avoid effects of EVs on EDNS.	29
Figure 8. Relation between EALCB and load profile of EVs.	34
Figure 9. Probability distribution function of daily travel distance of EVs.	45
Figure 10. Relation between HEAP and load profile of EVs.	46
Figure 11. Probability distribution function of arrival time of EVs.	48
Figure 12. Probability distribution function of departure time of EVs.	48
Figure 13. Relation between HEAP of the IEEE 123-node test feeder and load demand of EVs.	54
Figure 14. Selected regions of the IEEE 123-node test feeder for Case III and Case IV.	55
Figure 15. Charging/discharging period.	60
Figure 16. Smart charging/discharging architecture for a microgrid.	60
Figure 17. PDFs of (a) arrival times at homes and (b) departure times from homes.	64
Figure 18. PDFs of (a) arrival times at workplaces and (b) departure times from workplaces.	64
Figure 19. PDF of daily travel distances of EVs.	65
Figure 20. Algorithm to calculate the daily maximum HC.	66
Figure 21. Modified IEEE 33-bus.	68
Figure 22. EMHC of the modified IEEE 33-bus for selected nodes.	69
Figure 23. The Flowchart of the Interruptible/Curtailable Load Modeling.	71
Figure 24. Typical Demand Price Elasticity.	72
Figure 25. Load Profile of the IEEE-RTS with and without I/C Loads Program for a Typical Day.	76
Figure 26. The flowchart to calculate maximum penetration level of EVs at power system buses.	84
Figure 27. Load profiles for initial number of EVs for the RBTS.	92

Abbreviations

DEAE	Daily extra available energy
DR	Demand response
DS	Distribution system
EALCB-EVs	Extra accessible loading capacity of a bus for EVs
EDNS	Expected demand not supplied
EEAE-EVs	Extra effective available energy for EVs
EEEG-EVs	Extra effective required energy for EVs
EV	Electric vehicles
EMHC	Expected maximum hosting capacity
FORs	Forced outage rates
HEAG	Hourly extra available generation
HEAP	Hourly extra available power
HC	Hosting capacity
LOEE	Loss of expected energy
LOLP	Loss of load probability
MC	Monte Carlo
PHEVs	Plug-in hybrid EVs

Chapter 1. Introduction

The penetration level of EVs in power systems is anticipated to rise sharply in the upcoming years. For example, in the United States, the expected annual increase in the number of EVs is about 400% between the years of 2013 and 2022 [1]–[3]. Also, it has been forecasted that over 240 million light-duty electric cars and trucks, 7 million medium- and heavy-duty electric trucks, and 80,000 electric transit buses will be on the U.S. roads by 2050 [112]. This will cause an increase in the load demand of power systems. Consequently, challenges to maintain system reliability using existing system resources will increase. Also, changes in charging profiles of EVs in terms of charging times, duration, and locations that are governed by the behavior and preferences of drivers will cause uneven changes in the values of demand and reliability indices at system buses. Therefore, it is critical to build comprehensive load profiles for EVs that capture drivers' behavior and preferences to accurately model their impacts on power system reliability.

The need to equip power system operators and planners with the required resources to accommodate the huge increase in EVs has become evident and has triggered several ongoing efforts to construct energy consumption profiles for EVs to facilitate power system expansion projects. At present, there is no effective tool to assist power system operators and planners in making a well-informed choice from amongst a profusion of resource allocation alternatives that can potentially maintain/enhance the reliability of power grids against the sharp increase in EVs. Determining the maximum permissible amount of EV loads that a power system can accommodate while maintaining its reliability is an important factor for power system planning and operation. Also, determining the required extra generation to maintain power system reliability, if EV loads exceed systems' maximum permissible load, has become indispensable. Moreover, developing controlled charging strategies is important to ensure the efficient utilization of existing power system resources.

DR programs, which are defined as interdependency between electricity demand of customers and change of price over time, have the potential to decrease the negative impacts of EVs on the reliability of power systems. However, the effectiveness of DR programs on improving power system reliability strongly relies on the degree of customer participation. Therefore, it is important to create an economic model that considers both incentives and penalties and emulates customers' active participation in the DR programs.

1.1 Background

Analyses of load profiles of EVs have been reported in several technical reports and research papers [3]–[10]. Summary of in-home and public charging patterns at six electric utilities in the United States is presented in [3]. Similar analysis is given in [4] for several European countries. Charging patterns in the Ohio state are given in [7], in Xcel Energy-Colorado are given in [8], and in California and Portland are given in [10]. However, most power system reliability studies considering EVs either divide the charging profile of one year into winter and summer seasons or generalize charging data of one day to the entire year. Therefore, an hourly load profile for EVs that captures variations in the charging demand on different charging periods and locations based on drivers' behavior needs to be developed to analyze their impacts on power system reliability.

Several methods have been proposed in the literature to determine the effects of controlled charging of EVs on power system reliability [11]–[19]. The available power capacity of EVs that can be supplied to the reserve market and its effect on power system reliability have been analyzed in [11]. Vehicle to grid integration (V2G) techniques have been introduced in [12] and [13] to improve power system reliability. It has been found that V2G techniques can defer reliability-based generation expansions. Plug-in hybrid EVs (PHEVs) have been considered as dispatchable loads to demonstrate their effects on Portuguese electric power consumption profile in [14]. The work presented in [14] shows that the consideration of PHEVs as dispatchable loads can increase

systems' minimum load, increase base load utilization, reduce plant cycling, and defer investing in new generation. The impact of EVs on power system load profile and efficient solutions for peak load reduction to improve power system reliability have been discussed in [15]–[17]. Power system reliability evaluation for different charging strategies of PHEVs has been presented in [18] and [19]. The above-mentioned studies deal with increasing the amount of energy exchange between grid and EVs through controlled charging to improve system reliability. However, determining the maximum amount of EV loads that a power system can accommodate with its existing resources (i.e., maintain its reliability level through controlled charging) has not been addressed. Also, the maximum accessible energy to accommodate load demand of EVs needs to be determined for developing a charging schedule for EVs.

The influence of charging/discharging of EVs on power system reliability has been extensively analyzed in the literature [20]–[23]. The impacts of EVs on power system reliability considering battery exchange strategies and energy storage systems have been studied in [20]. The work reported in [20] concluded that the reliability of a given power system can be improved using the battery exchange mode. An optimization model for charging/discharging of EVs to meet a reliability criterion (e.g., a reliability index) has been proposed in [21]. Composite system reliability evaluation in the presence of PHEVs has been presented in [22]. In [23], the EVs have been modeled as moveable loads based on the drivers' behavior to investigate their effects on composite system reliability indices. However, determining the required extra generation to maintain the reliability of power systems prior to integrating EVs has not been given attention.

The impacts of EV charging loads on power systems have been analyzed from different standpoints in [23]–[29]. In [24], the authors have investigated the impacts of EVs on power system infrastructure. In [25], the authors have analyzed the impacts of EVs on power system constraints during different periods of a day. The impacts of EVs on the lifetime of residential transformers

have been studied in [26]. In [27], the authors have investigated the impacts of EV penetration on the operation and development of the Italian power system for a specific time period. The impacts of EVs on distribution networks have been analyzed in [28] with different charging levels (slow and fast). Also, the authors of [28] have introduced a smart charging technique to avoid aging of distribution system transformers. In [23], the effects of EVs are investigated on composite system reliability based on the behavior of drivers. In [23]–[28], the proposed methods have been developed to analyze the impacts of EVs on power system, which are essential for power system planning to handle EV loads. However, a method to quantify the maximum number of EVs at each bus needs to be developed to determine the maximum penetration level of EVs at power system buses with existing resources.

The impacts of EVs on DSs have been investigated in several papers [30]–[34]. An analytical framework considering diversity in both penetration and charging patterns of EVs has been developed to evaluate their impacts on DSs in [30]. The impacts of EVs on power losses and voltage limit violations have been analyzed in [31]. Also, a coordinated charging strategy has been proposed in [31] to both maximize the load factor and minimize power losses. An approach to evaluate the impacts of EVs on energy losses and investment costs has been developed in [32]. In [33], the authors have analyzed the impacts of electricity demand to charge EVs on the lifetime of distribution transformers. Battery capacities, state of charge, and daily energy consumption of EVs have been modeled based on the behavior of EV owners to analyze the impacts of EVs on DSs [34]. The impacts of EVs on distribution system constraints (i.e., current capacity, voltage limits, power losses, investment costs, and transformers lifetime) have been analyzed in [30]–[34]. However, determining the maximum hosting capacity of DSs to EVs while maintaining system constraints needs to be addressed.

Smart charging/discharging strategies have been proposed in [35]–[41] to increase financial benefits of EV charging/discharging process. In [35], a smart charging/discharging strategy has been proposed to maximize the number of EVs that are charged up to desired levels as well as financial benefits of both commercial stations and EV owners. An intelligent charging/discharging strategy has been proposed in [36] to determine optimal charging/discharging times and rates over 24 hours to maximize the overall profits of an EV parking deck. A game-theory-based smart charging/discharging strategy has been proposed in [37] to maximize the financial benefits of commercial buildings through optimizing energy consumption profiles. In [38], an hourly electricity price-based optimal charging/discharging scheme has been proposed to maximize the profits of parking lots. An optimal charging/discharging strategy has been developed in [39] to charge specific number of EVs at charging stations based on economic benefits. The strategies proposed in [35]–[39] have been developed mainly to increase financial benefits of EV owners and charging stations without providing much attention on quantifying the HC of power grids. A voltage constrained-based method to calculate the maximum HC of distribution systems to EVs for both fully controlled and uncontrolled charging has been developed in [40]. In [41], the maximum permissible number of EVs that can be penetrated at transmission system buses have been quantified using the extra hourly loading capacities. The developed methods in [40], [41] are aimed to determine the maximum HC considering only charging capability of EVs. However, a method to maximize the HC for both charging and discharging is required to ensure maximum utilization of existing resources as well as to determine appropriate times for the allocation of new resources.

In order to reduce the negative effects of EVs on power systems, controlled charging/discharging strategies for EVs based on electricity prices have been introduced in [42]–[57]. In [42] and [43], the charging/discharging of EVs has been modeled based on a nonlinear pricing method. An EV-Wind coordinated framework based on variable charging/discharging rates has been developed in [44] to minimize the unit emission-cost considering transmission network constraints.

The requirements of power quality for electric vehicle chargers to maintain stability of bulk power grids have been highlighted in [45]. In [46] and [47], a large amount of electricity consumption by EVs has been anticipated in the year of 2030 and provided recommendations to analyze the impacts of EVs on transmission systems for future system planning.

In [48], the authors have developed a model to determine optimum charging/discharging strategies at parking lots considering EVs as responsive demand in both incentive- and price-based DR programs. In [49], a DR program has been proposed based on optimal charging schedule for EVs that increases the allowable number of charging vehicles and reduces the electricity bill of charging stations. In [50], DR programs have been considered in developing a charging schedule for large scale EVs at public charging stations to maximize the benefits of both utilities and customers. In [51], the authors have developed a dynamic DR program that considers real-time price of charging plug-in hybrid EVs and interactions between utilities and customers. In [52], a DR-based vehicle to grid integration model has been developed to balance power demand of distribution networks. In [53], a DR-based charging and discharging strategy for EVs has been proposed to improve the stability and robustness of distribution networks. Also, a DR-based charging and discharging strategy for EVs has been developed in [54] to increase the EV penetration level at residential stations. In [55], an optimal planning-based method has been presented for siting and sizing of charging stations considering DR-based charging of EVs. In [56], power system reliability has been improved through controlling the charging of EVs based on a time of use price-based DR program. Also, a DR-based controlled charging strategy has been developed in [57] to improve the reliability of microgrids. In [43]–[57], DR programs have been applied on EV charging periods to both reduce the negative impacts of EVs on power systems and optimize the charging cost of EVs.

1.2 Contribution

In this dissertation, a load profile that depicts the charging time, duration, and location of EVs has been developed. The load profile is represented in terms of weekly, daily, and hourly charging load data over one year. Also, two adequacy metrics are proposed to quantify the maximum permissible EV loads for a power system without deteriorating its reliability and the required improvements to power systems to accommodate high penetrations of EVs. These metrics are defined as follows: 1) extra effective available energy for EVs' charging (EEAE-EVs) and 2) extra effective required generation to accommodate EVs (EERG-EVs). The EEAE-EVs provides a measure for the maximum amount of EV loads that a power system can accommodate without adding new generation while maintaining its reliability. The EERG-EVs provides a measure to the minimum amount of new generation that is needed to restore the reliability level of a power system if the load of EVs exceeds the maximum permissible load of the system. These metrics provide a decision aid to power system planners and operators on when and how to perform generation expansion. Moreover, an iterative approach is proposed to quantify the maximum permissible number of EVs at different power system buses based on extra accessible loading capacity at each bus. The maximum permissible number of EVs at each bus is calculated through maximizing their load demand.

The maximum hosting capacity of DSs to EVs is determined under both uncontrolled (actual) and controlled charging scenarios ensuring that voltage requirements are not violated. The maximum hosting capacity of EVs under the uncontrolled charging scenario is estimated based on load profile of EVs and hourly extra available power (HEAP). Also, a smart charging/discharging-based method is proposed to evaluate the expected maximum hosting capacity (EMHC) of power systems to EVs. The EMHC is calculated for charging stations at both homes and workplaces. Moreover, a reliability-constrained demand response-based method to maximize the permissible

penetration level of EVs at electric power system buses, which is developed based on a DR program and load profiles of EVs.

1.3 Dissertation Organization

This is a paper-based dissertation. Due to this format, each chapter contains the information for the given papers including their references for ease of reading. This dissertation includes eight chapters. Chapter 1 provides a comprehensive literature review regarding the proposed approaches to analyze impacts of EVs on power systems. Chapter 2 is based on [29], [61], and [108] where two new metrics are introduced to quantify the number of EVs in power systems under both controlled and uncontrolled charging scenarios. Also, this chapter presents the proposed approach to develop a load profile for EVs. Moreover, this chapter describes the most well-known reliability indices of power systems. Further, numerical simulations are presented to demonstrate the proposed metrics on IEEE reliability test system (IEEE-RTS). Chapter 3 is based on [41] where we develop a mathematical model to both develop load profile for EVs and analyze their impacts on power system buses. Also, the proposed approach is demonstrated on the IEEE-RTS through numerical simulations. Chapter 4 is constructed based on [40] in which a smart charging strategy for EVs is proposed based on their arrival and departure times at homes to increase the hosting capacity to EVs. The effectiveness of the proposed strategy is demonstrated on the IEEE 33-bus distribution system. Chapter 5 is based on [109] where a smart charging/discharging strategy for EVs considering their arrival and departure times at both home and workplaces is proposed to maximize the hosting capacity of power systems to EVs. This proposed strategy is also demonstrated on the IEEE 33-bus distribution system. Chapter 6 is developed based on [110] where a DR-based method is presented to increase the reliability of power systems. The proposed method is demonstrated on the IEEE-RTS. Chapter 7 is based on [111] where we propose a DR-based approach to maximize the penetration level of EVs at different buses of power systems under uncontrolled charging

scenarios using existing resources. A comprehensive numerical example is provided to demonstrate the proposed method on the Roy Billinton Test System (RBTS), IEEE-RTS, and IEEE 33-bus distribution system. Finally, several concluding remarks are provided in Chapter 8.

Chapter 2. Reliability-based Metrics to Quantify the Maximum Permissible Load

Demand of EVs

In this chapter, two new metrics are introduced to measure the capability of a power system to accommodate EV loads without deteriorating its reliability. These metrics are: 1) extra effective available energy for EVs' charging (EEAE-EVs) and 2) extra effective required generation to accommodate EVs (EERG-EVs). The EEAE-EVs measures the capability of a power system to accommodate EV loads through controlled charging while maintaining its reliability. The EERG-EVs determines the required generation expansion to maintain the reliability of a power systems if EV loads exceed the systems' maximum permissible load. These metrics help power system operators and planners to determine: 1) the capability of a power system in accommodating EV loads with existing resources and 2) the required generation expansion if the maximum system capability is reached. The EEAE-EVs is estimated by gradually increasing the number of EVs until the minimum daily extra available generation of a year is equivalent to the daily EV loads in that year. The minimum daily extra available generation of a year is estimated by taking the differences between the daily total generation capacity and total daily loads without EVs for a year considering forced outage rates (FORs) and outages due to scheduled maintenance of generating units. The EERG-EVs is iteratively determined by increasing EV loads and adding new generation while keeping the reliability level of the system unchanged. Also, a load profile for EVs is tabulated in forms of hourly, daily, and weekly load in percent of their maximum load. This load model considers drivers' behavior and preferences, which include weekdays/weekends and seasonal charging patterns. The load profile is built based on a comprehensive review of existing load profiles. The sequential Monte Carlo (MC) simulation method is used to: 1) calculate the daily available generation considering system load and FORs of the generating units; 2) determine the EEAE-EVs by gradually increasing the number of EVs until the daily available generation is met;

3) determine the EERG-EVs by gradually incrementing the generation level for a given EV penetration considering the initial reliability level as a stopping criterion; and 4) calculate power system reliability indices for each loading scenario. The importance and effectiveness of the proposed metrics are demonstrated on the IEEE-RTS.

2.1 Extra Effective Available Energy to Accommodate EVs

Determination of EEAE-EVs requires: 1) calculation of the HEAG; 2) calculation of the daily required energy to charge EVs; and 3) construction of a load profile for EVs. The proposed method to determine the EEAE-EVs is described as follows.

2.1.1 Hourly Generation Capacity

The hourly available generation capacity from generating units of a power system is not constant for a given period of time due to several factors including forced outages, scheduled maintenance, and network constraints. In this dissertation, we consider the forced outages and scheduled maintenance to determine the hourly available capacity from the generating units. Estimation of the hourly available generation of a power system depends on the rated capacity of the units and on their outage profiles. Outage profiles of generating units are generated using sequential MC simulation method. Mean time to failures (MTTFs), mean time to repairs (MTTRs), and outages due to scheduled maintenance of generating units are used to simulate the up and down periods.

The calculation processes begin with calculating the hourly available power from existing generating units using the sequential MC simulation method for the given number of years. Then, the total hourly available generation capacity of the system at each hour is calculated based on the availability of each generating unit at the corresponding hour for the simulated years. Finally, the average hourly available generation capacity of the system for each hour for one year is calculated by taking the average of the available capacity at the corresponding hours for the period of study.

In this study, the average hourly available capacity is calculated as follows,

$$P_h = \frac{1}{N_y} \sum_{i=1}^{N_y} G_{hi}, \quad h = 1, 2, \dots, 8760, \quad (2.1)$$

where N_y is the total number of simulated years, G_{hi} is the total amount of generation at the h^{th} hour of the i^{th} year, and P_h is the average hourly available generation. The total amount of generation, G_{hi} , at the h^{th} hour of the i^{th} year can be calculated as follows,

$$G_{hi} = \sum_{j=1}^{N_g} g_{hji}, \quad j = 1, 2, \dots, N_g, \quad (2.2)$$

where N_g is the total number of generating units and g_{hji} is the available capacity of unit j at hour h of year i .

2.1.1.1 Hourly Load Profile for Existing Load (Without EVs)

The amount of hourly load of a power system is another important factor to determine the HEAG and the EEAE-EVs. The hourly load demand of a day varies based on the energy consumption profile of that day. The peak load of each day in a year varies depending on the season as well as whether it is a weekday or weekend. The load profile is developed based on the load profile of the IEEE-RTS [59]. In [59], hourly, daily, and weekly load data are presented in percentages of the annual peak load which can be utilized to construct a load profile for a year.

2.1.1.2 Calculation of the HEAG

The HEAG of a power system is estimated by subtracting the electricity demand of each hour from the average available generation (given in Section 2.1.1) of the corresponding hour. Therefore, the resulting HEAG captures load variations as well as the unavailability of the generating units due to their forced outages. The hourly extra (average) available generation can be calculated as follows,

$$\zeta_h = P_h - L_h - R_h, \quad (2.3)$$

where P_h is calculated using (2.1), L_h is the amount of electricity demand at hour h , R_h is the amount of the required system reserve at hour h , and ζ_h is the hourly extra (average) available generation of the system. We introduce R_h if a specific reserve is required beyond forced outages.

2.1.2 Calculation of the Daily Required Energy to Charge EVs

The daily required energy to charge EVs is another important factor to calculate the EEAE-EVs. In contrast to traditional loads, challenges induced by EV loads are mostly related to the variability of the charging time, amount, duration, and location (commercial and residential). Modeling load profiles for EVs and determining the required resources to maintain the reliability of power systems are key factors in addressing these challenges.

Most power system reliability studies considering EVs either divide the charging profile of one year into winter and summer seasons or generalize charging data of one day to the entire year. These assumptions ignore seasonal as well as weekday and weekend differences. The daily required energy to charge EVs is estimated by calculating their daily cumulative charging energy. Daily travel distances and energy required to travel every mile are the main two factors to calculate the daily required energy. Different types of EVs (e.g., compact sedan, mid-size sedan, mid-size SUV, and full-size SUV) have different energy consumption per mile [61]. Considering these two factors, the daily required energy to charge EVs can be calculated as follows,

$$\text{Daily Required Energy} = \sum_{n=1}^N d_n \times EPM_n, \quad (2.4)$$

where N is the total number of EVs, d_n is the average daily distance traveled in miles by the n^{th} EV, and EPM_n is the average energy required to travel each mile by the n^{th} EV. The daily required energy to charge EVs is used to determine the initial number of EVs in calculating the EEAE-EVs.

2.1.3 Load Profiles of EVs

From the perspective of energy consumption, charging patterns of EVs dynamically change in terms of time, amount, and duration (weekdays or weekends) and location (commercial and/or residential) that are governed by drivers' behavior and preferences. This continuous growth with a highly variable load profile will dramatically reshape conventional load profiles of power systems. As a result, peak hours will not happen at the same time for different system buses. In other words, not only the time of traditional system peak load will be shifted but also the correlation between peak load locations will be significantly altered. In view of these reasons, building a load profile for EVs and determining the required resources to maintain the reliability of power systems has become indispensable. Hourly, daily, and weekly data of electricity demand for charging EVs are presented in percentages of the annual peak load. These data are collected from different sources including technical reports and research papers and are arranged based on the steps provided in Sections 2.1.3.1, 2.1.3.2, and 2.1.3.3. The procedure of creating load profile for EVs through establishing hourly, daily, and weekly loads is described as follows.

2.1.3.1 Hourly Charging Load of EVs

EVs can be charged at residential locations or public charging stations or both. However, charging patterns in terms of charging time and duration depend on the location of charging (residential or commercial). Therefore, it is important to distinguish the load profiles at residential charging stations from those of public charging stations. Load profiles for both residential and public charging stations have been provided in [3] and [5]–[7]. In [5] and [6], daily charging patterns for both residential and public charging stations have been considered to be identical and fixed for the entire year. However, due to the variability of driving patterns in weekdays and weekends, the data given in [5] and [6] will not capture this behavior. The charging patterns of EVs in weekdays are considered different from weekends in [3] and [7] for the residential charging

scenario. We used the data given in [3] rather than that given in [7] because the number of surveyed cars in [7] is much smaller than that of [3] (the data given in [7] resulted in a large standard deviation in comparison to [3]). In the survey reports of [3] and [7] for public charging, the differences between charging patterns in weekdays and weekends are negligible. Therefore, charging patterns in weekdays and weekends for the public charging scenario are considered identical. Table 1 shows the hourly load profiles for weekdays and weekends as percentages of daily peak load of residential and public charging stations, respectively.

Table 1. Hourly Peak Loads in Percent of Daily Peak Loads

Hour	Residential Charging		Public Charging	
	Weekdays	Weekends	Weekdays	Weekends
12 –1 am	54.41	100	33	33
1 – 2	39.71	78.95	28.5	28.5
2 – 3	35.29	63.16	26	26
3 – 4	32.35	52.63	27.5	27.5
4 – 5	26.47	39.47	35	35
5 – 6	17.65	26.32	54	54
6 – 7	10.29	15.79	71.5	71.5
7 – 8	11.03	15.79	79	79
8 – 9	11.76	15.79	91.5	91.5
9 – 10	11.62	20.79	100	100
10 – 11	11.76	27.63	95	95
11– Noon	13.97	39.47	91	91
Noon –1 pm	16.18	57.89	80	80
1 – 2	22.06	65.79	71	71
2 – 3	26.47	78.95	58	58
3 – 4	28.68	84.21	66	66
4 – 5	36.76	86.84	69	69
5 – 6	51.47	86.84	78	78
6 – 7	73.53	89.47	82	82
7 – 8	85.29	89.47	80	80
8 – 9	88.24	92.11	72	72
9 – 10	100	97.37	63	63
10 – 11	95.59	97.37	51.5	51.5
11 – 12	75	78.95	44	44

2.1.3.2 Daily Peak Load of Charging EVs

Daily peak loads are important for determining the hourly peak loads because hourly peak loads

are commonly given in percentages of daily peak loads. Two different peak loads for EVs have been provided in [3], [10], [58], and [5]–[7], which are a constant peak load for weekdays and a constant peak load for weekends. However, charging patterns will not be the same for all weekdays as well as for weekends due to drivers’ preferences. A survey that provides different daily peak loads for a week has been reported in [4]. In this dissertation, we have adopted the load profiles given in [4] to develop the peak loads of each day in a week. Table 2 shows the peak loads in each day of a week in percentages of weekly peak loads.

Table 2. Daily Peak Loads in Percent of Weekly Peak Loads

Day	Peak Load
Monday	100
Tuesday	66
Wednesday	89
Thursday	71
Friday	95
Saturday	59
Sunday	50

2.1.3.3 Weekly Peak Load of Charging EVs

Similarly, weekly peak loads are important to create a load profile for EVs for one year because weekly peak loads are commonly given in percentages of the annual peak load. In [4] and [58], two load profiles of EVs have been constructed for two different seasons (e.g., summer and winter) which are represented in only two peak loads for the entire year. This assumption may introduce inaccuracy in developing a load profile for EVs. Monthly peak loads for a year have been provided in [58]. In this dissertation, we have used the monthly load profile given in [58] to develop the weekly peak loads. Since the monthly peak loads are the best available temporal resolution for a year as of now, we considered the same peak load for each consecutive four weeks (i.e., peak of the corresponding month) as given in [58]. In each three months, the peak of the third month is used to calculate the peak of five weeks instead of four to account for the differences between the number of days in a month and the number of days in four weeks. Table 3 shows the weekly peak

loads of charging EVs as percentages of the annual peak load of charging EVs.

Table 3. Weekly Peak Loads in Percent of Annual Peak Loads

Week	Peak Loads	Week	Peak Loads
1	100	27	74.8
2	100	28	74.8
3	100	29	74.8
4	100	30	74.8
5	94.49	31	73.6
6	94.49	32	73.6
7	94.49	33	73.6
8	94.49	34	73.6
9	98.03	35	81.1
10	98.03	36	81.1
11	98.03	37	81.1
12	98.03	38	81.1
13	98.03	39	81.1
14	86.61	40	96.06
15	86.61	41	96.06
16	86.61	42	96.06
17	86.61	43	96.06
18	84.25	44	94.49
19	84.25	45	94.49
20	84.25	46	94.49
21	84.25	47	94.49
22	69.29	48	96.06
23	69.29	49	96.06
24	69.29	50	96.06
25	69.29	51	96.06
26	69.29	52	96.06

The given data in Table 1, Table 2, and Table 3 are composed with the annual peak load to create the daily peak load for 364 (52×7) days, assuming Monday is the first day of the year.

2.1.4 Calculation of the EEAE-EVs

An iterative method is proposed to calculate the EEAE-EVs. The solution process begins by estimating the HEAG. The HEAG is calculated based on two scenarios: 1) modeling the FORs and outages due to scheduled maintenance of the generating units while ignoring system reserve margin and 2) modeling the FORs and outages due to scheduled maintenance of the generating units while

considering a constant system reserve margin. These two scenarios are explained as follows.

2.1.4.1 Scenario I:

In this scenario, the hourly generation capacity of a power system is estimated using the process described in Section 2.1.1. This scenario considers the MTTF, MTTR, and outages due to scheduled maintenance for all generating units in the system. Thus, the estimated hourly generation capacity in this scenario provides the average available power at each hour without accounting for the reserve margin. Therefore, in this scenario, to calculate the HEAG using (2.3), the value of R_h (hourly reserve) in the right-hand side of (2.3) is always zero. Capturing forced outages and outages due to scheduled maintenance of the generating units in the available generation profile may substitute for making a reserve margin zero against potential generation outages. However, considering zero reserve margin will introduce the risk of encountering loss of load events.

2.1.4.2 Scenario II:

In this scenario, a constant reserve margin is maintained to meet the demand during failure events of the system. Although there is no commonly agreed upon reserve margin for power systems, the East Central Area Reliability Council maintains the reserve at least 3% of daily peak load for both spinning and non-spinning reserves [62]. The required reserve in the Western Systems Coordinating Council, the sum of 7% of the demand is satisfied by thermal generating units and 5% of the demand is satisfied by hydroelectric generating units [62]. In the mid-Atlantic region, the amount of spinning reserve is maintained as the capacity of the largest operating unit. However, if the capacity of the largest operating unit is less than 700 MW, then, the amount of spinning reserve is considered as 700 MW [62]. In Florida, the amount of spinning reserve is maintained as 25% of the largest operating unit and the supplemental reserve is maintained as 75% of the largest operating unit [63]. Following the same procedure to maintain the total reserve margin in Florida, we assume that the total reserve margin is equivalent to the size of the largest operating unit.

In the next step, the HEAG is used to calculate the EEAE-EVs under fully controlled charging. In order to calculate the EEAE-EVs under fully controlled charging, the EEAE for each day of a year is estimated as follows,

$$\xi^d = \sum_{\hat{h}=1}^{24} \xi_{\hat{h}}^d, \quad \hat{h} = 1, 2, \dots, 24; \quad d = 1, 2, \dots, 365, \quad (2.5)$$

where $\xi_{\hat{h}}^d$ is the extra available generation at hour \hat{h} and ξ_a is the EEAE on d day of the year.

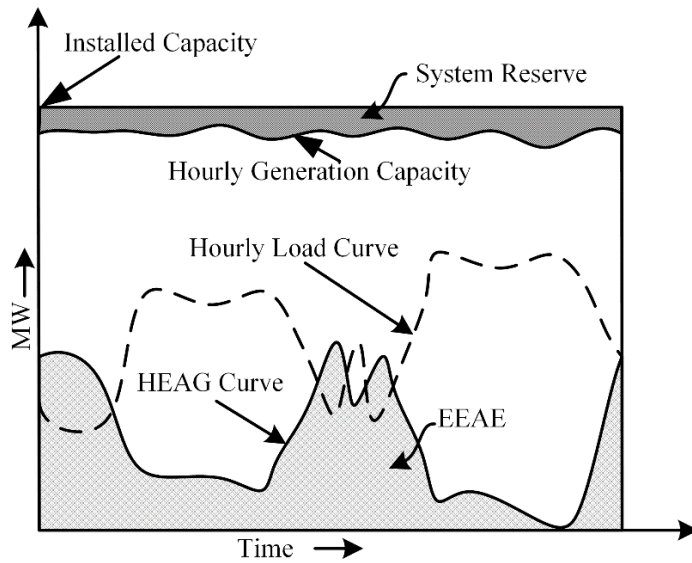


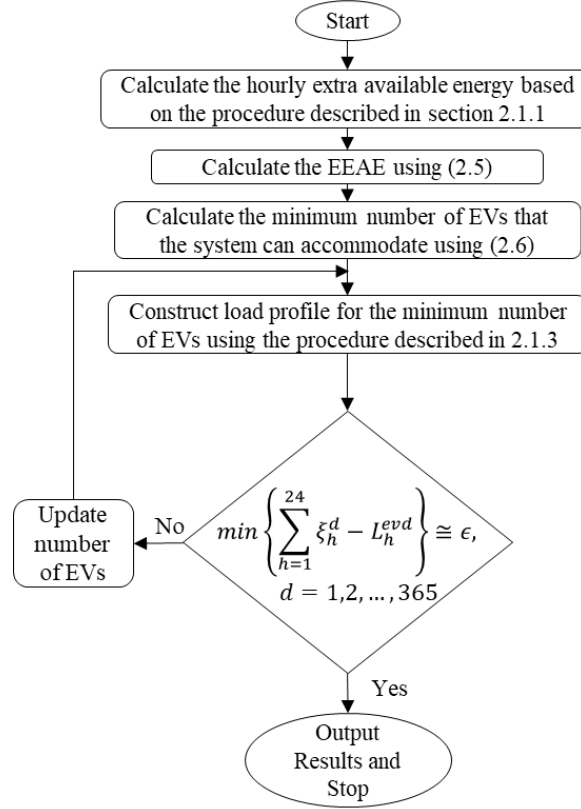
Figure 1. Relationship between generation capacity, system reserve, load profile, HEAG, and EEAE of a power system.

Figure 1 provides a typical relationship between hourly available generation capacity, load profile, HEAG, and EEAE of a power system. In general, the calculated ξ^d using Scenario I is expected to be higher than that of Scenario II.

After calculating the ξ^d for a year, the relationship given in (2.6) is developed using (2.4) and (2.5) to calculate the minimum number of EVs that can be incorporated into a power system without generation expansion for fully controlled charging.

$$\min(\xi^d) = \sum_{n=1}^{N_{ev}^{min}} d_n \times EPM_n, \quad (2.6)$$

where $\min(\xi^d)$ represents the minimum daily available energy of a year.



* $\xi_h^d - L_h^{evd}$ are the EEAE and charging load demand of EVs at hour h on day d .

Figure 2. Flowchart to calculate the EEAE-EVs under fully controlled charging.

Then, a load profile is constructed for the estimated minimum number of EVs using the data Tables provided in Section 2.1.3. Finally, the number of EVs is updated until the following relationship is satisfied.

$$\min\left\{\sum_{\hat{h}=1}^{24} (\xi_{\hat{h}}^d - L_{\hat{h}}^{evd})\right\} = \epsilon, \quad (2.7)$$

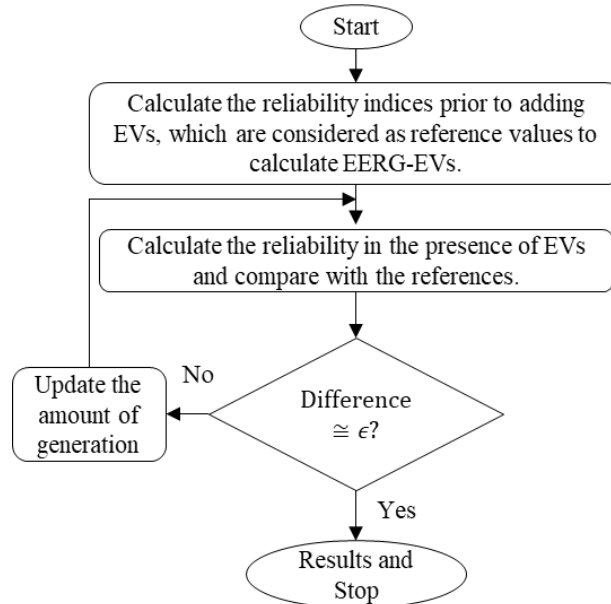
where d represents days of a year, \hat{h} represents hours of the d^{th} day, $\xi_{\hat{h}}^d$ is the extra available

generation at \hat{h}^{th} hour of the d^{th} day, $L_{\hat{h}}^{evd}$ is the amount of EV load at \hat{h}^{th} hour of the d^{th} day, and ϵ is the tolerance level.

If the value of ϵ for the initial number of EVs is positive or negative, then, the process is repeated by increasing or decreasing the number of EVs, respectively, until the stopping criterion described in (2.7) is satisfied. Finally, the EEAE-EVs under fully controlled charging is estimated by determining the equivalent charging load for the final number of EVs. The flowchart of the proposed method to calculate the EEAE-EVs is given in Figure 2.

2.2 Extra Effective Required Generation to Accommodate EVs

The EERG-EVs is used to estimate the required new generation to maintain the level of reliability of power systems. An approach similar to determining the capacity value of wind power [64]–[66] is developed to measure the new generation amount using the EERG-EVs metric.



*Difference= Reference -Reliability with EVs

Figure 3. Flowchart to calculate the EERG-EVs.

The reliability of power systems will be deteriorated after adding EV loads. Therefore, extra

generation will be required to restore the initial reliability level (i.e., the reliability level prior to adding the load of EVs). The calculation of the new generation amount to achieve the initial reliability level using the EERG-EVs metric begins by estimating the reliability indices of the system prior to adding EVs, which are used as references. In the next step, reliability indices are calculated in the presence of EVs, which are expected to increase compared to the references. Then, the generation in the system is gradually increased until the system reliability level reaches the reference point. The flowchart to calculate the EERG-EVs is given in Figure 3.

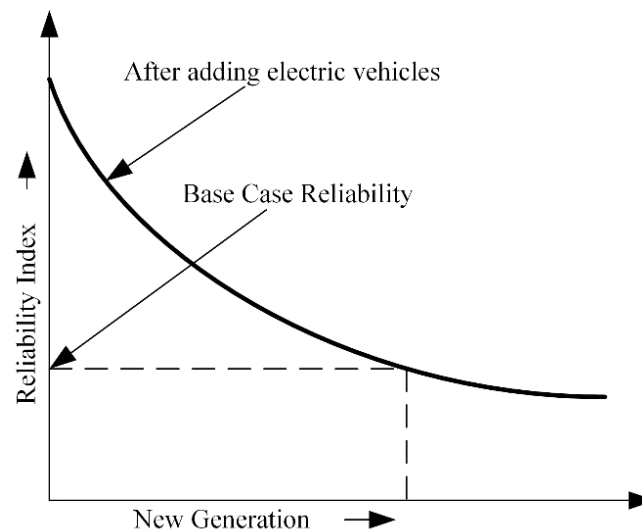


Figure 4. Calculation of the required generation based on the EERG-EVs concept.

A typical relationship between the increased generation and a reliability index is depicted in Figure 4. The loss of load probability (LOLP) and expected demand not supplied (EDNS) indices are used to estimate the required new generation amount using the EERG-EVs metric. These two indices may yield different values for the required generation and the planner or operator has the option to consider any of them. For instance, if the concern is about the probability that the customer experiences one or more loss of load events, the LOLP index decides the required new generation. On the other hand, if the concern is how much power interruption the customer may experience for each loss of load events, EDNS is used to calculate the required new generation.

2.3 Calculation of the Reliability Indices

In this dissertation, we have evaluated the most well-known reliability indices, Loss of Load Probability (LOLP), Loss of Load Frequency (LOLF), and Expected Demand Not Supplied (EDNS), of power systems. Simulation methods have been commonly implemented in sampling system states and evaluating the reliability indices of power systems. In evaluating the reliability indices, the expected values are used to evaluate the indices. If an index is denoted by η , the expected value of the index is calculated as follows,

$$\hat{\eta} = E[\eta], \quad (2.8)$$

where $E[\cdot]$ is the expectation operator.

2.3.1 Calculation of the LOLP Index

The probability of failure of the system to meet the demand is expressed by the LOLP index and is calculated as follows,

$$q = \sum_{m=1}^{n_f} P\{x_m: x_m \in X_f\}, \quad (2.9)$$

where q denotes the LOLP index, X_f is the set of failure states ($X_f \subset X$), X is the set of all states, x_m is the system state m , $P\{x_m: x_m \in X_f\}$ is the probability of the system being in state x_m , and n_f is the number of failure states.

Using sequential MC simulations, sampled states are evaluated and the failure probability index q is updated. In this regard, the estimated value of the LOLP index \hat{q} is calculated using sequential MC simulation as follows,

$$\hat{q} = \frac{1}{T} \sum_{m=1}^N v_m, \quad (2.10)$$

where T is the total duration of all sampled system states, N is the number of samples, and v_m can be expressed as follows,

$$v_m = \begin{cases} \tau_m, & \text{if } x_m \in X_f \\ 0, & \text{Otherwise} \end{cases}, \quad (2.11)$$

where τ_m is the time duration of state x_m .

2.3.2 Calculation of the EDNS Index

The EDNS index measures the expected load that will be curtailed in cases of failure states. The EDNS index is calculated using the following where ρ denotes the EDNS index.

$$\rho = \sum_{m=1}^{n_f} P\{x_m: x_m \in X_f\} \cdot L_c\{x_m: x_m \in X_f\}, \quad (2.12)$$

where $L_c\{x_m: x_m \in X_f\}$ is the amount of load curtailment of state x_m .

Using sequential MC simulations, sampled states are evaluated and the EDNS index ρ is updated based on the amount of load curtailment. The estimated EDNS index $\hat{\rho}$ is calculated using sequential MC simulation as follows,

$$\hat{\rho} = \frac{1}{T} \sum_{m=1}^N \psi_m, \quad (2.13)$$

where ψ_m represents the amount of curtailment and is expressed as follows:

$$\psi_m = \begin{cases} \tau_m \cdot L_{cm}, & \text{if } x_m \in X_f \\ 0, & \text{Otherwise} \end{cases}, \quad (2.14)$$

2.3.3 Calculation of Frequency of Failure Index:

Frequency and duration indices provide measures for how often and how long a load is curtailed. It is worth mentioning here that calculation of frequency and duration indices using MC state sampling method is not a straightforward process as is for probability and energy indices [90]. Some manipulations to the MC state sampling method have been introduced in [91]–[93] to

calculate the frequency and duration index. For this reason, the MC next event method is used in this dissertation. The estimated LOLF index ($\hat{\phi}$) is calculated as follows,

$$\hat{\phi} = \frac{1}{T} \sum_{m=1}^N \phi_m \times 8760, \quad (2.15)$$

where ϕ_m is a binary indicator for the transitions between success and failure states, which is expressed as follows,

$$\phi_m = \begin{cases} 1, & \text{if } x_{m-1} \in X_s \text{ and } x_m \in X_f \\ 0, & \text{Otherwise} \end{cases} \quad (2.16)$$

where X_s is the set of success states ($X_s \subset X$).

2.4 Simulation Results

The proposed approaches in this chapter is demonstrated on the IEEE-RTS, which has been extensively tested for power system reliability analysis. The detailed data of the IEEE-RTS (e.g., the capacities of generating units, failure and repair rates of the system components, and the load profile) are given in [59].

In [5], the peak demand of 100 EVs is considered as 79.05 kW for home charging scenario and 74.18 kW for public/home charging scenario. In [60], the peak demand for 100 EVs ranges from 62.5 to 80 kW based on a utility factor (the percentage of total miles driven by vehicles with electric energy) of the EVs. Therefore, following the same range of peak loads, we considered 75 kW as the annual peak demand for 100 EVs. This peak load is scaled for the number of EVs used in this study. The percentages of charging EVs in public and residential stations are considered 40% and 60%, respectively, as provided in [5]. The percentages of different types of vehicles are considered as follows: 60.85% sedan, 11.94% mid-sedan, 13.1% mid-SUV, and 14.11% full-SUV [67]. The most common daily travel distance in the United States is about 25–30 miles [60]. Therefore, we considered 30 miles as the daily driving distance to estimate the total daily electricity demand for

charging EVs. The required energy to travel each mile for different types of vehicles are considered as follows: sedan 0.3225 kWh/mile, mid-sedan 0.3605 kWh/mile, mid-SUV 0.4375 kWh/mile, and full-SUV 0.5075 kWh/mile [60]. The daily required energy to charge EVs is calculated based on daily travel distance using (2.4).

Four different case studies are carried out to demonstrate the effectiveness of the proposed metrics on the IEEE-RTS, which are as follows:

- Case I: IEEE-RTS Base Case,
- Case II: Analyzing the Effects of EVs on System Reliability,
- Case III: Calculation of EEAE-EVs, and
- Case IV: Calculation of EERG-EVs.

2.4.1 Case I: IEEE-RTS Base Case

In this case, the original load profile of the IEEE-RTS and existing generating units are used without adding EVs. System states are sampled using the sequential MC simulation method. The second row of Table 4 shows the estimated LOLP and EDNS for this case.

2.4.2 Case II: Analyzing the Effects of EVs

In this case, the impacts of EVs on the IEEE-RTS is illustrated with real EV charging data. Therefore, the constructed load profiles for residential and public charging stations of EVs are combined with the system load profile. In [5] and [6], the penetration level of EVs have been considered as 12–24% of the peak system load. Therefore, following the same range of assumptions, we have considered 330–660 MW EV loads (11.58–23.16% EV penetrations of the total load of IEEE-RTS) to illustrate the effects of EVs on system reliability. The estimated reliability indices for different amounts of EV loads are shown in Table 4

2.4.3 Case III. Calculation of EEAE-EVs:

In this case, the time and duration for scheduled maintenance of generating units of the IEEE-RTS provided in [59] and [68] are adopted to calculate the EEAE-EVs. The EEAE-EVs of the IEEE-RTS is calculated for both Scenario I and Scenario II described in Section 2.1.4.

Table 4. Calculated Reliability Indices for the IEEE-RTS

Cases	Added EV load (MW)	LOLP	EDNS (MW/Yr)
Case I	-	0.00107	0.1393
Case II	330 (11.58%)	0.0028	0.3936
	386 (13.54%)	0.0032	0.4352
	441 (15.47%)	0.0036	0.5078
	496 (17.40%)	0.0041	0.5890
	552 (19.36%)	0.0047	0.6798
	607 (21.29%)	0.0054	0.7806
	660 (23.16%)	0.0061	0.8909

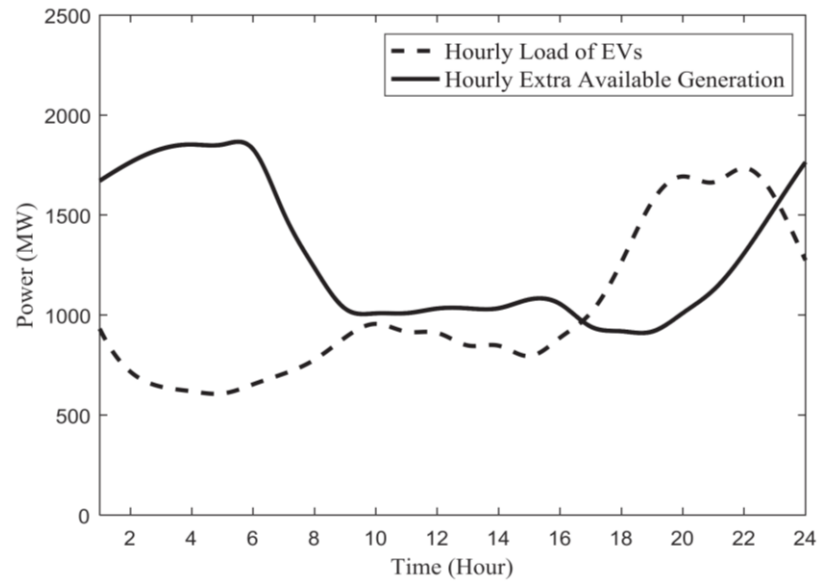


Figure 5. EV loads based on the EEAE-EVs concept for IEEE-RTS.

2.4.3.1 EEAE-EVs of IEEE-RTS under Scenario I:

To calculate the EEAE-EVs of the IEEE-RTS under this scenario, first, we have calculated the

HEAG of the IEEE-RTS using the algorithm described in Section 2.1.4.1 under Scenario I. Then, the HEAG is used to calculate the ξ_d for the IEEE-RTS using (2.5). In the next step, the initial number of EVs is estimated using (2.6) which is found to be 971,200 cars or 10,716.77 MWh daily EV loads. Then, a load profile for this initial number of EVs is developed using the algorithm described in Section 2.2. The condition of determining the EEAE-EVs is checked using (2.7) and the number of EVs is updated in each iteration until this condition is satisfied. The step size is considered as 100 EVs. Finally, the EEAE-EVs is estimated for the final number of EVs.

The estimated number of EVs that the IEEE-RTS can accommodate daily with fully controlled charging is 1,462,667 cars without adding any new generating unit. Therefore, the EEAE-EVs of the IEEE-RTS is the daily equivalent charging load of 1,462,667 cars for fully controlled charging, which is approximately 16,139.89 MWh. Figure 5 shows the HEAG and the EEAE-EVs of the IEEE-RTS for a typical day of a year.

2.4.3.2 EEAE-EVs of IEEE-RTS under Scenario II:

In this scenario, the HEAG of the IEEE-RTS is estimated using the algorithm described in 2.1.4.2 under Scenario II. In this scenario, the assumed reserve capacity for the IEEE-RTS is 400 MW (the maximum generation capacity of the largest unit of the IEEE-RTS). The EEAE-EVs of the IEEE-RTS for this scenario is estimated using the procedure described in Section 2.1.4. The estimated minimum number of EVs for this scenario is 559,250 cars or 6,171.08 MWh daily EV loads. The final number of EVs that can be added to the IEEE-RTS for Scenario II without adding generation is also calculated using the relationship (2.7), which is found to be 9,32,000 cars or 10,284.22 MWh daily EV loads. Therefore, the estimated EEAE-EVs for the IEEE-RTS under this scenario is 10,284.22 MWh daily EV loads for a fully controlled charging strategy.

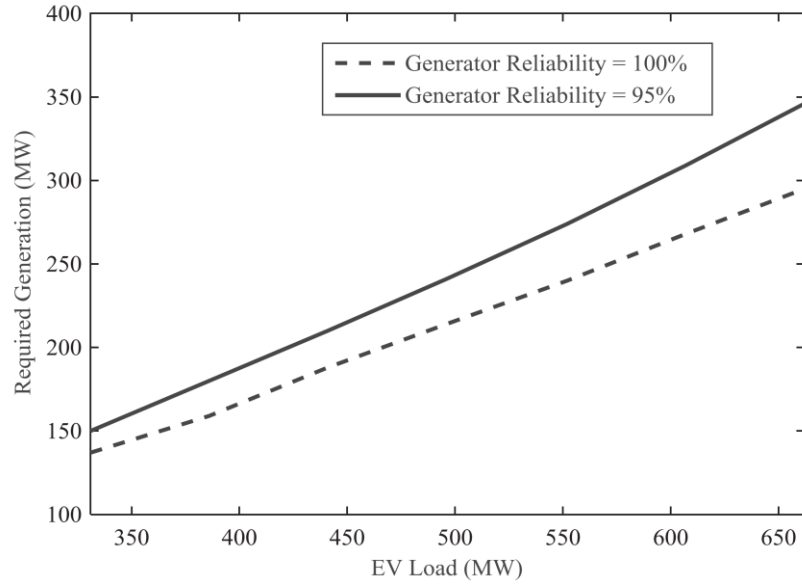


Figure 6. Required generation to avoid effects of EVs on LOLP.

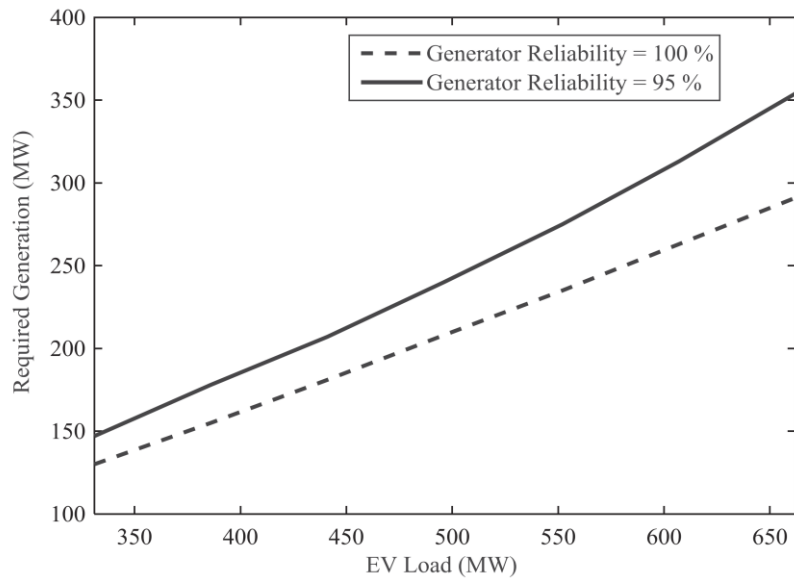


Figure 7. Required generation to avoid effects of EVs on EDNS.

2.4.1 Case IV. Calculation of EERG-EVs:

In this case, the EERG-EVs using the algorithm described in Section 2.2. The amount of extra generation is estimated for generators with two different reliability parameters (e.g., perfectly reliable and with 95% availability). The estimated required extra generation amount to restore the

initial system reliability for different penetration levels of EVs is shown in Table 5. Figure 7 and Figure 8 are the graphical representations of EV penetrations versus new generating units.

Table 5. Required Generation to Maintain LOLP and EDNS with EVs

Penetration Charging Load of EVs (MW)	Added Generation (MW) to Restore			
	Base Case LOLP		Base Case EDNS (MW/Yr)	
	Perfectly Reliable	Availability (95%)	Perfectly Reliable	Availability (95%)
331	137	150	130	147
386	159	180	155	178
441	188	210	181	207
496	214	241	208	240
552	240	274	235	275
607	268	309	263	313
660	295	346	291	354

2.5 Discussion

The reliability indices for Case I and Case II are evaluated using the sequential MC simulation method. The reliability indices are given in Table 4. Table 4 also shows the effect of increasing the amount of EV loads on the LOLP and EDNS indices. Further, Table 4 shows that the increase of EV loads increases the LOLP and EDNS indices. Although, the increase in the LOLP and EDNS indices is low for a small number of EVs, as the amount of EV loads increases, the increase in the LOLP and EDNS indices becomes large. From Table 4, it can be seen that the increase in the LOLP and EDNS indices is 0.0004 and 0.0416, respectively, for increasing the amount of EV loads from 330 to 386 MW. On the other hand, the increase in the LOLP and EDNS indices becomes 0.0007 and 0.1103 for increasing the amount of EV loads from 607 to 660 MW, respectively. Therefore, it can be concluded that the developed load profiles can be used effectively to analyze their impacts on power system reliability.

In Case III, the EEAE-EVs for the IEEE-RTS is estimated with the calculated HEAGs under Scenarios I and II as described in Section 2.1.4. From the results of Case III, it can be seen that the

EEAE-EVs for the IEEE-RTS is higher for Scenario I than Scenario II (Scenario I considers MTTR, MTTF, and outages due to scheduled maintenance of the generating units and ignores the reserve margin whereas Scenario II considers both). The results of Case III also show that the IEEE-RTS is capable of maintaining its reliability level for a maximum of 16,139.89 MWh of daily EV loads without adding new generating units for Scenario I. Moreover, the results of Case III show that the IEEE-RTS is capable of maintaining its reliability level for a maximum of 10,284.22 MWh of daily EV loads without adding new generating units for a constant system reserve of 400 MW (Scenario II). However, in order to include this amount of EV loads, the charging of EVs needs to be controlled fully based on the HEAG to maintain the reliability level. Although the number of EVs for Scenario I is different from Scenario II, the reliability indices for both scenarios are the same. This happens because the EEAE-EVs is developed based on maintaining power system reliability.

In Case IV, only the second metric (EERG-EVs) is demonstrated on the IEEE-RTS under uncontrolled charging of EVs. Table 5 shows the estimated required amount of extra generation to restore the initial reliability for different number of EVs with two different reliability levels for the generators (i.e., perfectly reliable and 95% availability). From Table 5, it can be seen that the amount of the new generation needed to restore the EDNS index is lower than that required to restore the LOLP index. Also, Figure 6 and Figure 7 show that the amount of the new generation needed to restore the initial reliability indices is low for perfectly reliable generators compared to the generators with 95% availability, which is not a surprise.

From the above-discussed case studies, it can be concluded that the proposed EEAE-EVs metric is effective in calculating the amount of EV loads that can be incorporated in a power system without adding any resources under fully controlled charging. Also, the proposed EERG-EVs metric has significant potential benefits to both analyze the effects of EVs on power systems and to estimate the required amount of generation to maintain/enhance system reliability.

Chapter 3. Maximum Permissible Load Demand for EVs at Power System Buses

In this chapter, an index to determine the “extra accessible loading capacity of a bus” for EVs (EALCB-EVs) to allocate EVs at system buses is proposed. The EALCB-EVs can be used to determine the maximum permissible number of EVs at system buses with existing resources under both controlled and uncontrolled (actual) charging scenarios. The EALCB-EVs of a bus is estimated through updating the number of EVs iteratively until the cumulative charging load of EVs is satisfied with extra accessible loading capacity of the respective bus. The hourly extra accessible loading capacities of power system buses are estimated by taking the difference between hourly maximum loading capacities and existing hourly loads of the buses respectively. The maximum penetration level of EV loads in a bus is evaluated through calculating the equivalent charging load for maximum permissible number of EVs of the respective bus. The proposed method is demonstrated on the IEEE-RTS. The linear programming is used to calculate extra accessible loading capacities at power system buses.

3.1 Extra Accessible Loading Capacity

The EALCB-EVs concept to determine the maximum permissible number of EVs at power system buses has three main steps, which are described in the following sections.

3.1.1 Maximum Permissible Number of EVs at System Buses

The procedure to calculate the maximum permissible number of EVs at power system buses using the EALCB-EVs concept follows an iterative process. The process begins by estimating the extra accessible loading capacities of system buses (EALCB). Then, the load profile for an initial number of EVs is constructed. The detail of the procedures to calculate the EALCB and to construct the load profile for EVs are described in Sections 3.1.2 and 3.1.3. In the next step, the maximum

permissible number of EVs for power system buses are calculated under fully controlled and uncontrolled charging scenarios based on the following procedures.

3.1.1.1 EALCB-EVs under Fully Controlled Charging Scenario:

In this scenario, after calculating the EALCB, daily extra accessible energy at power system buses is calculated as follows,

$$\xi_e^{id} = \sum_{h=1}^{24} \xi_e^{ihd}, \quad \begin{cases} i = 1, 2, \dots, N_b \\ h = 1, 2, \dots, 24, \\ d = 1, 2, \dots, 365 \end{cases} \quad (3.1)$$

where N_b is the total number of buses, ξ_e^{ihd} is the extra accessible loading capacity of bus i at hour h of day d , and ξ_e^{id} is the extra accessible energy of bus i on day d of the year.

The daily required energy to charge an initial number of EVs can be estimated as follows,

$$L_{ev}^{id} = \sum_{h=1}^{24} L_{evd}^{ih}, \quad (3.2)$$

where L_{evd}^{ih} is the load demand of the anticipated number of EVs for bus i at hour h of day d and L_{ev}^{id} is the total required energy to charge the anticipated number of EVs at bus i on day d .

Then, a stopping criterion for controlled charging scenario with the tolerance level, ϵ , is expressed as follows,

$$\min(\xi_e^{id} - L_{ev}^{id}) \approx \epsilon \quad (3.3)$$

The results of (3.3) are used to determine the maximum number of EVs that can be charged at the respective bus under fully controlled charging. A typical relationship between the EALCB and load profile of EVs is shown in Figure 8.

Under fully controlled charging, the area under the EALCB curve has to be equal to the area under the EV load profile curve to accommodate the EVs with existing resources. Also, the amount

of EV load that is represented by the area B in Figure 9 should be shifted to areas A and C under fully controlled charging.

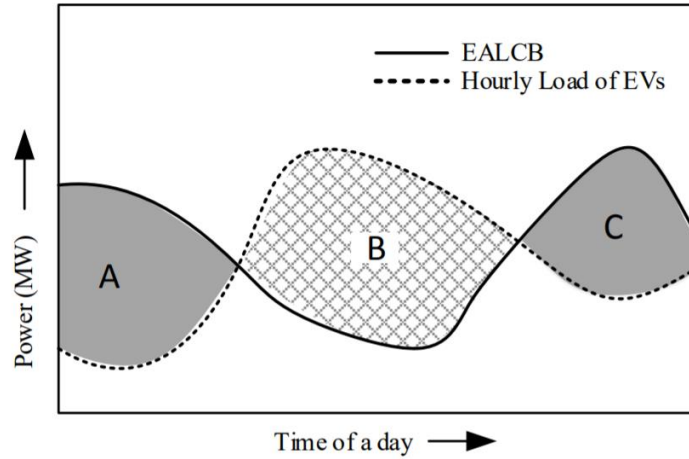


Figure 8. Relation between EALCB and load profile of EVs.

3.1.1.2 EALCB-EVs under Uncontrolled Charging Scenario:

Also, in this scenario, after calculating the EALCB, the load profile for initial number of EVs is constructed. A stopping criterion for uncontrolled charging scenario is as follows,

$$\min(\xi_e^{ih} - L_{ev}^{ih}) \approx \epsilon, \quad h = 1, 2, \dots, 8760, \quad (3.4)$$

where ξ_e^{ih} is the extra accessible loading capacity of bus i at hour h and L_{ev}^{ih} is the load of EVs of bus i at hour h .

Also, in this scenario, the estimated final number of EVs using (3.4) for a bus is the maximum number of EVs that can be charged at the respective bus with existing resources under uncontrolled charging scenario.

3.1.2 Calculation of EALCB

The EALCB at the buses is calculated using the maximum hourly loading capacities and existing hourly loads.

3.1.2.1 Evaluation of Maximum Hourly Loading Capacities of Buses

The calculation of the maximum hourly loading capacities at system buses is important to calculate the EALCB. The maximum hourly loading capacity of buses is not constant for a given period of time due to the network topology (i.e., rated capacity and outage profiles of generating units and transmission lines etc.). Therefore, we calculate the hourly maximum loading capacity of buses based on the capacity and outage profiles of the generating units and transmission lines for several years using the MC simulation. Then, we calculate the average of maximum loading capacity at each hour for all the simulated years. Also, the linear programming with an objective function of maximizing bus loading capacities is used to calculate the maximum loading capacities at buses. However, in the calculation of maximum hourly loading capacity of buses, there can be multi optimum situations. Depending on the manner in which the program scans the vertices of the feasible polytope, it can favor maximizing loading capacities at certain buses depending on how the buses are numbered. This bias can be removed by dynamic numbering of the buses, i.e., altering the bus numbers after the occurrence of each event in the simulation. The average of the hourly maximum loading capacities of buses is calculated as follows,

$$\xi_{max}^{ih} = \frac{1}{N_y} \sum_{j=1}^{N_y} \xi_{max}^{ijh}, \quad (3.5)$$

where N_y is the total number of simulated years, ξ_{max}^{ijh} is the maximum loading capacity at hour h of j^{th} year for bus number i , and ξ_{max}^{ih} is the average of the maximum loading capacity at hour h of the i^{th} bus.

3.1.2.2 Construction of Hourly Load Profile:

Existing load profiles at power system buses are also important factors to determine the EALCB. The existing load profiles at system buses are constructed based on the hourly, daily, and weekly data of load demand of the IEEE-RTS load profile [59]. The peak load of a bus is composed

with the hourly, daily, and weekly data of load demand to construct the load profile for a year of the respective bus.

3.1.2.3 Calculation of EALCB:

Finally, the EALCB is calculated by subtracting actual hourly loads from average maximum hourly loading capacities of buses. The EALCB of a power system can be calculated as follows,

$$\xi_e^{ih} = \xi_{max}^{ih} - L_{hi}^a, \quad (3.6)$$

where L_{hi}^a is the actual load demand at hour h of bus i .

3.1.3 Load Profiles of EVs

In order to calculate the EALCB-EVs, it is also important to construct load profiles for EVs. The EVs may charge either at public charging stations or at residential charging stations where charging patterns of EVs depend on the type of the charging station. For example, at public charging station, peak amount of the charging happens at around midday. On the other hand, at residential stations, the maximum amount of charging happens at midnight. Therefore, it is important to construct load profiles for EVs for both public and residential charging stations. The load profiles of EVs for both residential and public charging stations at system buses are constructed using the annual peak demands of EVs of corresponding buses and the given hourly, daily, and weekly data in Chapter 2 Section 2.1.4.

3.2 Network Modeling

Typically, voltage limits are taken into account in loadability calculation of power systems. On the other hand, in composite system reliability evaluation where repetitive simulations are needed, the DC power flow model is commonly performed due to the high computation demand for the case of the AC power flow model. Following the same convention, we have calculated the

maximum EV loadability limit using the DC power flow with the power balance equation, generation capacity limits, and transmission line carry capability limits. The power balance equation represents an equality constraint and the generation and transmission limits represent inequality constraints [69]. In this dissertation, we do not consider the impacts of voltage limits on the number of EVs. However, the voltage limits will have an impact on the number of EVs that can be accommodated. The linear programming is used to calculate the maximum hourly loading capacity. The linear programming model of the network with DC load flow is as follows,

$$\text{Maximum Loading Capacity} = \max \sum_{i=1}^{N_b} L_i, \quad (3.7)$$

Subject to,

$$\begin{aligned} \hat{B}\delta + G - L &= 0 \\ G &\leq G_{max} \\ -F_{max} &\leq b\hat{A}\delta \leq F_{max} \\ G, L &\geq 0 \\ -\pi &\leq \theta \leq \pi \end{aligned} \quad (3.8)$$

In (3.7) and (3.8), N_b is number of buses, N_t is number of transmission lines, \hat{B} is the augmented node susceptance matrix ($N_b \times N_t$), b is the transmission line susceptance matrix ($N_t \times N_t$), \hat{A} is the element-node incidence matrix ($N_b \times N_b$), δ is the vector of node voltage angles ($N_b \times 1$), L is the vector of bus loading capacity ($N_b \times 1$), G_{max} is the vector of maximum accessible generation ($N_b \times 1$), F_{max} is the vector flow capacities of lines ($N_t \times 1$), respectively, and G is the solution vector of the generation at buses ($N_b \times 1$). To get a feasible solution for the standard problem, we assume that one of the bus angles is zero of the constraints given in (3.8).

In the optimization problem, charging demand for EVs is considered as nonbasic variables, while the other variables (e.g., real power generation) of DC power flow are considered as basic variables. In the simplex method of LP, if none of the constraints is violated, the optimization

algorithm follows an iterative process to adjust values of the variables within their limits to find an optimal solution. In this case, the generators are set at their maximum values. However, if one or more constraints are violated, the LP provides ordered weights to dispatch power from available generators based on their locations in the coefficient matrix to maximize the objective function. The description for LP solution algorithms and limitations can be found in [112]–[113].

3.3 Case Studies

The proposed EALCB-EVs method is applied on the IEEE-RTS. The IEEE-RTS consists of 32 generating units, 38 transmission lines, and 24 buses. The total generation capacity of the IEEE-RTS is 3405 MW and the total peak load is 2850 MW. The detailed data of the IEEE-RTS are given in [59]. In [5], the peak demand for 100 EVs has been given as 79.05 kW and 74.18 kW for home and public charging scenario respectively. In [60], the peak demand for 100 EVs ranges from 62.5 kW to 80 kW based on the utility factor of the EVs. Therefore, following the same range of peak loads, 75 kW is assumed as the annual peak demand for 100 EVs, which is scaled for the number of EVs in this study. The assumed percentage of charging EVs at public and residential stations are 40% and 60%, respectively [5]. Four different case studies are carried out to demonstrate the proposed method.

3.3.1 Case I:

In this case, the EALCB-EVs is calculated for all load buses of the IEEE-RTS under fully controlled charging scenario. The EALCB is calculated using the procedure described in Section 3.1.2, and the daily EALCB for the load buses are calculated using (3.1). The load profile for an initial number of EVs is constructed using the procedure described in Section 3.1.3. The daily required energy to charge this initial number of EVs is calculated using (3.2). Finally, the maximum number of EVs that can be allocated at each load bus of the IEEE-RTS under fully

controlled charging are calculated using (3.3). Also, the annual peak demand for the maximum number of EVs at each load bus is calculated by scaling the assumed peak demand for EVs. The results of this case study are given in the second, third, and fifth column of Table 6.

3.3.2 Case II:

In this case, the EALCB-EVs for the IEEE-RTS load buses are calculated under uncontrolled (actual) charging scenario. The calculated EALCB and the constructed load profile for an initial number of EVs in case I are also used in this case. The maximum permissible number of EVs for load buses of the IEEE-RTS under uncontrolled charging scenario is estimated using (3.4). The results of this case are shown in the fourth and sixth column of Table 6.

Table 6. Maximum EVs Load Allocation at Load Buses of the IEEE-RTS

Bus No.	Maximum ξ^{id}	EALCB-EVs (MW)		EALCB-EVs (No.)	
	For EVs (MWh)	Case I	Case II	Case I	Case II
1	551.7	49.0	26.5	65,333	35,333
2	396.0	50.00	26.65	66,667	35,533
3	803.6	82.00	34.25	109,333	45,667
4	516.3	55.00	16.00	73,333	21,333
5	546.7	59.00	15.00	78,667	20,000
6	469.2	48.00	21.00	64,000	28,000
7	2268	198.00	91.00	264,000	121,333
8	666.5	70.00	26.00	93,333	34,667
9	989.3	103.00	35.00	137,333	46,667
10	917.0	95.00	34.00	126,667	45,333
13	1693	179.00	35.00	238,667	46,667
14	1469	150.00	55.00	200,000	73,333
15	1855	194.00	46.00	258,667	63,448
16	1910	197.00	68.00	262,666	90,667
18	5122	530.00	156.00	706,667	208,000
19	2163	219.00	83.00	292,000	110,667
20	2215	230.00	70.00	306,667	93,333

3.3.3 Case III:

In this case, the EALCB-EVs for selected load buses of the IEEE-RTS is calculated under fully controlled charging. The EALCB for the selected load buses is calculated through maintaining the constant loading capacities of the other buses. Then, the daily EALCB for the selected load buses

is calculated using (3.1). The constructed load profile for an initial number of EVs and the calculated daily required energy to charge this initial number of EVs in case I are again used in this case. Finally, the maximum number of EVs that can be allocated at the selected load buses of the IEEE-RTS under fully controlled charging are calculated using (3.3). Also, the peak demand for the calculated maximum number of EVs are determined. The results of this case are given in the second, third, and fifth column of Table 7.

Table 7. Maximum EVs Load Allocation at Selected Load Buses of the IEEE-RTS

Bus No.	Maximum ξ^{id}	EALCB-EVs (MW)		EALCB-EVs (No.)	
	For EVs (MWh)	Case III	Case IV	Case III	Case IV
1	803.5	72	38.00	96,000	50,667
5	1218.4	128	36.00	170,667	48,000
7	2571.5	226	121.00	301,333	161,333
8	1070.7	112	37.00	149,333	49,333
10	1642.1	170	55.00	226,667	73,333
13	4390.2	462	100.00	616,000	133,333
14	2390.6	244	85.00	325,333	113,333
15	3970.9	411	129.00	548,000	172,000
18	6768.0	680	249.00	906,667	332,000

3.3.4 Case IV:

In this case, the EALCB-EVs is calculated for selected load buses of the IEEE-RTS under uncontrolled charging scenario. Again, the calculated EALCB for the selected load buses in case III and the constructed load profile for an initial number of EVs in case I are used in this case. The final number of EVs for the selected buses is calculated using (3.4). The results of this case are given in the fourth and sixth column of Table 7.

3.4 Results and Discussion

From Table 6, it can be seen that among all load buses of the IEEE-RTS, the maximum number of EVs can be allocated at bus 18 followed by bus 7 for both the fully controlled and uncontrolled charging scenario. This is not a surprise because both buses of the IEEE-RTS have high generation

capacity. Therefore, the maximum loading capacities of bus number 18 and 7 are higher than that of the other load buses. Table 6 also shows that, the maximum number of EVs for all buses under fully controlled charging are much higher than uncontrolled charging. This happens because in the proposed fully controlled charging, most of the charging occurs during maximum extra accessible loading capacity periods which is not possible for uncontrolled charging. Moreover, Table 6 shows that bus 1 has low daily maximum EALCB for EVs but high EV allocation capability compared to bus number 6. This happens because the maximum number of EVs at a system bus under fully controlled charging not only depends on the daily maximum EALCB-EVs but also depends on the difference between daily EALCB and daily demand for EVs of the corresponding bus. On the other hand, the maximum number of EVs at a bus under uncontrolled charging scenario depends only on the difference between hourly EALCB and hourly demand for EVs of the respective bus.

From Table 6 and Table 7, it can be seen that the calculated EV allocation capacity of a specific bus is higher for the cases of selected buses than for the cases of all load buses. For example, in case III, the maximum number of EVs that can be allocated at bus 18 is 28.3% higher compared to case I. In same way, in case IV, the calculated maximum number of EVs for bus 18 is 59.61% higher compared to case II. This happens due to the fact that in case III and case IV, the linear programming distributes the extra accessible generation amount among the selected buses based on their line capacity. On the other hand, in case I and case II, the extra accessible generation amount is distributed among all the load buses. Therefore, the loading capacity of a bus is higher for case III and case IV compared to case I and case II respectively.

From the above case studies, it can be concluded that the proposed EALCB-EVs concept is effective in calculating the number of EVs that can be incorporated—under both the fully controlled and uncontrolled charging scenarios—at power system buses without adding any resources. This will be beneficial for the system operators and planners to plan for the deployment of charging

stations at system buses. Also, the EALCB-EVs concept is effective to calculate the maximum number of EVs that can be accommodated at a transmission level bus, which provides the total number of EVs that can be charged at the aggregated distribution system at that bus. Furthermore, the proposed concept has significant potential to estimate the required amount of resources to handle the demand increase due to penetration of EVs.

Chapter 4. Determining Maximum Hosting Capacity of Electric Distribution Systems to EVs

A voltage constrained-based approach to determine the maximum hosting capacity of (DSs) to EVs is proposed in this chapter. The maximum hosting capacity under uncontrolled (actual) charging scenario is estimated through gradually increasing the penetration of EVs until the minimum difference between load profile of EVs and hourly extra available power (HEAP) of the DS becomes zero. The final number represents the maximum hosting capacity of the DS to EVs under the uncontrolled charging scenario. Load profile for EVs is constructed using probability distribution functions of daily travel distance, departure time, and arrival time. These distribution functions are constructed using survey data collected from several technical reports. The HEAP is calculated by taking the differences between maximum hourly loading capacities and hourly loads at each node. The maximum loading capacities are calculated through gradually increasing the spot loads until the voltage constraints are violated. For fully controlled charging scenario, daily extra available energy (DEAE) and daily required energy to charge EVs are used to estimate the maximum hosting capacity of EVs. The DEAE of a DS is estimated using the HEAP. Daily required energy to charge EVs is calculated based on daily travel distance and energy required to travel each mile. OpenDSS is used to check the voltage constraints and to estimate the HEAP. The proposed approach is demonstrated on the IEEE 123-node test feeder through several case studies.

4.1 Maximum Hosting Capacity of DSs to EVs

The proposed voltage constrained-based approach to calculate the maximum hosting capacity of DSs to EVs follows an iterative method. The process begins by selecting nodes (e.g., all the nodes or some selected nodes) of the DS to host EVs. Then, the HEAP at each of the selected nodes is estimated. After calculating the HEAP, initial number of EVs that can be accommodated at the

selected nodes is estimated using the constructed load profile of EVs and the minimum HEAP of the respective nodes. The procedures to construct the load profile for EVs and calculate the HEAP are described in Sections 4.2.1 and 4.2.2 respectively. Finally, the maximum hosting capacity of EVs in the DS is calculated under uncontrolled and fully controlled charging scenarios based on the following procedure.

4.1.1 Maximum Hosting Capacity of DSs under Uncontrolled Charging Scenario

In this scenario, after calculating the HEAP at the selected nodes, the initial number of EVs for each of the selected nodes is calculated as follows,

$$\min P_{i,j,k} = \max \sum_{n=1}^{N_k^{u,min}} P_{i,j,k,n}^{ev} \quad (4.1)$$

where i is the index for hours of a day, j is the index for days of a year, k is the index for number of buses of a DS, n is the index for number of EVs, $N_k^{u,min}$ is the minimum number of EVs under uncontrolled charging scenario for node k , $P_{i,j,k}$ is the extra available power at the i^{th} hour of j^{th} day for node k , and $P_{i,j,k,n}^{ev}$ is the demand to charge the n^{th} EV at i^{th} hour of j^{th} day for node k .

After calculating the initial number of EVs, the expression provided in (4.2) is developed to update the number of EVs at each node.

$$\min(P_{i,j,k} - \sum_{n=1}^{N_k^u} P_{i,j,k,n}^{ev}) \approx \epsilon, \quad (4.2)$$

where N_k^u is the number of EVs under uncontrolled charging scenario for node k and ϵ is the tolerance level.

The final number of EVs calculated for each node using (4.2) represents the maximum hosting capacity of DSs at the respective node under uncontrolled charging scenario. The summation of the

maximum hosting capacities at each of the selected nodes is the maximum HC of DSs to EVs under this scenario.

4.1.2 Maximum Hosting Capacity of DSs under Fully Controlled Charging Scenario

In this scenario, after calculating the HEAP, the DEAE of the DS is calculated as follows,

$$W_j = \sum_{k=1}^{N_b} \left(\sum_{n=1}^{24} P_{i,j,k} \right), \quad (4.3)$$

where W_j is the extra available energy on the j^{th} day of the year.

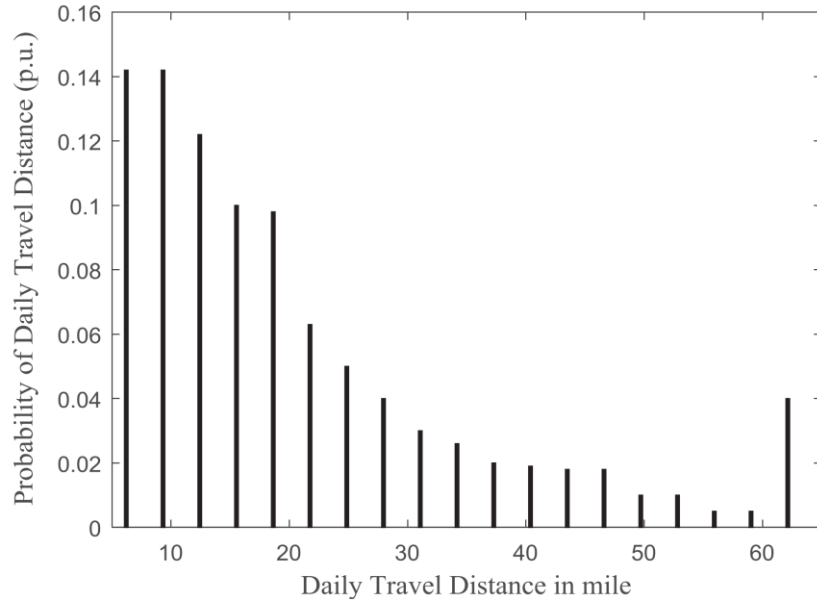


Figure 9. Probability distribution function of daily travel distance of EVs.

The initial number of EVs that can be accommodated in the DS under fully controlled charging scenario is calculated as follows,

$$\min W_j = \max \left(\sum_{m=1}^{N^{c,min}} W_{j,m}^{ev} \right), \quad m = 1, 2, \dots, N^{c,min}, \quad (4.4)$$

where $N^{c,min}$ is the minimum number of EVs under fully controlled charging scenario and $W_{j,m}^{ev}$ is the required energy to charge m^{th} EV on j^{th} day. The $W_{j,m}^{ev}$ is calculated as follows,

$$W_{j,m}^{ev} = D_{j,m} \times W_m^{ev}, \quad (4.5)$$

where $D_{j,m}$ is the travel distance by the m^{th} EV on j^{th} day and W_m^{ev} is the required energy to travel each mile by the m^{th} EV.

The PDF of daily travel distance by conventional cars is used to sample the daily travel distance. The PDF for daily travel distance is shown in Figure 9, which is developed using the survey data provided in [70].

In the next step, number of EVs is updated using the following stopping criterion.

$$\min(W_j - \sum_{m=1}^{N^c} W_{j,m}^{ev}) \approx \epsilon, \quad m = 1, 2, \dots, N^c, \quad (4.6)$$

where N^c is the number of EVs under the fully controlled charging scenario.

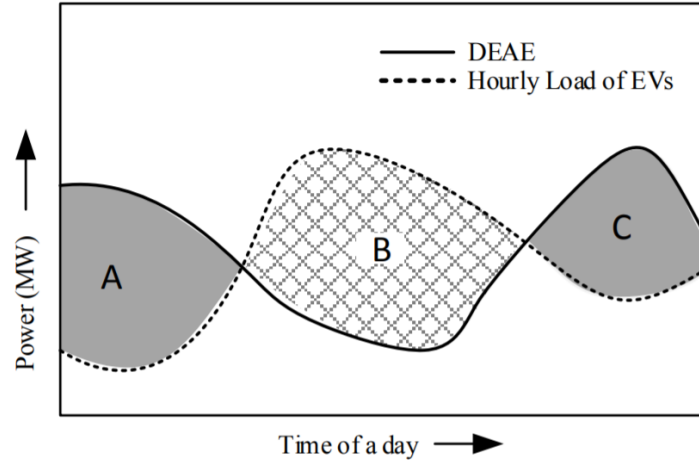


Figure 10. Relation between HEAP and load profile of EVs.

The final number of EVs calculated using (4.6) is used to determine the maximum hosting capacity of EVs in the DS under the fully controlled charging scenario. A typical relationship between the DEAE and demand profile of EVs is shown in Figure 10.

Under fully controlled charging, the area under the DEAE curve has to be equal to the area under the curve of load profile for EVs to accommodate the EVs with existing resources. Also, the amount of EV load that is represented by the area B in Figure 10 should be shifted to areas A and C under fully controlled charging.

4.2 Construction of Load Profiles for EVs and Calculation of HEAP

In the proposed approach, calculate hourly load demand to charge EVs and calculation of the HEAP are two important factors to calculate the maximum hosting capacity of a DS to EVs. The procedure to construct load profiles for EVs and calculate the HEAP is as follows.

4.2.1 Hourly Load Demand to Charge EVs

The procedure to calculate hourly load demand to charge EVs based on daily required energy, parking duration, and charging duration is described as follows.

4.2.1.1 Calculation of Parking Duration of EVs

Parking duration of each EV is an important factor to calculate hourly load demand to charge EVs. The parking duration at home and public charging stations are calculated as follows,

$$H_j = HA_j - HD_j, \quad (4.7)$$

where HA_j is the arrival time at a home charging station on the j^{th} day, HD_j is the departure time from a home charging station on the j^{th} day, and H_j is the parking duration at a home charging station on the j^{th} day of an EV, respectively.

$$P_j = PA_j - PD_j, \quad (4.8)$$

where PA_j is the arrival time at a home charging station on the j^{th} day, PD_j is the departure time from a home charging station on the j^{th} day, and P_j is the parking duration at a home charging station on the j^{th} day of an EV, respectively.

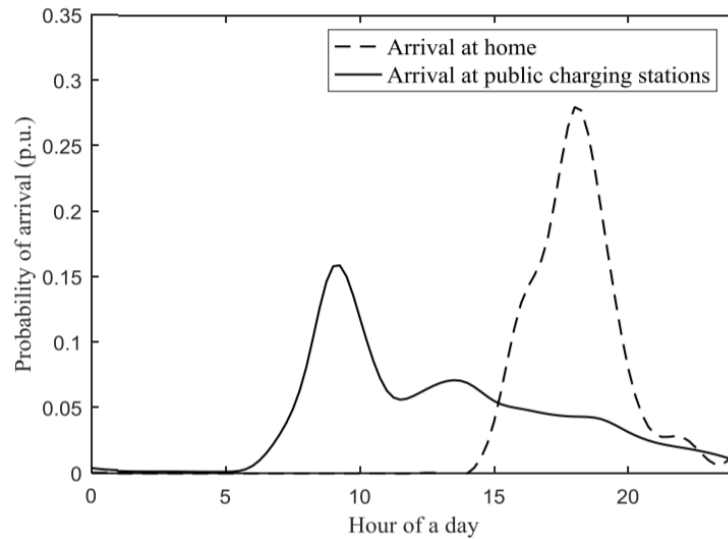


Figure 11. Probability distribution function of arrival time of EVs.

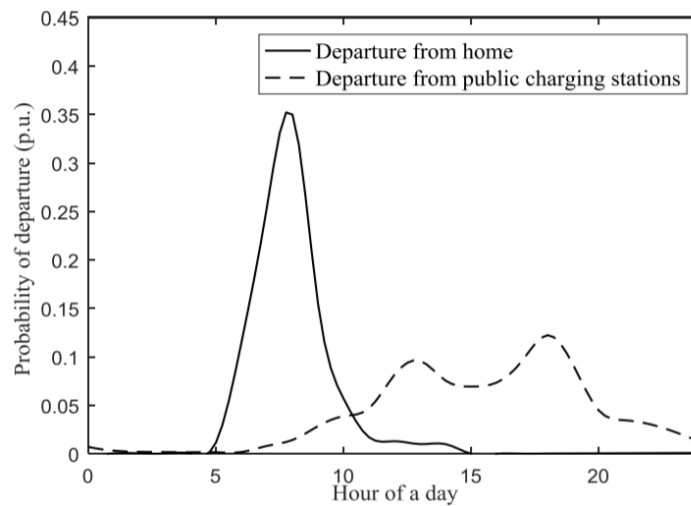


Figure 12. Probability distribution function of departure time of EVs.

The daily arrival and departure times of EVs change dynamically due to the behavior and preference of drivers. This dynamic change is captured by sampling the arrival and departure times

of EVs using the PDFs of departure and arrival times of conventional cars. The PDFs for arrival and departure times of EVs at home are developed using the survey data provided in [70], [71]. The PDFs for arrival and departure times of EVs at public charging stations are developed based on the data collected from [72]. The PDFs are shown in Figure 11 and Figure 12, respectively.

4.2.1.2 Calculation of Charging Duration of EVs

The calculation of required charging duration at each day is another important factor to construct load profiles for EVs. The charging duration at home and public stations are calculated using (4.9) and (4.10), which are derived using (4.5).

$$H_{j,m} = \frac{f_m^H \times W_{j,m}^{ev}}{R^h}, \quad (4.9)$$

where f_m^H is the fraction of required energy to charge the m^{th} EV at a home charging station on the j^{th} day, $CH_{j,m}$ is the charging duration at a home charging station of the m^{th} EV on the j^{th} day, and R^h is the charging rate at home charging stations.

$$CP_{j,m} = \frac{f_m^P \times W_{j,m}^{ev}}{R^p}, \quad (4.10)$$

where f_m^P is the fraction of required energy to charge the m^{th} EV at a public charging station on the j^{th} day, $CP_{j,m}$ is the charging duration at a public charging station of the m^{th} EV on the j^{th} day, and R^p is the charging rate at public charging stations.

4.2.1.3 Construction of Load Profiles for EVs

It is assumed that EV owners immediately plug in their vehicles after arrival and provide inputs about their departure time and required energy. After calculating the parking and charging duration, if the required charging time is larger than or equal to the parking duration, then the charging happens during the entire parking duration, which is expressed as follows,

$$\begin{aligned}
CH_{j,m} &\geq H_{j,m}, \\
CP_{j,m} &\geq P_{j,m},
\end{aligned}
\tag{4.11}$$

where $H_{j,m}$ is the parking duration at home charging stations of the m^{th} EV on the j^{th} day and $P_{j,m}$ is the parking duration at public charging stations of the m^{th} EV on the j^{th} day.

On the other hand, if the required charging time is less than the parking duration, then the charging happens during the entire charging duration, which is expressed as follows,

$$\begin{aligned}
CH_{j,m} &< H_{j,m}, \\
CP_{j,m} &< P_{j,m},
\end{aligned}
\tag{4.12}$$

For the conditions described in (4.11), hourly demand at home and public charging stations are calculated as follows,

$$P_{i,j,m}^H = \begin{cases} R^h, & i = HA_{j,m}, HA_{j,m} + 1, \dots, HA_{j,m} + H_{j,m}, \\ 0, & \text{Otherwise} \end{cases}
\tag{4.13}$$

where $P_{i,j,m}^H$ is the hourly demand at a home charging station for m^{th} EV on the j^{th} day.

$$P_{i,j,m}^p = \begin{cases} R^p, & i = PA_{j,m}, PA_{j,m} + 1, \dots, PA_{j,m} + P_{j,m}, \\ 0, & \text{Otherwise} \end{cases}
\tag{4.14}$$

where $P_{i,j,m}^p$ is the hourly demand at a public charging station for m^{th} EV on the j^{th} day.

The hourly demand at home and public charging stations for the conditions described in (4.12) are calculated as follows,

$$P_{i,j,m}^H = \begin{cases} R^h, & i = HA_{j,m}, HA_{j,m} + 1, \dots, HA_{j,m} + CH_{j,m}, \\ 0, & \text{Otherwise} \end{cases}
\tag{4.15}$$

$$P_{i,j,m}^p = \begin{cases} R^p, & i = PA_{j,m}, PA_{j,m} + 1, \dots, PA_{j,m} + CP_{j,m}, \\ 0, & \text{Otherwise} \end{cases}
\tag{4.16}$$

After calculating hourly demand for all home and public charging stations, the load profile for EVs at a given node is constructed using the expression provided in (4.17), which is derived using (4.13), (4.14), (4.15), and (4.16).

$$P_{i,j,k}^{ev} = \sum_{m=1}^{N_k^u} P_{i,j,m}^H + P_{i,j,m}^P, \quad (4.17)$$

where $P_{i,j,m}^H$ and $P_{i,j,m}^P$ are the calculated hourly demand to charge EVs at home and public stations at bus k , respectively.

4.2.2 Calculation of HEAP

The procedure to calculate the HEAP of a DS using the maximum hourly loading capacities and hourly loads is described as follows.

4.2.2.1 Evaluation of the maximum loading capacity

The maximum loading capacities at the selected nodes for EV charging are calculated by gradually increasing the spot loads until voltage limits are violated. We consider the voltage limits for DSs based on the recommendation provided by American National Standards Institute (DS voltage have to be maintained within 5% of base voltage) [73]. The OpenDSS and MATLAB are used to perform power flow to check voltage limits. The maximum amount of spot loads that can be incorporated at each of the selected nodes is considered as the maximum loading capacities.

4.2.2.2 Construction of hourly load profile

Existing load profiles at each of the selected nodes are also important factors to determine the HEAP. The existing load profiles at the selected nodes are constructed based on the developed load profile for DSs by the Electric Power Research Institute (EPRI) [74]. In [74], hourly data of load demand are presented in percentages of the annual peak (spot) load which are combined to construct the load profile for a year. The peak load of a node is combined with the hourly data of load demand to construct the load profile for a year of the respective node.

4.2.2.3 Calculation of HEAP

Finally, the HEAP is calculated by subtracting actual hourly loads from the maximum loading capacity at each node. The HEAP of a node is calculated as follows,

$$P_{i,j,k} = P_{i,j,k}^{\max} - L_{i,j,k}, \quad (4.18)$$

where $P_{i,j,k}^{\max}$ and $L_{i,j,k}$ are the maximum loading capacity and actual load demand of node k at the i^{th} hour on the j^{th} day, respectively, and $P_{i,j,k}$ is the HEAP of the k^{th} node at the i^{th} hour on the j^{th} day.

4.3 Case Studies

The proposed method to calculate the maximum hosting capacity of DSs to EVs is applied on the IEEE 123-node test feeder. The total amount of spot load of the IEEE 123-node test feeder is 3490 kW. The detailed data are given in [75]. Typically, three types of chargers are available [76]: Level 1: charging rate of 1 kW/h, Level 2: charging rate of 6 kW/h, and Level 3: charging rate of 50 kW/h. However, Level 3 is very expensive and frequent uses of fast chargers reduces the lifetime of batteries. Therefore, Level 1 is used at most of home charging stations and Level 2 is used at most of public charging stations. It is assumed that average charging rates at home and public charging stations are 3 kW/h and 5 kW/h respectively. We calculate the maximum hosting capacity of the IEEE 123-node test feeder under both the uncontrolled and controlled charging scenarios for two types of node selection as follows,

- EV loads are distributed at all load nodes with the same percentage of their existing spot loads.
- EV loads are distributed in two different regions (i.e., region1: residential and urban area and region2: residential and industrial area).

EVs are distributed in region1 and region2 based on the given ratio (the ratio of vehicles per home in region1 is 0.6 and the ratio of vehicles per home in region2 is 0.45) in [32]. The required energy to travel each mile by different types of vehicles is as follow: sedan 0.3225 kWh/mile, mid-sedan 0.3605 kWh/mile, mid-SUV 0.4375 kWh/mile, and full-SUV 0.5075 kWh/mile [60]. We have assumed that the required energy—average of the above-mentioned energy consumption per mile—to travel each mile by an EV is 0.407 kWh/mile. The percentages of EVs at residential and public stations are assumed 40% and 60%, respectively as provided in [5].

The HEAP of the IEEE 123-node test feeder is calculated using the procedure described in Section 4.2. The daily travel distance, arrival time, and departure time of the EVs are sampled using the PDFs described in Figure 10, Figure 11, and Figure 12 respectively. The daily electricity demand, parking duration, and minimum charging duration of the EVs are calculated using (4.5), (4.7), (4.8), (4.9), and (4.10) respectively. Four different case studies are carried out to demonstrate the proposed method, which are explained as follows.

4.3.1 Case I: Maximum Hosting Capacity for All Nodes under Uncontrolled Charging

In this case, the maximum hosting capacity of the IEEE 123-node test feeder to EVs is calculated under uncontrolled charging scenario for all load nodes. The EV loads are distributed with the same percentage of spot loads at each node. The HEAP is calculated for each load node. The initial number of EVs that can be incorporated at each node with existing resources under this scenario is calculated using (4.1). The hourly load demand to charge EVs is calculated using the procedure described in Section 4.2. The maximum hosting capacities for all the nodes under the uncontrolled charging scenario are calculated using (4.2). Finally, the maximum hosting capacity of the IEEE-123 test feeder under this scenario is calculated by taking the summation of the maximum hosting capacities of EVs of all nodes. The results of this case are given in the second row of Table 8.

Table 8. Maximum Hosting Capacity for All the Nodes

Case I	Number of Cars	Peak Load (kW)
	438	595
Case II	Number of Cars	Peak Daily Energy (kWh)
	1510	13015

4.3.2 Case II: Maximum Hosting Capacity for All Nodes under Fully Controlled Charging Scenario

In this case, the maximum hosting capacity of the IEEE 123-node test feeder to EVs is calculated for all load nodes under fully controlled charging scenario. Same as Case I, EVs are distributed with the same percentage of spot loads at each node in this case. The calculated HEAP for each load node of the IEEE 123-node test feeder in Case I is used for this case. The DEAE of the IEEE 123-node test feeder is calculated using (4.3). The initial number of EVs for this scenario is calculated using (4.4). The maximum hosting capacity of the IEEE 123-node test feeder to EVs under this scenario is calculated using (4.6). The results of this case study are given in the fourth row of Table 8.

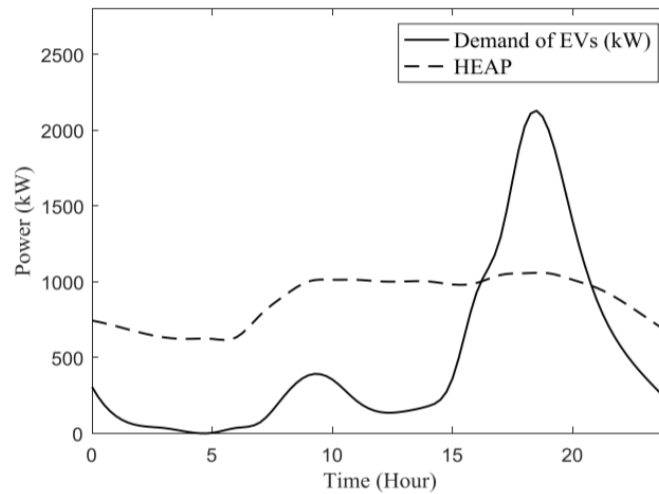


Figure 13. Relation between HEAP of the IEEE 123-node test feeder and load demand of EVs.

Figure 13 shows the relationship between the HEAP of the IEEE 123-node test feeder and load demand of EVs in a typical day under this scenario.

4.3.3 Case III: Maximum Hosting Capacity for Selected Nodes under Uncontrolled Charging

In this case, the maximum hosting capacity in two different regions of the IEEE 123-node test feeder to EVs is calculated under uncontrolled charging scenario. The selected regions of the IEEE 123-node test feeder for this case is shown in Figure 14.

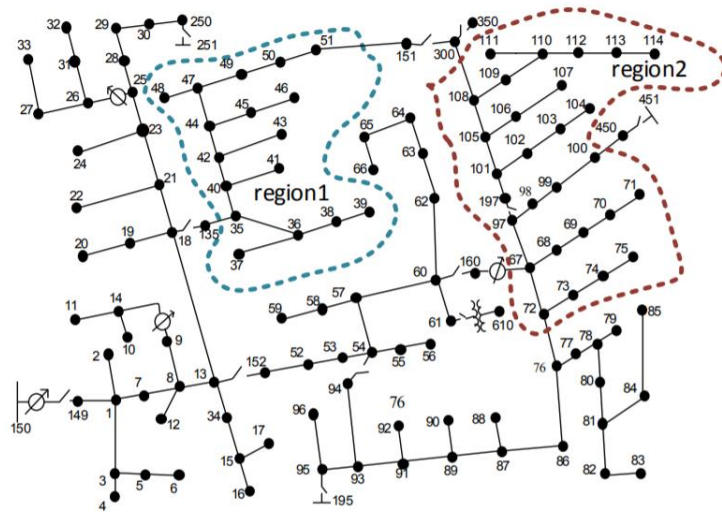


Figure 14. Selected regions of the IEEE 123-node test feeder for Case III and Case IV.

The penetration level of EV loads in region1 is considered as 1.3 times of the penetration level in region2 based on the given ratio in [31]. The EV loads at different nodes in both region1 and region2 are distributed with the same percentage of their existing spot loads. The HEAP of the IEEE 123-node test feeder is calculated for the selected nodes in region1 and region2. Same as Case I, (4.1) is used to calculate the initial number of EVs and the procedure described in Section 4.2.1 is used to hourly load demand to charge EVs at the selected nodes. The maximum hosting capacities for the selected nodes under this scenario are calculated using (4.2). The summation of the maximum hosting capacities of the selected nodes represents the maximum hosting capacity of

the IEEE 123-node test feeder under this scenario. The results of this case are given in the second row of Table 9.

Table 9. Maximum Hosting Capacity for the Selected Nodes

	Region	Number of Cars	Peak Load (kW)
Case I	region1	106	188
	region2	124	205
	Total	230	393
Case II		Number of Cars	Peak Daily Energy (kWh)
	region1	423	3811
	region2	489	4455
	Total	912	8266

4.3.4 Case IV: Maximum Hosting Capacity for Selected Nodes under Fully Controlled Charging

In this case, the maximum hosting capacity in two different regions of the IEEE 123-node test feeder is calculated under fully controlled charging. The calculated HEAP in Case III is used to calculate the hosting capacity. Same as Case II (4.3), (4.4), and (4.6) are used to calculate the DEAE, initial number, and the maximum hosting capacity of EVs in the IEEE 123-node test feeder respectively under this scenario. The results of this case are given in the fourth row of Table 9.

4.4 Results and Discussion

From Table 8, it can be seen that the maximum hosting capacity of the IEEE 123-node test feeder to EVs under Case I (uncontrolled charging for all buses) and Case II (controlled charging for all buses) are 438 cars (595 kW) and 1510 cars (13015 kWh) respectively. Table 8 also shows that the hosting capacity in terms of number of EVs under Case II is 244.75% larger than Case I.

From Table 9, we can see that the hosting capacity in terms of the number of EVs in region1 under Case IV (controlled charging scenario) is 299% larger than Case III (uncontrolled charging scenario). Also, from Table 9, it can be seen that the hosting capacity in terms of number of EVs in region2 under Case IV is 294.35% larger than Case III. Moreover, Table 9 shows that the total

maximum hosting capacity in terms of the number of EVs under Case IV is 296.52% larger than Case III. From Table 9, we can also see that the hosting capacity in region2 under both the Case III and Case IV is larger than region1. This happens because the penetration level of EVs as well as the number of nodes in region2 is high compared to region1.

From Table 8 and Table 9, it can be seen that the maximum hosting capacity of EVs under fully controlled charging scenario (case II and case IV) is high compared to uncontrolled charging scenario (case I and case III). This is not a surprise because under fully controlled charging scenario, the maximum DEAE is used to charge the EVs which is not possible under uncontrolled charging scenario due to the charging preferences of the EVs' owners. From Table 8 and Table 9, we can also see that the maximum hosting capacity for selection of all nodes is high compared to the selection for some specific nodes. The maximum hosting capacity of EVs in case I and case II are 90.43% and 65.57% high compared to case III and case IV respectively. This happens because the calculated HEAE while maintaining the network constraints in case I is high compared to case III.

From the above case studies, it can be concluded that the proposed approach is effective in calculating the maximum hosting capacity of DSs to EVs under both the fully controlled and uncontrolled charging scenarios. This will be beneficial for the system operators and planners to plan for the deployment of charging stations at different locations of DSs. Also, the proposed approach has potential to estimate the required amount of resources to handle the demand increase due to penetration of EVs.

Chapter 5. A Method to Evaluate the Maximum Hosting Capacity of Power Systems to EVs

The proposed smart charging/discharging to calculate the expected maximum hosting capacity (EMHC) of power systems to EVs is described in this chapter. The proposed smart charging/discharging strategy is developed based on the daily energy demand and parking duration of EVs. Probability distribution functions (PDFs) of arrival and departure times are used to calculate the parking duration. The daily energy demand is calculated based on the energy required to travel each mile and PDF of daily travel distances. An optimization problem to maximize the HC is formulated based on network constraints (e.g., voltage limits, generation and line capacities, and loads), charging/discharging limits of smart chargers, and daily energy demand and parking durations of EVs. To relieve the computational burden, a linearized AC power flow model is leveraged to capture the nonlinear characteristics of network constraints. The EMHC is calculated for charging stations at both homes and workplaces using MC simulation. The proposed method is demonstrated on the modified IEEE 33-bus system.

5.1 Smart Charging/Discharging Strategy to Maximize the Hosting Capacity

In the proposed smart charging/discharging strategy, the rates are controlled by a central controller based on network constraints and provided inputs (e.g., departure time, next travel distance, and type of vehicle) to smart chargers. This section illustrates the overall system architecture for the proposed framework and describes the formulation of the optimization problem to maximize the HC of power systems to EVs.

5.1.1 System Architecture

We introduce a smart charging/discharging architecture which is composed of smart chargers, a communication layer, and a central controller. The smart chargers have input panels in which EV

owners provide their departure time, next travel distance, and type of vehicle. Also, it is assumed that the EV owners plug in their vehicles immediately after arrival. The smart chargers can read arrival times and initial SOCs of EVs and calculate parking duration by taking the difference between arrival and departure times. Different types of EVs (e.g., sedan, mid-sedan, SUV, and mid-SUV) have different energy consumption per mile. The smart chargers are also capable of determining the energy required to travel each mile based on vehicle type. Moreover, the smart chargers calculate the required charging energy as follows,

$$E = D \times \eta_E, \quad (5.1)$$

where D is the expected travel distance by an EV, η_E is the required energy for the EV to travel each mile, and E is the total energy demand of the EV.

The departure time, calculated parking duration, and energy demand are fed as inputs to the central controller by smart chargers using a communication channel. Also, the central controller gathers network information such as voltage levels, hourly generation capacities, line capacities, and loads. This information is used to control charging/discharging rates without violating network constraints. Each day of a year is divided into 24 time-intervals to control charging/discharging rates. However, the time-intervals can be adjusted based on the requirements. The total number of intervals that are suitable for charging and discharging depends on the arrival and departure times. The charging and discharging of an EV cannot occur simultaneously within a time interval and charging/discharging power during a time interval remain unchanged. Figure 15 shows an example for the timeline of charging and discharging periods.

Figure 15 shows that the arrival time, t_a^n , departure time, t_f^n , and parking duration of the n^{th} EV are 8, 19, and 11 respectively. Thus, the total number of time intervals for charging/discharging is

11. The initial and desired final energy levels are E_{ini}^n and E_{final}^n , respectively. The value of E_{final}^n must be less than or equal to the maximum energy limit of the EV battery.

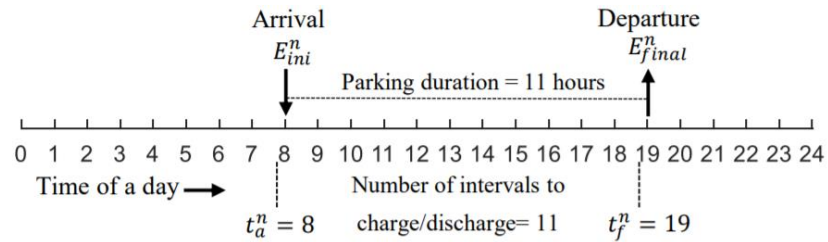


Figure 15. Charging/discharging period.

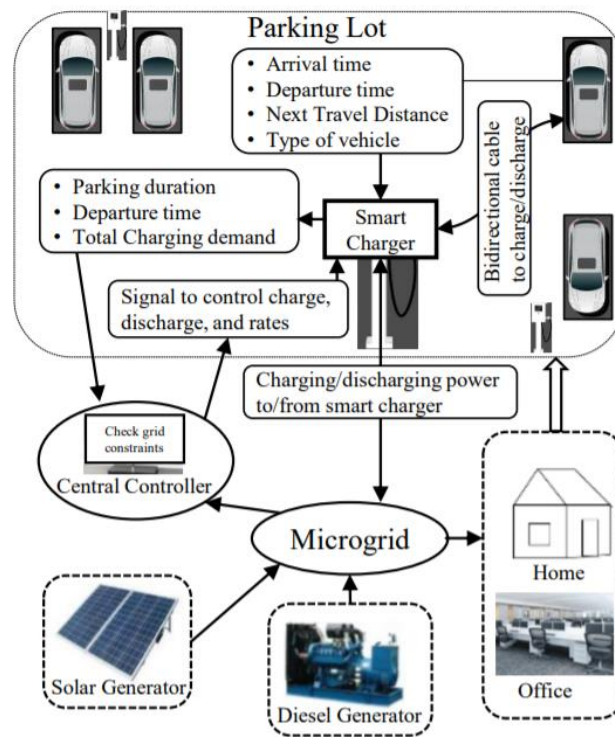


Figure 16. Smart charging/discharging architecture for a microgrid.

If the network has additional capacity after satisfying its existing demand (without EV), then the EV is charged. On the other hand, if the network fails to satisfy its existing demand (without EV), then the EV is discharged. The charging/discharging rate during an entire interval remains constant which is determined by the optimization model described in Section 5.1.2 and Section 5.1.3, respectively. This procedure is repeated for all possible time intervals. Also, in the proposed smart

charging/discharging strategy, it is ensured that the EV battery will achieve the desired final energy level at the time of departure. A schematic diagram of the proposed smart charging/discharging strategy for a microgrid is shown in Figure 16.

5.1.2 Objective Function

In the proposed smart charging/discharging strategy, the objective is to maximize the number of EVs. The objective function to maximize the HC of power systems to EVs, is expressed as follows,

$$H^{ev,max} = \max\left(\sum_{n \in N} E^{n,d}\right), \quad \forall d \quad (5.2)$$

where d is the index for days of a year, running from 1 to 365, N is the set for all candidate EVs to be charged/discharged. $E^{n,d}$ is the required energy of the n^{th} EV on the d^{th} day, and $H^{ev,max}$ is the maximum HC of a power system to EVs.

The LP follows same procedure described in Chapter 3 section 3.2 to dispatch power from generators to maximize the HC.

5.1.3 Network Constraints

We leverage the linearized AC power flow model proposed in [77] to describe the network constraints.

Power balance equations,

$$\begin{aligned} B^{t,d}\theta^{t,d} - G^{t,d}V^{t,d} + P_g^{t,d} + P_{dis}^{t,d} &= P_{ch}^{t,d} + P_l^{t,d} & \forall t, \forall d \\ G^{t,d}\theta^{t,d} + B^{t,d}V^{t,d} + Q_g^{t,d} &= Q_l^{t,d} & \forall t, \forall d \end{aligned} \quad (5.3)$$

where t is the index for hours of a day, running from 1 to 24; $B^{t,d}$ and $G^{t,d}$ are the modified susceptance and conductance matrices at time t on day d , respectively; $B^{t,d}$ and $G^{t,d}$ are the

conventional susceptance and conductance matrices at time t on day d , respectively; $\theta^{t,d}$ and $V^{t,d}$ are the vectors of nodal voltage angles and magnitudes at time t on day d , respectively; $P_g^{t,d}$ and $Q_g^{t,d}$ are the vectors of real and reactive power generations at time t on day d , respectively; $P_{dis}^{t,d}$ and $P_{ch}^{t,d}$ are the vectors for discharging and charging power of EVs at time t on day d , respectively; and $P_l^{t,d}$ and $Q_l^{t,d}$ are the vectors of real and reactive power demand (without EVs) at time t on day d , respectively.

EV energy level at each hour for charging/discharging,

$$E^{n,t,d} + \frac{1}{\eta_{dis}} P_{dis}^{n,t,d} \Delta t - \eta_{ch} P_{ch}^{n,t,d} \Delta t = E^{n,t-1}, \quad \forall t, \forall d \quad (5.4)$$

where Δt is the duration of each time interval; η_{ch} and η_{dis} are the efficiency coefficients of charging and discharging, respectively; $P_{dis}^{n,t,d}$ and $P_{ch}^{n,t,d}$ are the discharging and charging power of n^{th} EV at time interval t on day d , respectively; and $E^{n,t,d}$ and $E^{n,t-1}$ are the energy level of n^{th} EV at time $t - 1$ and t on day d , respectively.

Daily EV energy demand constraints,

$$\sum_{t=t_a^{n,d}}^{t_f^{n,d}} \left(\frac{1}{\eta_{dis}} P_{dis}^{n,t,d} \Delta t - \eta_{ch} P_{ch}^{n,t,d} \Delta t \right) \geq E^{n,d} \quad \forall d \quad (5.5)$$

$$E^{n,min} \leq E^{n,d} \leq E^{n,max} \quad \forall d$$

where $t_a^{n,d}$ and $t_f^{n,d}$ are the arrival and departure times of the n^{th} EV on the d^{th} day, respectively; $E^{n,min}$ and $E^{n,max}$ are the minimum and maximum battery capacity of the n^{th} EV, respectively.

Charging/discharging constraints,

$$0 \leq P_{ch}^{n,t,d} \leq P_{ch}^{max} \quad \forall d, \forall t \quad (5.6)$$

$$0 \leq P_{dis}^{n,t,d} \leq P_{dis}^{max} \quad \forall d, \forall t$$

where P_{ch}^{max} and P_{dis}^{max} are the maximum charging and discharging rates of smart chargers, respectively.

Real and reactive power generation constraints,

$$\begin{aligned} P_g^{min} \leq P_g^{t,d} \leq P_g^{max} & \quad \forall d, \forall t \\ Q_g^{min} \leq Q_g^{t,d} \leq Q_g^{max} & \quad \forall d, \forall t \end{aligned} \quad (5.7)$$

where P_g^{min} and P_g^{max} are the vectors of minimum and maximum real power generation, respectively; and Q_g^{min} and Q_g^{max} are the vectors of minimum and maximum reactive power generation, respectively.

Feeder capacity constraints,

$$\begin{aligned} S_F^{t,d} \leq S_F^{max} & \quad \forall d, \forall t \\ S_R^{t,d} \leq S_R^{max} & \quad \forall d, \forall t \end{aligned} \quad (5.8)$$

where S_F^{max} and S_R^{max} are the vectors of maximum forward and reverse feeder flow capacities, respectively; and $S_F^{t,d}$ and $S_R^{t,d}$ are the vectors of forward and reverse feeder flows at time t on day d , respectively.

Voltage constraints,

$$V^{min} \leq V^{t,d} \leq V^{max} \quad \forall d, \forall t \quad (5.9)$$

where V^{min} and V^{max} are the vectors of minimum and maximum bus voltage magnitudes, respectively.

Angle constraints,

$$\pi \leq \theta^{t,d} \leq \pi \quad \forall d, \forall t \quad (5.10)$$

5.2 Calculation of the EMHC

The proposed algorithm to calculate the EMHC of power systems to EVs follows an iterative process, which starts with computing the maximum HC at each day of a year. To determine the HC at each day, we assume that there are enough number of smart chargers deployed at both homes and workplaces to plug in EVs immediately after arrival.

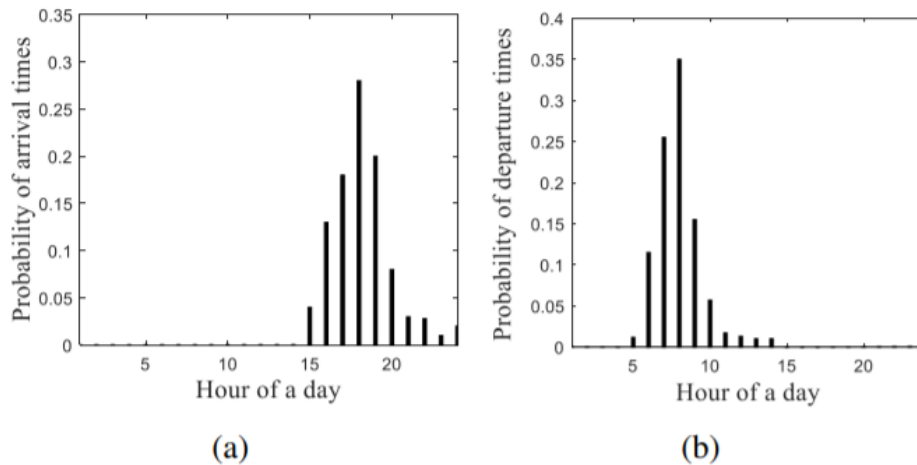


Figure 17. PDFs of (a) arrival times at homes and (b) departure times from homes.

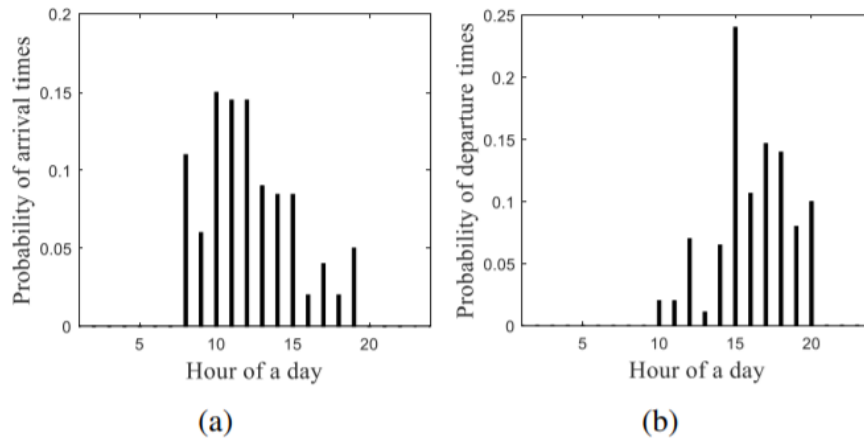


Figure 18. PDFs of (a) arrival times at workplaces and (b) departure times from workplaces.

Then, the arrival times, departure times, and next travel distances on the first day of a year for an initial number of EVs for both homes and workplaces are determined. The arrival and departure

times are determined based on the PDFs provided in Figure 17 and Figure 18. The PDFs for arrival and departure times at homes are developed using the survey data for conventional cars provided in [70], [71]. The PDFs for arrival and departure times at workplaces are developed using the survey data [78]. The next travel distances are calculated based on the PDF of daily travel distances for conventional cars shown in Figure 19, which is developed using the survey data provided in [70].

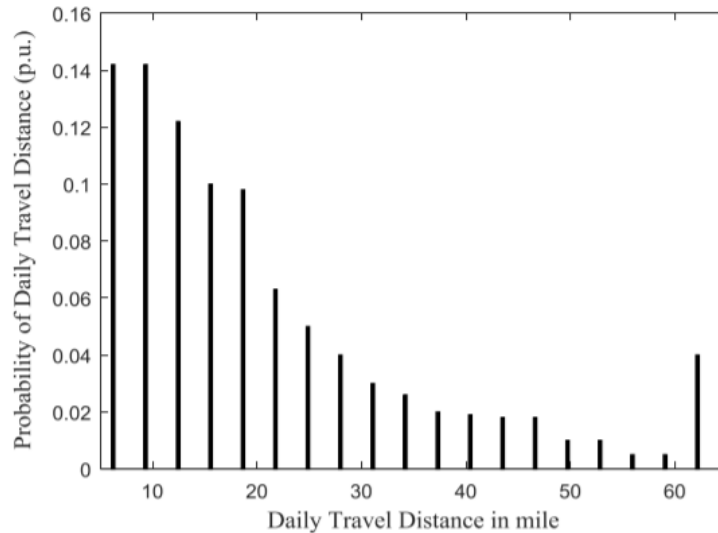


Figure 19. PDF of daily travel distances of EVs.

In the next step, parking duration, required charging energy, and initial SOC level for each EV are determined. The parking duration is calculated by taking the difference between arrival and departure times. The required charging energy is calculated using (5.1). The initial SOC level is determined randomly between 10% to 30% of the maximum battery capacity. The hourly demand for existing loads (without EVs) is calculated using data tables provided in [59].

Then, the optimization problem described in Section 5.1 is solved by using linear programming solver. The number of EVs is updated until the obtained solution for the optimization problem is infeasible. The final number of EVs is the maximum HC on first day of the year. The above procedure is repeated 365 times to calculate the maximum HC for each day of a year. A flowchart to calculate the maximum HC at each day is provided in Figure 20.

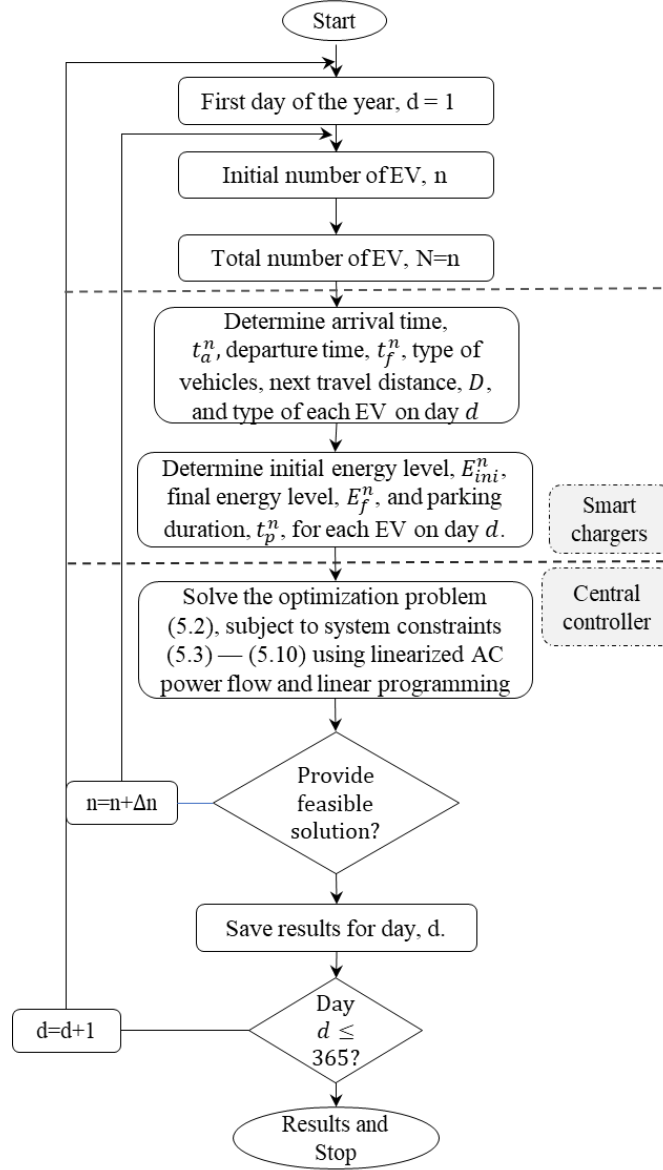


Figure 20. Algorithm to calculate the daily maximum HC.

To calculate the EMHC capacity, the above procedure is repeated for N_y years. Then, the expected maximum hosting capacity at each day of a year is calculated as follows,

$$\xi_m^d = \frac{1}{N_y} \sum_{y=1}^{N_y} \xi_y^d \quad (5.11)$$

where N_y is the number of simulated years; ξ_y^d is the maximum HC of power systems to EVs on the d^{th} day of y^{th} year; and ξ_m^d is the EMHC on the d^{th} day of a year.

Finally, the EMHC of the power system to EVs is calculated by taking the minimum value of daily EMHC. Following the stopping criterion provided in [79] to evaluate power system reliability using the MC simulation, we introduce a stopping criterion based on the coefficient of variance of EMHC as follows,

$$\sigma = \frac{\sqrt{|V(\xi_m)|}}{\xi_m} \quad (5.12)$$

where ξ_m is the EMHC of power systems to EVs; $V(\xi_m)$ is the variance of the EMHC of power systems to EVs; and σ is the coefficient of variance. Typically, the value for σ to calculate the reliability indices is ≤ 0.025 , which is adopted for the proposed algorithm.

The variance of EMHC, $V(\xi_m)$, is calculated as follows,

$$V(\xi_m) = \frac{1}{N_y}(\xi_m - \xi_m^2) \quad (5.13)$$

5.3 Numerical Examples

To validate the proposed method, simulations are carried out on the modified IEEE 33-bus distribution system. The IEEE 33- bus test system is characterized by 33 nodes, 32 branches, 5 tie-lines, 3 laterals, and operating voltage of 12.66 kV [80]. In the modified IEEE 33-bus system, locations of the generating units and ratings of the photovoltaic (PV) units are selected based on the provided modification in [81]. The total peak demand of the modified IEEE 33-bus test system is 2972 kW [81]. The limits of hourly generation amount of the PV units are calculated using PVWatts calculator developed by the National Renewable Energy Laboratory [82].

A specific node of a distribution system may have only home charging stations or only workplace charging stations or both types of charging stations. In this dissertation, we consider that a node contains either only home charging stations or only workplace charging stations. Also, the charging stations can be installed in all or several selected nodes of distribution systems. We randomly select 10 nodes to install charging stations. The locations of the generators and charging

stations in the modified IEEE 33-bus distribution system are shown in Figure 21. The ratings of all the generating units are given in Table 10.

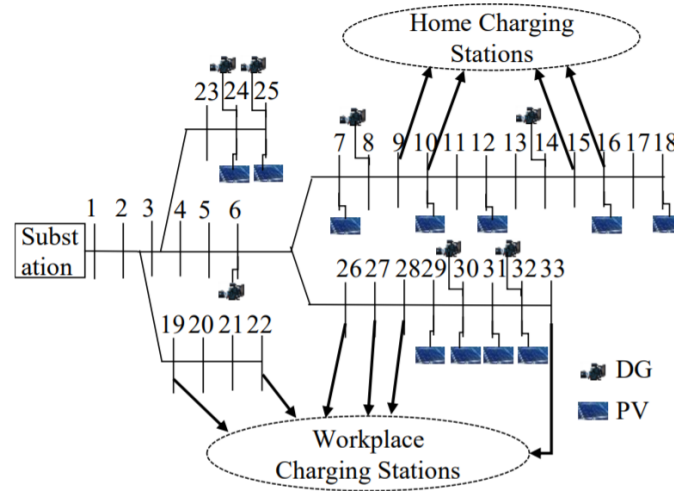


Figure 21. Modified IEEE 33-bus.

Table 10. Ratings of Generators of the Modified IEEE 33-Bus

Types of Generators	Locations (Node No.)	Rating (kW)	Types of Generators	Locations (Node No.)	Rating (kW)
DG	6	1200	PV	12	50
DG	8	400	PV	16	50
DG	14	400	PV	18	100
DG	24	800	PV	24	300
DG	25	800	PV	25	250
DG	30	400	PV	29	100
DG	32	400	PV	30	200
PV	7	100	PV	31	150
PV	10	100	PV	32	50

Typically, two types of chargers: Level 1: charging rate of 1 kW/h and Level 2: charging rate of 6 kW/h are used at home and workplaces [76]. Therefore, we assume that charging/discharging rates of smart chargers vary from 0–6 kW/h.

The U.S. Department of Energy is welcoming employers to sign the pledge for workplace charging challenges to increase the percentage of charging at workplaces [83]. Also, the employers usually provide free charging to their employees to increase employee satisfaction. Therefore, we

consider that the employees fulfill their entire charging demand at workplaces. The employment rates in the United States at each month of 2019 varied between 60–61% [84]. Thus, the distribution of EVs between homes and workplaces are considered as 40% and 60%, respectively. The distribution ratios of EVs between nodes are same as the distribution ratios of existing loads. The EMHC at each day of a year is calculated using the algorithm described in Section 5.2. The voltage limits to calculate the EMHS are maintained within 5% of base voltage [73]. The value for σ is considered as 0.2. The energy consumption to travel each mile by various types of EVs are provided in [60], which are as follow: full-SUV 0.5075 kWh/mile, mid-SUV 0.4375 kWh/mile, mid-sedan 0.3605 kWh/mile and sedan 0.3225 kWh/mile. We assume an average (0.407 kWh/mile) of these energy consumptions per mile as the energy required to travel each mile by an EV. The required number of simulation years to achieve the convergence is 27 years. The calculated daily EMHC is shown in Figure 22.

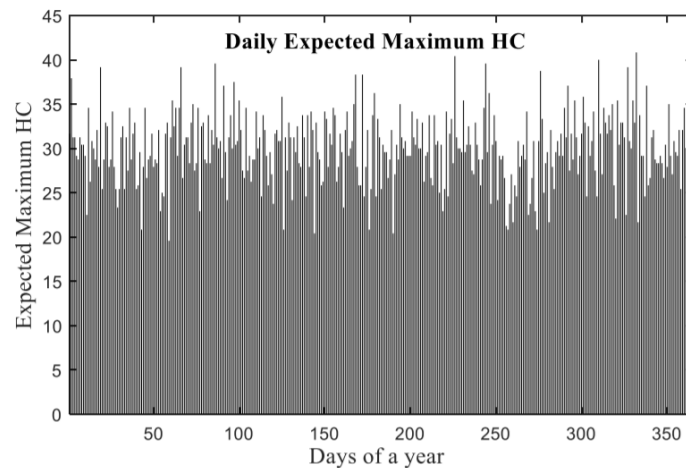


Figure 22. EMHC of the modified IEEE 33-bus for selected nodes.

From Figure 22, we can see that the calculated daily EMHC varies between 20–41 cars. Thus, the EMHC of the modified IEEE 33-Bus system is 20 cars. Therefore, it can be deduced that the power system planners can use the proposed method to calculate the EMHC of power systems to EVs for the allocation of resources.

Chapter 6. Demand Response-based Power System Reliability Enhancement

In this chapter, a novel demand response (DR) method based on interruptible/curtailable (I/C) loads has been developed and incorporated in the power system reliability evaluation. In deriving this model, economic incentives and penalties are both considered. Also, the mathematical model of I/C loads is developed based on demand-price elasticity and customer benefit. In this method, customers are categorized based on the amount of consumption in order to apply the I/C load programs. The proposed technique is demonstrated on the IEEE-RTS and reliability indices are calculated using MC simulation.

6.1 Modeling of Demand Response Considering Interruptible/Curtailable Loads

Shifting load demand from one hour to another is known as DR which can be represented as I/C loads. DR programs based on I/C loads have potential significant contributions to reduce the peak demand of power systems. The following sections presents the modeling of I/C load programs and describe the strategy of selecting participating consumers.

6.1.1 Interruptible/Curtailable Load Modeling Approach

Modeling of I/C loads starts with selecting the customers who can participate in I/C loads program. In general, the amount of I/C loads are much smaller than the total load. Therefore, small-scale consumers of electric power are usually not considered in I/C loads program. The typical minimum size of the customer eligible for I/C loads ranges from 200 kW to 3 MW depending on the size and circumstances of electricity markets [85]. Customers who are involved in I/C load programs must agree to curtail either a predetermined amount or a specified block of load [86]. Customers usually have to curtail the loads within 30–60 minutes after being acknowledged by the utility through advanced metering infrastructure (AMI) [85]. The degree of DR implementation depends on the acuity of the AMI in the power system [87]. The total number of interruption hours

is predetermined and all types of loads that are suitable for I/C programs are identified based on the procedure given in [85].

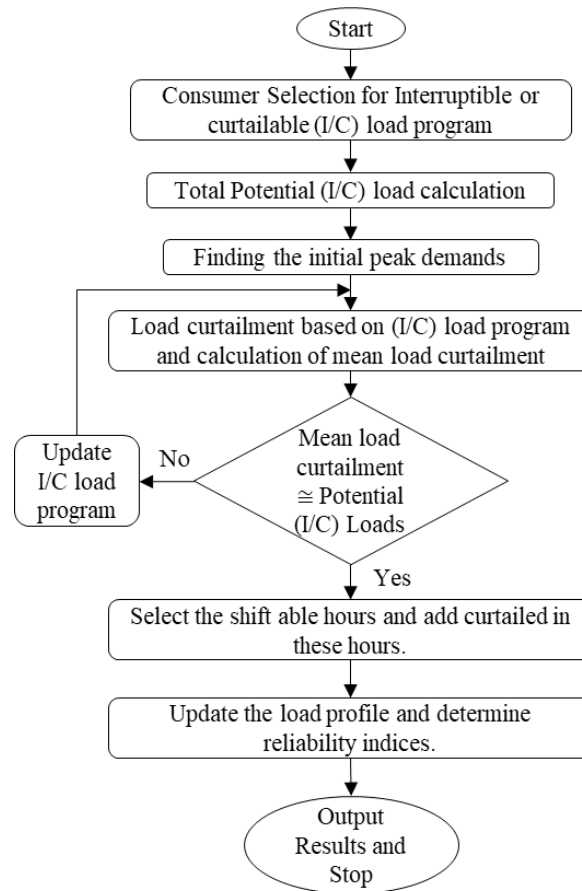


Figure 23. The Flowchart of the Interruptible/Curtailable Load Modeling.

In the next step, total potential amount of I/C loads are calculated as a percentage of peak load. After this point, loads are curtailed from peak load based on optimum amount of incentive and penalty. Incentive and penalty tariffs may vary for different electricity markets (e.g., in 2001, total incentive for I/C load programs was 7000 \$/MW month against the electricity price of 65 \$/MWh in California power market) [88]. If the curtailed load is close to the potential amount of I/C loads, the load profile is restructured by shifting the curtailed load to the off-peak hours. Finally, the algorithm ends after determining the reliability indices for the modified load profile. The modeling approach for I/C load is described in a flowchart as shown in Figure 23.

6.1.2 Interruptible/Curtailable Load Modeling Approach

In order to ensure the effective participation of the customers in the DR program, a suitable economic load model needs to be developed based on the change of customers' power consumption with the change of electricity prices, benefits, and penalties applied to the customers [85]. In general, the load demand of customers who participate in the DR programs is inversely proportional with the electricity price as shown in Figure 24 [89].

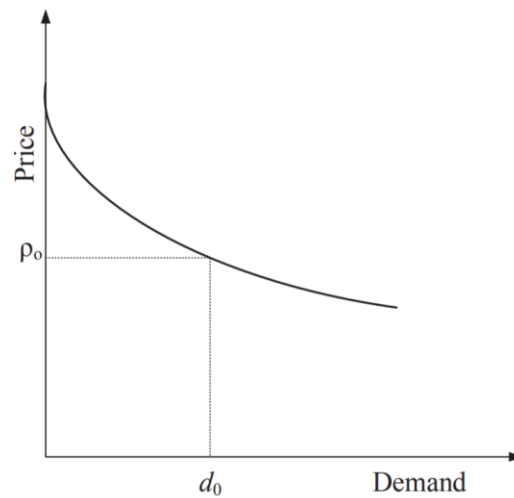


Figure 24. Typical Demand Price Elasticity.

Demand-price elasticity is defined as the ratio of rate of change of demand to the rate of change of price as follows [89].

$$\epsilon = \frac{\delta d/d_0}{\delta \rho/\rho_0} \quad (6.1)$$

where ϵ is the elasticity, d_0 is the demand at price ρ_0 for a given equilibrium point, and δd is the change of demand due to the change of price of $\delta \rho$.

Based on the allocation of loads at different time slots, electrical loads can be divided into two categories: single-and multi-period loads. Single period loads cannot be moved from one time slot to another (e.g., illuminating loads) and elasticity related to these loads are known as “self-

elasticity” [85]. On the other-hand, multi-period loads are movable from peak hours to off-peak or low hours and elasticity related to these loads are known as “cross-elasticity” [11]. The self-elasticity and cross-elasticity can be represented as follows [89]:

$$\epsilon(i, i) = \frac{\delta d(i)/d_0}{\delta \rho(i)/\rho_0} \quad (6.2)$$

$$\epsilon(i, j) = \frac{\delta d(i)/d_0}{\delta \rho(j)/\rho_0} \quad (6.3)$$

where $\delta d(i)$ and $\delta \rho(i)$ are the change of load and price at the i^{th} period respectively, $\delta \rho(j)$ is the price change at the j^{th} period, $\epsilon(i, i)$ is the self-elasticity, and $\epsilon(i, j)$ is the crosselasticity; the value of self-elasticity is always negative and the value of cross-elasticity is always positive [85], [89]. Based on self-elasticity and cross-elasticity, the single- and multi-period loads are modeled as follows.

In order to calculate the potential amount of I/C load of the system, the following equation is introduced.

$$L_{IC} = \sum_{k=1}^N L_{IC}(k) \quad (6.4)$$

where N denotes the total number of I/C loads, $L_{IC}(k)$ is the vector of power consumption of the I/C loads, and L_{IC} represents the total amount of I/C power.

Assume that the customers load demand at the i^{th} period changes from its initial value of $d_0(i)$ to $d(i)$ due to the incentive and penalty imposed on the customer. Hence, the total change of load, $\delta d(i)$, can be represent as follows.

$$\delta d(i) = d(i) - d_0(i) \quad (6.5)$$

If the economic incentive for each kWh load curtailment at i^{th} hour is defined as $Incen(i)$ (\$/kWh), then the total incentive, $I(i)$, of the customer for participating in I/C load program can be expressed as follows.

$$I(i) = Incen(i) \cdot [d(i) - d_0(i)] \quad (6.6)$$

If the agreed amount of load curtailment at the i^{th} hour is $C(i)$ and the imposed penalty on the customer is $pen(i)$ (\$/kWh) for not responding to the committed load curtailment, then the total amount of penalty, $P(i)$, will be as follows.

$$P(i) = pen(i) \cdot [C(i) - (d(i) - d_0(i))] \quad (6.7)$$

The demand response model considering I/C load program is given in (6.8).

$$d(i) = d_0(i) \left\{ 1 + \epsilon(i, i) \cdot \frac{[\rho(i) - \rho_0(i) + I(i) + P(i)]}{\rho_0(i)} - \sum_{\substack{j=1 \\ j \neq i}}^{24} \epsilon(i, j) \cdot \frac{[\rho(i) - \rho_0(j) + I(i) + P(i)]}{\rho_0(j)} \right\} \quad (6.8)$$

The I/C load at the i^{th} hour can be calculated using (6.9) which is derived from (6.4), (6.5), and (6.8).

$$\delta d(i) = d_0(i) \left\{ \epsilon(i, i) \cdot \frac{[\rho(i) - \rho_0(i) + I(i) + P(i)]}{\rho_0(i)} - \sum_{\substack{j=1 \\ j \neq i}}^{24} \epsilon(i, j) \cdot \frac{[\rho(i) - \rho_0(j) + I(i) + P(i)]}{\rho_0(j)} \right\} \leq L_{IC} \quad (6.9)$$

6.2 Simulation Results

The proposed method is demonstrated on the IEEE-RTS. The detailed data of the IEEE-RTS (e.g., the capacities of generating units, the line carrying capabilities of the transmission lines, the failure rate of the system components, the repair rates of system components, and the load profile)

are given in [59]. The total generation capacity of the system is 3405 MW and the total peak load is 2850 MW. Table 11 shows the self- and cross-elasticities for peak and off-peak hours [95].

Table 11. Self-Cross Elasticities

	Peak	Off Peak
Peak	-0.200	0.032
Off Peak	0.032	-0.200

In order to evaluate the impact of the I/C loads on the reliability of the IEEE-RTS, the reliability indices are calculated with and without considering (I/C) loads. The load profile is divided into three categories: low load period ($\leq 50\%$ of annual peak load), off-peak load ($> 50\%$ of annual peak load to $\leq 85\%$ of annual peak load), and peak load ($> 85\%$ of annual peak load). Two case studies are performed. In these case studies, the considered initial and final peak hour electricity prices are 36.543 ¢/kWh and 37 ¢/kWh respectively, and off-peak price (flat rate) is 6.148 ¢/kWh [96]. In both case studies, the reliability indices for the base case (without (I/C) loads program) are calculated. The case studies are presented in the following sections.

6.2.1 Case Study I

In this case study, the total potential I/C loads are considered as 10% of annual peak load. The incentive and penalty are adjusted gradually to achieve the assumed potential load curtailment based on the method presented in Section 6.1.2. The load curtailment with different penalties and incentives are shown in Table 12. The optimum penalty and incentive are determined by solving (6.9). The summation of optimum penalty and incentive for this case study is 20 ¢/kWh (assumed penalty is 7.5 ¢/kWh and incentive 12.5 ¢/kWh).

In the next step, the curtailed load based on the I/C loads program is shifted to the low load hours and the load profile is updated. Figure 25 represents the daily load profile with and without I/C loads program. Finally, the reliability indices are calculated for base case and after applying I/C

loads program which are given in Table 13.

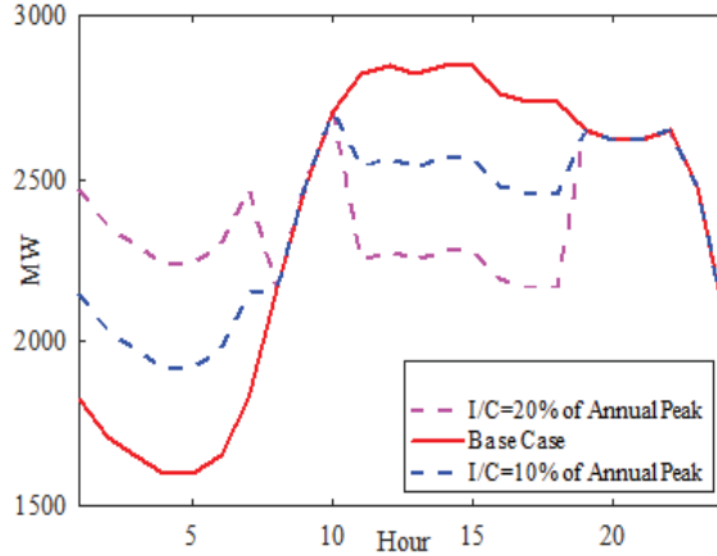


Figure 25. Load Profile of the IEEE-RTS with and without I/C Loads Program for a Typical Day.

From Table 13, it can be seen that for I/C load program considering potential I/C load to be 10% of annual peak load, the LOLP is reduced approximately by 59%, the EDNS is reduced by 63.4%, and the LOLF is reduced by 48% of the base case.

6.2.2 Case Study II

This case study is similar to case study I, except that the potential load curtailment is assumed 20% of annual peak demand. The load curtailment with different penalties and incentives for this case study are given in Table 14. The summation of optimum penalty and incentive by solving (6.9) is determined as 40.7 ¢/kWh (assumed penalty is 15.0 ¢/kWh and incentive 25.7 ¢/kWh).

Table 12. Load Curtailment with Different Penalties and Incentives for Case Study I

Incentive (¢/kWh)	Penalty (¢/kWh)	Load Curtailment (MW)	Percentage Annual Peak
7.5	2.5	144.610	5.074%
10.0	5.0	213.755	7.50%
12.5	7.5	282.900	9.93%

Table 13. Annual Reliability Indices of the IEEE-RTS with and without I/C Loads Program for Case Study I

	LOLP	LOLE (hr/yr)	LOLF (occ./yr)	EDNS (MW/yr)	LOEE (MWh/yr)
Without I/C	0.00110	9.5850	1.9280	0.1380	1209.2
With I/C	0.00045	3.9390	1.0025	0.0505	442.7

Table 14. Load Curtailment with Different Penalties and Incentives for Case Study II

Incentive (¢/kWh)	Penalty (¢/kWh)	Load Curtailment (MW)	Percentage Annual Peak
20.4	10.0	426.72	14.97%
23.1	12.5	498.63	17.50%
25.7	15.0	569.16	19.97%

Table 15. Annual Reliability Indices of the IEEE-RTS with and without I/C Loads Program for Case Study II

	LOLP	LOLE (hr/yr)	LOLF (occ./yr)	EDNS (MW/yr)	LOEE (MWh/yr)
Without I/C	0.00110	9.5850	1.9280	0.1380	1209.2
With I/C	0.00037	3.2615	0.9300	0.0424	371.6

The calculated reliability indices for this case study are presented in Table 15. For this case study, the LOLP is reduced by 66%, the EDNS is reduced by 69.3%, and the LOLF is reduced by 51.7% for I/C load program compared to the base case.

From the above case studies, it can be concluded that the reliability of a power system is improving with the increasing of potential I/C loads.

Chapter 7. A Reliability-constrained Demand Response-based Method to Increase the Hosting Capacity of Power Systems to EVs

The focus of this chapter is to develop a method to calculate the maximum permissible penetration level of EVs at power system buses while maintaining the system reliability level. The major contributions of this chapter can be summarized as follows.

- A reliability-constrained DR program-based iterative method is proposed to maximize the permissible penetration level of EVs in power systems.
- A method to calculate the initial number of EVs for the proposed iterative method is developed based on total demand for all the I/C loads and peak load of EVs.
- A mathematical model to construct load profiles for EVs considering drivers' behavior and preferences in terms of charging times, periods, and locations is presented; this model also considers drivers' uncertain movements between charging stations.
- A mathematical model to restructure load profiles at power system buses using load profiles of EVs and I/C loads-based DR program is developed.

The proposed method starts with developing a mathematical model to construct load profiles for EVs considering dynamic movements of EV loads between buses due to drivers' behavior and preferences. Then, I/C loads-based DR program is implemented to restructure load profiles at power system buses with EVs. Finally, the maximum permissible penetration level of EVs in a power system is calculated through updating the numbers of EVs until systems' prior reliability level is achieved. The proposed method is demonstrated on the Roy Billinton Test System (RBTS), IEEE-RTS, and IEEE 33-Bus Distribution System through several case studies. MC simulation is performed to calculate the well-known reliability indices of power systems.

7.1 Maximizing Permissible Penetration Level of EVs in Power Systems

The proposed method to construct the load profiles for EVs at power system buses considers travel patterns of EVs, locations of charging stations, and charging behavior of drivers. The detailed model based on these factors is described in this section.

7.1.1 Restructuring Bus Load Profiles

All or selected power system buses may contain EV loads. The mathematical expression to modify load profiles of power system buses that contain EV loads is expressed as follows.

$$P_{i,j,k} = P_{i,j,k}^0 + P_{i,j,k}^{ev} \pm \delta P_{i,j,k}^{ic}, \quad \begin{cases} \forall i \in N \\ j = 1, 2, \dots, 24 \\ k = 1, 2, \dots, 365 \end{cases} \quad (7.1)$$

In (7.1) $P_{i,j,k}^{ev}$, and $\delta P_{i,j,k}^{ic}$, are calculated based on the load profiles of EVs and DR program, respectively. Mathematical models to construct load profiles for EVs and to calculate demand for I/C loads-based DR program are as follows.

7.1.1 Constructing Load Profiles for EVs

The mathematical expression to construct load profiles for EVs is modeled based on locations of charging stations and mobility of EVs, which is explained as follows.

7.1.1.1 Load Profiles of EVs Considering Charging Locations

The demand of EVs at power system buses changes due to preferences of drivers and location of charging stations (e.g., residential and public). For instance, the peak amount of charging at residential stations happen at around midnight. On the other hand, the maximum amount of charging at public stations happen at midday [3]. Therefore, determining charging patterns of public and residential stations is indispensable to build load profiles for EVs at each bus. The hourly load profiles of EVs at each bus for a year considering charging patterns of public and residential stations

can be constructed as follows.

$$P_{i,j,k}^{ev} = P_{i,j,k}^{ev,c} + P_{i,j,k}^{ev,r} \quad (7.2)$$

where $P_{i,j,k}^{ev}$ is the amount of EV loads at the i^{th} bus on j^{th} hour of k^{th} day; $P_{i,j,k}^{ev,c}$ is the amount of charging load of EVs at public charging stations of i^{th} bus at j^{th} hour of k^{th} day; and $P_{i,j,k}^{ev,r}$ is the amount of charging load of EVs at residential charging stations of i^{th} bus at j^{th} hour of k^{th} day.

In a given power system, a bus may contain only residential or public charging stations or both. Therefore, load profiles of EVs at a bus depend on the type of installed charging stations. In Chapter 2, Section 2.1.3, data tables are provided to represent hourly, daily, and weekly EV loads of both residential and public stations in terms of percentages of annual peak load. These data tables can be used to calculate the hourly charging loads at residential and public stations. However, it is worth mentioning here that considering fixed hourly charging patterns at public and residential stations is not practical due to the behavior and preferences of drivers. In [97], it has been reported that the peak hours on weekdays and weekends of both public and residential stations vary randomly depending on parking hours at offices, schools, malls, and houses. Therefore, uncertain amount of load may shift from residential charging stations to public charging stations or vice versa. Consequently, the hourly charging loads at a bus for public and residential stations considering all these factors can be modeled as follows.

$$P_{i,j,k}^{ev,c} = \begin{cases} (f_{i,j,k}^{ev,c} + \gamma_{i,j,k}) \times P_i^{ev,m}, & \text{if } i \in N^p \\ 0, & \text{Otherwise} \end{cases} \quad (7.3)$$

$$P_{i,j,k}^{ev,r} = \begin{cases} (f_{i,j,k}^{ev,r} + \chi_{i,j,k}) \times P_i^{ev,m}, & \text{if } i \in N^r \\ 0, & \text{Otherwise} \end{cases} \quad (7.4)$$

where N^p is the number of buses that contain public charging stations ($N^p \subset N^{ev}$); N^r is the number of buses that contain residential charging stations ($N^r \subset N^{ev}$); $P_i^{ev,m}$ is the peak demand for the initial number of EVs; $f_{i,j,k}^{ev,c}$ is the fraction of annual peak load of EVs at the i^{th} bus that contains public stations at j^{th} hour of k^{th} day; and $f_{i,j,k}^{ev,r}$ is the fraction of annual peak load of EVs

at the i^{th} bus that contains residential stations at j^{th} hour of k^{th} day. The value of $f_{i,j,k}^{ev,c}$ and $f_{i,j,k}^{ev,r}$ are calculated using the data tables provided in Chapter 2, Section 2.1.3.

7.1.1.2 Load Profiles of EVs Considering Drivers' Movement between Buses

Charging profiles of EVs at public and residential charging stations also depend on the preferences of EV owners. In [3], it has been reported that about 76%, 20%, and 4% of EVs were charged during off-peak, peak, and mid-peak periods, respectively in 2014. Also, in [3], it has been reported that the major percentages of EVs charging happen at residential charging stations from 7:00 pm–3:00 am. On the other hand, the major percentages of EVs were charged at public charging stations from 9:00 am to 7:00 pm [3]. However, daily travel patterns, driving distances, and arrival times of the commuters vary dynamically due to change in their working hours and travel needs on weekdays and weekends. Therefore, uncertain movement of EVs between power system buses may happen. Consequently, the dynamic movement of EV loads may happen from peak hours to off-peak hours or vice versa due to uncertainty in behavior and preferences of drivers. This uncertainty can be captured considering load variations due to uncertain future connections [98] and plug-in and plug-off times [99] of EVs. The expression to capture all these factors is as follows.

$$P_{i,j,k}^{ev,f} = \left(1 + \sum_{\substack{n=1 \\ n \neq j}}^{24} (\alpha_{i,n,k} - \beta_{i,n,k}) \right) \times P_{i,j,k}^{ev} \quad (7.5)$$

where $P_{i,j,k}^{ev,f}$ is the amount of charging load of EVs of i^{th} bus at j^{th} hour of k^{th} day considering all the uncertain movements.

Finally, load profiles of EVs considering both charging locations and drivers' movement between buses are constructed using (7.2) – (7.5).

7.1.2 Calculation of I/C Loads based on DR Program

Load profiles of power systems can be restructured using DR programs to improve system reliability. An I/C loads-based DR program is used to modify bus load profiles to increase the penetration level of EV loads at system buses while maintaining system reliability. Modeling of I/C loads-based DR programs has three main elements which are as follows: (i) calculating the total amount of suitable I/C loads, (ii) selecting eligible customers, and (iii) notifying customers in advance before curtailing I/C loads. A mathematical model for the I/C loads-based DR program was developed in Chapter 6. In this chapter, we will not reproduce the detailed derivation for DR program; rather, we will present the expressions that are necessary to derive mathematical formula to restructure load profiles with EVs.

The expression to restructure load profiles at power system buses for the I/C loads-based DR program is as follows.

$$P_{i,j,k}^{ic} = P_{i,j,k}^0 \left(1 + \frac{\epsilon_{j,j}(\delta P_j + I_j + \rho_j)}{P_j^0} - \sum_{\substack{n=1 \\ n \neq j}}^{24} \frac{\epsilon_{j,n}(\delta P_n + I_n + \rho_n)}{P_n^0} \right) \quad (7.6)$$

where $P_{i,j,k}^0$ is the amount of existing load (without EV) at the i^{th} bus on j^{th} hour of k^{th} day; $P_{i,j,k}^{ic}$ is the load demand (without EV) at the j^{th} hour of the k^{th} of i^{th} bus after implementing demand response program; P_j^0 and P_n^0 are the initial electricity prices at j^{th} and n^{th} hours, respectively; ρ_j and ρ_n are the total amount of penalties at j^{th} and n^{th} hours, respectively; δP_j and δP_n are the change of prices at j^{th} and n^{th} hours, respectively; and $\epsilon_{j,j}$ and $\epsilon_{j,n}$ are the self and cross elasticities, respectively.

The total amount of I/C loads that can be curtailed or interrupted based on the DR program is calculated using (7.7).

$$P_i^{ic} = \sum_{o=1}^{M^{ic}} P_{i,o}^{ic} \quad (7.7)$$

where M^{ic} is the total number of suitable I/C loads for DR program at i^{th} bus; $P_{i,o}^{ic}$ is the amount of load demand for the o^{th} I/C load of i^{th} bus; and P_i^{ic} is the total demand for the existing I/C loads in the i^{th} bus.

The expression provided in (7.8) is derived using (7.6) and (7.7) to calculate the amount of I/C loads at the j^{th} hour based on incentives and penalties imposed by utilities and demand-price elasticity.

$$\Delta P_{i,j,k}^{ic} = P_{i,j,k}^0 \left(\frac{\epsilon_{j,j}(\delta P_j + I_j + \rho_j)}{P_j^0} - \sum_{\substack{n=1 \\ n \neq j}}^{24} \frac{\epsilon_{j,n}(\delta P_n + I_n + \rho_n)}{P_n^0} \right) \leq P_i^{ic} \quad (7.8)$$

where $\Delta P_{i,j,k}^{ic}$ is the amount of added or curtailed I/C loads at the i^{th} bus on the j^{th} hour of the k^{th} day based on DR program.

The summation of optimum incentives and penalties for a specific amount of I/C loads can be calculated using (7.8).

In the proposed method, load profile at each bus is modified using load profiles of EVs and added/curtailed I/C loads at the selected hours based on the DR program. The mathematical expression to restructure load profile at each bus using load profiles of EVs and added/curtailed I/C loads is provided in (7.9), which is derived using (7.1), (7.5), and (7.8).

$$P_{i,j,k} = P_{i,j,k}^0 + \Delta P_{i,j,k}^{ic} \left(1 + \sum_{\substack{n=1 \\ n \neq j}}^{24} (\alpha_{i,n,k} - \beta_{i,n,k}) \right) \times P_{i,j,k}^{ev} \quad (7.9)$$

7.2 Calculation of Maximum Permissible Penetration

The proposed method to maximize the permissible penetration level of EVs starts with

calculating the power system reliability indices for existing loads (without EVs) at system buses, which are considered as reference values. Then, the load profiles at power system buses are restructured for an initial number of EVs using (7.9).

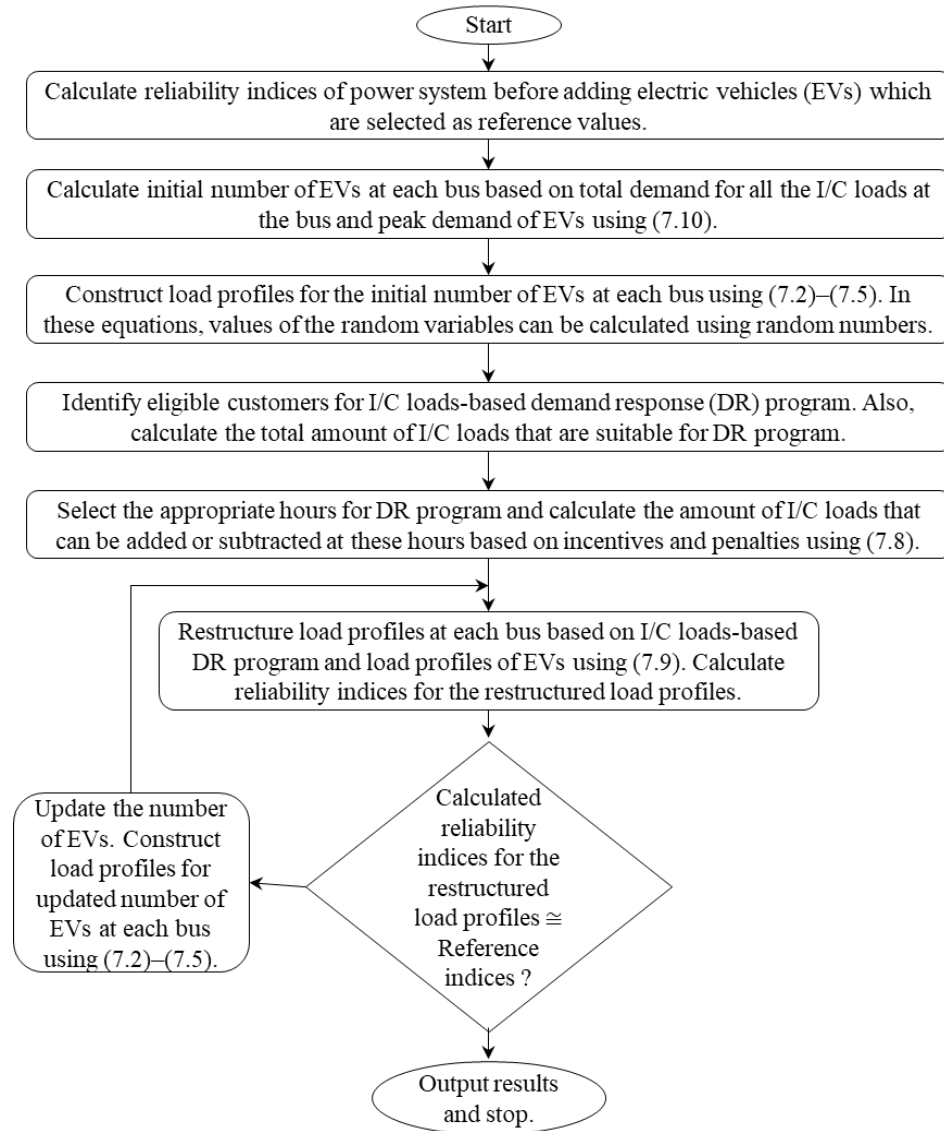


Figure 26. The flowchart to calculate maximum penetration level of EVs at power system buses.

The initial number of EVs for a bus is calculated based on the total demand of existing I/C loads in the bus and peak load of EVs. In other words, if the total demand for all the I/C loads at a bus is P_i^{ic} kW and the peak demand for a specific number of EVs is P_i^{ev} kW, then the initial number of

EVs is calculated as follows,

$$|P_i^{ev,m} - P_i^{ic}| \leq \xi \quad (7.10)$$

where P_i^{ic} is the demand for all the I/C loads at the i^{th} bus; and ξ is the tolerance level.

After restructuring the load profiles for the initial number of EVs using (7.9), the reliability indices are calculated for the restructured load profiles. Then, the calculated reliability indices are compared to the reference values and the number of EVs is updated until the following criterion is satisfied.

$$|RI^{rs} - RI^{ref}| \leq \epsilon \quad (7.11)$$

where RI^{rs} is the calculated reliability index using the restructured load profiles; RI^{ref} is the reference reliability index; and ϵ is the tolerance level.

The final number of EVs at each bus represents the maximum permissible penetration level of EVs at corresponding buses. The proposed method to maximize the penetration level at power system buses with existing resources is shown in Figure 26.

7.3 Reliability Evaluation Using the MC

The MC simulation has been used extensively to evaluate the reliability of power systems. Three main steps (sampling system states, classifying sampled system states, and check convergence) need to be followed to evaluate composite power system reliability using MC simulation, which are explained as follows.

7.3.1 Sampling System States

In composite system reliability evaluation, power system states are sampled using the operating states of system components (e.g., generators and transmission lines). The operating state of a

component is represented using a binary string (i.e., “1” represents functioning or up state and “0” represents malfunctioning or down state). In order to sample states of a given power system using MC simulation, random numbers are generated and compared to FORs of system components. A power system state can be sampled using the MC simulation as follows.

$$S = \begin{cases} 0, & \text{if } r^q \leq FOR^q, \\ 1, & \text{Otherwise} \end{cases} \quad q = 1, 2, \dots, N_q \quad (7.12)$$

where N_q is the total number of system components; r^q is the generated random number for q^{th} component; FOR^q is the forced outage rate of the component; and S is a $N_q \times 1$ vector which represents the system state.

As each component can be in either “up” or “down” state, the maximum space size of the system states is $2N_q$. The FOR of a component can be calculated as follows.

$$FOR^q = \frac{\mu^q}{\lambda^q + \mu^q} \quad (7.13)$$

where λ^q and μ^q are the failure and repair rates of the q^{th} component, respectively.

7.3.2 Classifying System States

In power system reliability evaluation, power flow is usually performed to classify sampled system states into failure (loss of load) and success (no loss of load) states. Typically, three types of power flow models are used in composite system reliability evaluation (Transportation/capacity flow, DC power flow, and AC power flow) [100]. The transportation/capacity flow model utilizes only the transmission line capacity constraints, which is not appropriate for composite but excellent for multi-area reliability evaluation. On the other hand, the DC power flow model has been widely used in transmission system reliability studies due to its easiness in terms of formulation and implementation [92], [101]–[105]. However, the DC power flow model is not suitable for the distribution systems as it ignores voltage and reactive power constraints. Evaluation of power system reliability using the AC power flow is not only extremely demanding in terms of

computation but also takes a long time to converge, which makes the AC power flow as an inappropriate choice to evaluate composite power system reliability [92], [101]–[105]. Therefore, we have leveraged a linearized AC power flow model that has been developed in [77] to capture the system constraints as well as to reduce the computation burden and simulation time. The linearized AC power flow is used to classify sampled system states. The constraints related to the linearized AC power flow model is described in (7.15). After classifying the sampled states, an optimization problem is usually used to minimize load curtailments in case of failure states. The optimization problem described in (7.14) is used to minimize the load curtailment [69]. The linear programming is used to solve this optimization problem. If any type of contingencies (e.g., outage of transmission lines or failure of generators) happens in a power system and the available power from the system fails to satisfy its demand, the linear programming minimizes the quantity of load to be curtailed.

$$\text{Minimize (Load Curtailment)} = \min \sum_{i=1}^N P_{ci} \quad (7.14)$$

Subject to,

$$\begin{aligned} B'\theta - GV + P_g + P_c &= P_d \\ G'\theta + BV + Q_g + Q_c &= Q_d \\ P_{gi}^{min} &\leq P_{gi} \leq P_{gi}^{max} \\ Q_{gi}^{min} &\leq Q_{gi} \leq Q_{gi}^{max} \\ 0 &\leq P_c \leq P_d \\ 0 &\leq Q_c \leq Q_d \\ |V^{min}| &\leq V \leq |V^{max}| \\ -F^{max} &\leq B_l A \theta \leq F^{max} \\ -\pi &\leq \theta \leq \pi \end{aligned} \quad (7.15)$$

where P_{ci} is the load curtailment at i^{th} bus; B' and G' are the modified susceptance and conductance matrices [77], respectively of buses with dimension of $(N \times N)$; B and G are the susceptance and

conductance matrices, respectively of buses with dimension of $(N \times N)$; θ is the vector of nodal voltage angles $(N \times 1)$; P_g and Q_g are the vectors of real and reactive power generations, respectively at buses with dimension of $(N \times 1)$; P_{gi}^{min} and Q_{gi}^{min} are the minimum real and reactive power generation limits, respectively at bus i ; P_{gi}^{max} and Q_{gi}^{max} are the maximum real and reactive power generation limits, respectively at bus i ; P_C and Q_C are the vectors of real and reactive load curtailments at buses with dimension of $(N \times 1)$; P_d and Q_d are the vectors of real and reactive power demand, respectively at buses with dimension of $(N \times 1)$; N_t is the total number of transmission lines; F^{max} is the vector of maximum power flow capacities of lines $(N_t \times 1)$; B_l is the susceptance matrix of transmission lines $(N_t \times N_t)$; and A is the matrix of element-bus incidence $(N \times N)$. In order to achieve a feasible solution, one of the bus angles has been assumed as zero for the given constraints in (7.15).

The LP follows same procedure described in Chapter 3 section 3.2 to dispatch power from generators to minimize load curtailments.

7.3.3 Convergence Criterion

Typically, in composite system reliability evaluation using the MC simulation, energy indices require the largest number of samples to converge [104]. Therefore, a convergence criterion considering the EDNS index is used to terminate the MC simulation. The convergence criterion can be expressed as follows.

$$\frac{\sqrt{V(EDNS)}}{EDNS} \leq \sigma \quad (7.16)$$

where $V(EDNS)$ is the variance of the EDNS and σ is the tolerance level. The value of σ is very small (typically ≤ 0.025) [103].

7.4 Numerical Examples

Simulations are carried out on three different systems, which are RBTS (sub transmission system), IEEE-RTS (transmission system), and IEEE 33-bus distribution systems to analyze the effectiveness of the proposed method on sub-transmission, transmission, and distribution systems. The total number of EVs is distributed among load buses based on the distribution ratio of their existing loads for all the systems. In [5], it has been reported that 40% of total charging happens in public stations, and the remaining 60% charging happens in public stations. Thus, we consider the distribution of total EV loads between residential and public stations as 40% and 60%, respectively.

The hourly loads of a day are classified into three different categories: low load hours, off-peak hours, and peak hours. The I/C loads are curtailed from peak hours of a day and added to low load hours of the respective day. To emulate customers' active participation in the DR program, the amount of incentive is selected as double of the penalty. The electricity prices at different hours are selected based on the electricity prices of Nevada Power Company-NV Energy. The low load hour electricity price (flat rate) is 6.1 ¢/kWh and initial and final electricity prices during peak hours are 36.6 ¢/kWh and 37.2 ¢/kWh, respectively [9]. Also, it is important to find eligible hours for the implementation of DR programs. Implementation of DR programs in inappropriate hours may increase the peak loads, which will have negative impacts on system reliability. The considered low, off-peak, and peak hours are as follows: low load hours (hours where the loads are 70% of annual peak load), off-peak hours (hours where the loads are in between 71% and 85% of annual peak load), and peak hours (hours where the loads are >85% of annual peak load). These percentages are selected in such a way that peak load of the restructured load profile using DR program is less than the peak load of actual load profile. The amount of added/curtailed loads at the low/peak load hours are calculated using (7.8). The cross- and self-elasticities for peak and low load hours are provided in Table 11 [95].

7.4.1 Case Studies for the RBTS

The total number of generators, transmission lines, and buses of the RBTS are 11, 9, and 6, respectively. The detailed data of the RBTS (e.g., annual peak load, load profile, total generation capacity, transmission lines carrying capabilities limits, generation capacities of the generating units, and failure and repair rate of the system components) are provided in [106]. The effectiveness of the proposed method to maximize the permissible penetration level of EVs at the RBTS buses is demonstrated through four different case studies:

- Case I: Base case
Case II: Calculation of maximum permissible penetration level of EVs based on the proposed method (considering both DR program and uncertainty in movements of EVs).
- Case III: Analyzing the impacts of uncertainty in movements of EVs on reliability indices.
- Case IV: Analyzing the effectiveness of the proposed method to improve reliability of the RBTS.

The above-mentioned cases are explained in detail as follows.

Case I: The load profile (without adding EVs) of the RBTS is assumed in this case. The MC simulation is performed to sample system states. The generating units are represented by up state and down state. The load levels are modeled using the clustering method [92]. To model the loads at system buses, the annual peak load (185 MW) of the RBTS is considered as 1.0 p.u., and the loads at system buses are divided into several clusters. It is found that 20 clusters are enough to capture the variability in hourly loads of the RBTS. Each cluster associated with a probability, which is used to sample system loads. The results of this case study are shown in the second row of Table 16 and second column of Table 17.

Case II: In this case, the maximum number of EVs that can be penetrated at load buses of the RBTS is calculated based on the procedure described in Section 7.1. In [85], it has been mentioned that the total demand for all the existing I/C loads of a power system ranges from 10–20% of its peak load. Therefore, we consider the total demand of eligible I/C loads for the DR program as 15% of annual peak load of the RBTS. The calculated amount of incentives and penalties for the demand of eligible I/C loads using (7.8) are 18.244 ¢/kWh and 9.0317 ¢/kWh, respectively. The calculated initial number of EVs using (7.11) is 37, 000 cars or 27.75 MW EV loads.

Table 16. Reliability Indices of Cases for the RBTS

Case No.	No. of EVs	LOLP	LOLE (hr/yr)	EDNS (MW/yr)	LOEE (MWH/yr)
Case I	-	0.01242	108.50	0.0381	333.02
Case II	15,333	0.00549	47.96	0.0365	319.08
Case III	15,333	0.00552	48.22	0.356	311.39
Case IV	15,333	0.02215	193.5	0.0574	501.02

Table 17. Bus EDNS of Cases for the RBTS.

Bus No.	Case I	Case II		Case III		Case IV	
	EDNS $\times 10^{-4}$	No. of EVs	EDNS $\times 10^{-4}$	No. of EVs	EDNS (MW/yr)	No. of EVs	EDNS $\times 10^{-4}$
2	70.12	1658	76.18	1658	66.12	1658	117.89
3	65.27	7044	58.13	7044	72.13	7044	118.09
4	85.34	3315	80.05	3315	70.84	3315	117.89
5	81.68	1658	76.40	1658	87.07	1658	109.73
6	78.77	1658	74.03	1658	60.03	1658	109.92

The load profiles given in Figure 27 are constructed for the initial number of EVs based on the actual (expected) EVs movements between public and residential charging stations. However, these load profiles are constructed based on the average of hourly loads where standard deviations are high. Also, changes in the amount of hourly loads due to drivers' behavior and preferences are not reflected in these profiles. Therefore, these load profiles are restructured using (7.2)–(7.5) to capture changes in charging times and mobility of EVs between charging stations due to drivers' behavior and preferences.

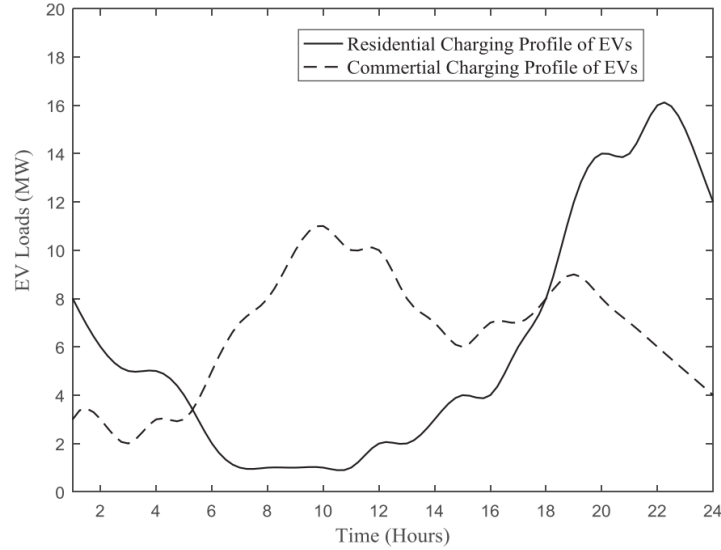


Figure 27. Load profiles for initial number of EVs for the RBTS.

In order to capture the mobility of EVs between charging stations due to drivers' behavior and preferences using (7.3) and (7.4), the selected values of random variables $\gamma_{i,j,k}$ and $\chi_{i,j,k}$ for weekdays and weekends are as follows: On weekdays, from 7:00 am to 1:00 pm, $\gamma_{i,j,k}$ are randomly selected in between 0 and 15% of the hourly charging loads of residential stations to capture mobility of EVs from residential to public stations. Also, from 6:00 pm to 12:00 am, the values of $\chi_{i,j,k}$ are randomly selected in between 0 and 10% of the hourly loads of public stations to capture mobility of EVs from EV public to residential stations. On weekends, from 6:00 pm to 12:00 am, the values of $\gamma_{i,j,k}$ are randomly selected in between 0 and 15% of the hourly charging loads of residential stations. On the other hand, from 7:00 am to 11:00 am, $\chi_{i,j,k}$ are randomly selected in between 0 and 10% of charging loads at public stations. To capture changes in charging times due to drivers' behavior using (7.5), the values of random variables $\alpha_{i,n,k}$ and $\beta_{i,n,k}$ are selected as follows: On weekdays, some commuters may go for work in the early morning and arrive home in the early evening. Therefore, on weekdays, from 4:00 am to 9:00 am, the values for $\alpha_{i,n,k}$ are selected as negligible while the values for $\beta_{i,n,k}$ are selected randomly in between 0–10% of

hourly charging loads of a given bus. On the other hand, from 1:00 pm to 6:00 pm, the values for $\alpha_{i,n,k}$ are selected randomly in between 0–10% of hourly charging loads while values for $\beta_{i,n,k}$ are selected as negligible. On weekends, some commuters may stay at home in the morning and go for shopping in the late afternoon. Therefore, on weekends, from 10:00 am–4:00 pm, the values for $\alpha_{i,n,k}$ and $\beta_{i,n,k}$ are 0–10% of hourly EV loads and negligible, respectively. On the other hand, from 10:00 pm to 6:00 am, the values for $\alpha_{i,n,k}$ and $\beta_{i,n,k}$ are selected as negligible and (0–10)% of hourly EV loads, respectively.

After constructing load profiles for the initial number of EVs and calculating the added/curtailed loads, load profiles of the RBTS are restructured using (7.9). The reliability indices of the RBTS for the restructured bus load profiles are calculated. Then, the procedure described in Section 7.1 is used to update the number of EVs. The tolerance level to update the number of EVs is assumed as 0.0002 MW/yr. The results of this case study are shown in the third row Table 16 and third and fourth columns of Table 17.

Case III: In this case, the impacts of uncertain movements of EV loads between buses due to drivers' behavior and presences are analyzed. Therefore, the maximum number of EVs that can be penetrated at load buses of the RBTS is calculated based on the proposed method. However, mobility of EV loads due to drivers' behavior and preferences of charging is ignored for this case. Same as Case II, the total demand of eligible I/C loads for the DR program and initial number of EVs are 27.75 MW and 37,000 cars, respectively. Also, the calculated amount of incentives and penalties for the demand of eligible I/C loads using (7.8) are 18.244 ¢/kWh and 9.0317 ¢/kWh, respectively. Moreover, the low, off-peak, and peak hours for the RBTS are same as case II. The amount of added/curtailed loads at the low/peak load hours are calculated using (7.8). Load profiles of the RBTS are restructured using (7.9) for the constructed load profiles of the initial number of EVs and calculated added/curtailed loads. The reliability indices of the RBTS using the restructured

bus load profiles are calculated. Then, the procedure described in Section 7.1 is used to update the number of EVs. Same as Case I, the tolerance level to update the number of EVs is assumed as 0.0002 MW/yr. The results of this case study are shown in the fourth row of Table 16 and fifth and sixth columns of Table 17.

Case IV: In this case, the effectiveness of the proposed method to improve power system reliability with EVs is analyzed. Therefore, the reliability indices with the calculated number of EVs in Case II are calculated without applying the DR program. The load profiles for the EVs are constructed using (7.5). Then, load profiles at each bus of the base case (Case I) are updated through combining the load profiles for final number of EVs in Case II. Finally, the reliability indices are calculated using the updated load profiles of the RBTS for this case. The results of this case study are shown in the fifth row of Table 16 and seventh and eighth columns of Table 17.

7.4.2 Case Studies for the IEEE-RTS

The IEEE-RTS has 32 generators, 38 transmission lines, and 24 buses. The detailed data of the IEEE-RTS are provided in [59]. Three different case studies are carried out to demonstrate the effectiveness of the proposed method to determine the maximum permissible penetration level of EVs at the IEEE-RTS buses.

- Case V: Base case
- Case VI: Calculation of penetration level of EVs based on the proposed method.
- Case VII: Analyzing the effectiveness of the proposed method to improve reliability of the IEEE-RTS.

The above-mentioned cases are explained in detail as follows.

Case V: The load profile of the IEEE-RTS is assumed in this case. The MC simulation is performed to sample system states. The generating units are represented by up state and down state. The load levels are modeled using the clustering method. To model the loads at system buses, the annual peak load (2850 MW) of the IEEE-RTS is considered as 1.0 p.u., and the loads at system buses are divided into 50 clusters. These clusters and associated probabilities are used to sample the system loads. The results of this case study are shown in the second row of Table 18 and second column of Table 19.

Case VI: In this case, the maximum number of EVs that can be penetrated at load buses of the IEEE-RTS is calculated based on the proposed method. The total demand of eligible I/C loads for the DR program is considered as 10% of annual peak load of the power systems [85]. The initial number of EVs are calculated using (7.11). Load profiles for the initial number of EVs are constructed based on the actual (expected) EVs movements between public and residential charging stations. After constructing load profiles for EVs and calculating the amount of added/curtailed loads, load profiles of the IEEE-RTS are restructured using (7.5). The reliability indices of the IEEE-RTS using the restructured bus load profiles are calculated and compared to the reference values. Then, the procedure described in Section 7.1 is used to determine the maximum number of EVs that can be penetrated at system buses. The results of this case study are shown in the third row of Table 18 and third and fourth columns of Table 19.

Table 18. Reliability Indices of Cases for the IEEE-RTS

Case No.	No. of EVs	LOLP	LOLE (hr/yr)	EDNS (MW/yr)	LOEE (MWh/yr)
Case V		0.00132	11.50	0.1395	1218.35
Case VI	10,667	0.00140	12.30	0.1293	1129.46
Case VII	10,667	0.00169	14.78	0.1906	1664.83

Case VII: In this case, the load profiles at each bus of the base case (Case IV) are updated through combining (without DR program) the load profiles for final number of EVs in Case V.

Then, the reliability indices are calculated using the updated load profiles of the IEEE-RTS. The results of this case are shown in the fourth row Table 18 and fifth and sixth columns of Table 19.

Table 19. Bus EDNS of Cases for the IEEE-RTS.

Bus No.	Case I	Case II		Case IV	
	EDNS	No. of EVs	EDNS	No. of EVs	EDNS
1	0.0085	4042	0.0055	4042	0.0105
2	0.009	3630	0.011	3630	0.0143
3	0.0089	6737	0.0048	6737	0.0117
4	0.0037	2770	0.0061	2770	0.0049
5	0.0053	2657	0.0055	2657	0.0077
6	0.0076	5090	0.0038	5090	0.0081
7	0.007	4678	0.0045	4678	0.0076
8	0.0076	6400	0.0038	6400	0.0061
9	0.004	6550	0.0086	6550	0.0084
10	0.0108	7299	0.0143	7299	0.0169
13	0.0119	9918	0.0102	9918	0.0122
14	0.0061	7261	0.0096	7261	0.0145
15	0.0083	11864	0.0104	11864	0.0132
16	0.0081	3743	0.0063	3743	0.0145
18	0.0094	12463	0.0081	12463	0.0202
19	0.012	6775	0.0119	6775	0.0129
20	0.011	4791	0.0048	4791	0.0067

7.4.3 Case Studies for the IEEE 33-bus Distribution System

The IEEE 33-Bus Distribution System is characterized by 33 busses, 32 branches, 5 tie-lines, 3 laterals, and operating voltage of 12.66 kV [80]. The total peak demand of the system is 3715 kW. The detailed data of the IEEE 33-Bus Distribution System can be found in [80]. The effectiveness of the proposed method to maximize the permissible penetration level of EVs at the IEEE 33-Bus Distribution System is demonstrated through four different case studies:

- Case VIII: Base case
- Case IX: Calculation of maximum permissible penetration level of EVs based on the proposed method (considering both DR program and uncertainty in movements of EVs).
- Case X: Analyzing the impacts of uncertainty in movements of EVs on reliability indices.

- Case XI: Analyzing the effectiveness of the proposed method to improve reliability of the IEEE 33-Bus Distribution System.

The above-mentioned cases are explained in detail as follows.

Case VIII: The load profile (without adding EVs) of the IEEE 33-Bus Distribution System is assumed in this case. Bus 1 is considered as slack bus. To model the loads at system buses, the annual peak load (3715 kW) of the IEEE 33-Bus Distribution System is considered as 1.0 p.u., and the loads at system buses are divided into 50 clusters. These clusters and associated probabilities are used to sample the system loads. The results of this case study are shown in the second row of Table 20 and second column of Table 21.

Table 20. Reliability Indices of Cases for the IEEE 33-Bus

Case No.	No. of EVs	LOLP	LOLE (hr/yr)	EDNS (kW/yr)	LOEE (kWh/yr)
Case VIII	-	0.01508	131.77	11.918	104118.7
Case IX	268	0.01508	131.77	12.434	108626.1
Case X	268	0.01508	131.77	12.433	108620.9
Case XI	268	0.01508	131.77	12.438	108658.1

Case IX: In this case, the maximum number of EVs that can be penetrated at each bus of the IEEE 33-Bus Distribution System is calculated based on the proposed method as described in Section 7.1. The total demand of eligible I/C loads for the DR program are considered as 15% of annual peak load of the IEEE 33-Bus Distribution System. The calculated initial number of EVs using (7.11) is 743 cars or 557.25 kW EV loads. To capture changes in the amount of hourly loads due to drivers' behavior and preferences, the values of random $\gamma_{i,j,k}$, $\chi_{i,j,k}$, $\alpha_{i,n,k}$, and $\beta_{i,n,k}$ for weekdays and weekends are selected as same as *Case II*. After constructing load profiles for the initial number of EVs and calculating the added/curtailed loads, load profiles of the IEEE 33-Bus Distribution System are restructured using (7.9). Then, the reliability indices of the IEEE 33-Bus Distribution System for the restructured bus load profiles are calculated. Finally, the procedure

described in Section 7.1 is used to update the number of EVs. The results of this case study are shown in the third row of Table 20 and third and fourth columns of Table 21.

Table 21. Bus EDNS of Cases for the IEEE 33-Bus

Bus No.	Case VIII	Case IX		Case X		Case XI	
	EDNS	No. of EVs	EDNS	No. of EVs	EDNS	No. of EVs	EDNS
2	15.94	7	16.61	7	16.62	7	16.63
3	17.15	6	17.88	6	17.89	6	17.89
4	25.55	9	26.63	9	26.64	9	26.66
5	14.09	4	14.69	4	14.69	4	14.71
6	15.85	4	16.53	4	16.53	4	16.54
7	58.26	15	60.75	15	60.76	15	21.03
8	62.82	15	65.53	15	65.55	15	65.56
9	20.15	4	21.02	4	21.02	4	21.03
10	22.1	4	23.05	4	23.05	4	23.06
11	17.84	3	18.61	3	18.61	3	18.62
12	25.27	4	26.35	4	26.36	4	26.36
13	26.62	4	27.77	4	27.77	4	27.78
14	57.37	9	59.88	9	59.88	9	59.87
15	29.86	4	31.17	4	31.17	4	31.17
16	31.49	4	32.86	4	32.86	4	32.86
17	32.83	4	34.26	4	34.26	4	34.26
18	51.55	7	53.8	7	13.79	7	53.79
19	16.52	7	17.23	7	17.23	7	17.25
20	18.75	7	19.54	7	19.55	7	19.57
21	21.03	7	21.9	7	21.9	7	21.94
22	23.17	7	24.14	7	24.15	7	24.18
23	19.31	7	20.16	7	20.16	7	20.16
24	101.6	30	106.11	30	106.11	30	106.12
25	113.3	30	118.23	30	118.22	30	118.2
26	17.21	4	17.95	4	17.96	4	17.95
27	18.68	4	19.48	4	19.49	4	19.5
28	20.37	4	21.25	4	21.25	4	21.26
29	43.27	9	45.15	9	45.15	9	45.16
30	76.33	15	79.6	15	79.62	15	79.65
31	60.57	11	63.15	11	63.16	11	63.2
32	90.06	15	93.92	15	95.94	15	93.97
33	26.92	4	28.07	4	28.08	4	28.09

Case X: In this case, the maximum number of EVs that can be penetrated at each bus of the IEEE 33-Bus Distribution System is calculated using the proposed method to analyze the impacts of uncertain movements of EV loads between buses due to drivers' behavior and preferences. However, mobility of EV loads due to drivers' behavior and preferences of charging is ignored for this case. Same as Case IX, the total demand of eligible I/C loads for the DR program and initial

number of EVs are 557.25 kW and 743 cars, respectively. Also, the low, off-peak, and peak hours for the IEEE 33-Bus Distribution System are same as case IX. The amount of added/curtailed loads at the low/peak load hours are calculated using (7.8). Load profiles of the IEEE 33-Bus DS are restructured using (7.9) for the constructed load profiles of the initial number of EVs and added/curtailed loads. The reliability indices are calculated using the restructured load profiles for each bus. The number of EVs is updated using the procedure described in Section 7.1. The results of this case are shown in the fourth row of Table 20 and fifth and sixth columns of Table 21.

Case XI: In this case, the effectiveness of the proposed method to improve reliability of distribution systems with EVs is analyzed. Therefore, the reliability indices with the calculated number of EVs in Case IX are calculated without applying the DR program. The load profiles for the EVs are constructed using (9.5). Then, load profiles at each bus of the base case (Case VIII) are updated through combining the load profiles for final number of EVs in Case IX. Finally, the reliability indices are calculated using the updated load profiles for this case. The results of this case study are shown in the fifth row of Table 20 and seventh and eighth columns of Table 21.

7.5 Results and Discussion

The reliability indices for the previously mentioned case studies are given in Table 16–21. From these tables, it can be observed that the maximum penetration level of EVs in a power system with existing resources while maintaining the system reliability can be calculated using the proposed method.

Table 16 and Table 17 show the results for the cases of the RBTS. From Table 16, we can see that the number of EVs that can be penetrated at the RBTS with existing resources based on proposed method is 15,333 cars. The equivalent load for this number of cars is 11.5 MW. Table 16 also shows that for Case IV (effects of EVs), the increase in the LOLP and EDNS compared to

Case I (base case) are about 78.34% and 50.66%, respectively for the calculated penetration level in Case II. This indicates that the calculated penetration level of EVs in the RBTS based on the proposed method is 11.5 MW with existing resources while the reduction in the LOLP and EDNS for this penetration level is 78.34% and 50.66%, respectively.

Table 17 shows the penetration level of EVs at the RBTS buses based on the proposed method. From Table 17, it can be seen that the maximum number of EVs can be penetrated at bus 3 followed by bus 4 of the RBTS with existing resources. This happens because the maximum penetration levels at different buses are calculated based on the ratio of their existing loads. Table 17 also shows that the calculated bus reliability indices for Case II (with EVs and DR based on proposed method) are approximately same as the base case (Case I). Thus, we can say that the proposed method is capable to maintain the reliability level of the system with EVs. Moreover, Table 17 shows that the calculated bus reliability indices for Case II (considering mobility of EV loads due to drivers' behavior and preferences) are different from Case III (ignoring mobility of EV loads due to drivers' behavior and preferences). The difference between the calculated reliability indices for Case II and Case III ranges from 11.50% to 24.09%. Therefore, it can be concluded that the uncertain mobility of EV loads between buses due to drivers' behavior and preferences has significant impacts on reliability indices of system buses. Further, Table 17 shows the bus reliability indices for Case IV (with EVs only). The increment in reliability indices of Case IV compared to the base case (Case I) ranges from 34.34% to 80.93%. The highest increment in EDNS happens at bus 2 of the RBTS because the penetration level at bus 2 of the RBTS is high compared to the other buses. This indicates that the penetration of EVs decreases the reliability level of power system buses unevenly.

The results for the cases of the IEEE-RTS are given in Table 18 and Table 19. From Table 18, we can see that the maximum permissible penetration of EVs in the IEEE-RTS based on the proposed method is 106,667 cars or 80 MW EV loads. Table 18 also shows that the increase in the

LOLP and EDNS for Case VII compared to Case V are about 28.03% and 36.63%, respectively for the calculated penetration level in Case VI. Thus, the maximum penetration level of EVs in the IEEE-RTS based on the proposed method is 106,667 cars with existing resources while the reduction in the LOLP and EDNS for this penetration level is 28.03% and 36.63%, respectively.

Table 19 shows the penetration level of EVs at the IEEE-RTS buses based on the proposed method. From Table 19, we can see that the maximum number of EVs that can be penetrated at bus 18 followed by bus 15 and bus 13 of the IEEE-RTS with existing resources. Table 19 also shows that the calculated bus reliability indices for Case VI (with EVs and DR based on proposed method) are approximately same as the base case indices. This proves the effectiveness of the proposed method to conserve the reliability level of the IEEE-RTS with EVs. Moreover, Table 19 shows that bus reliability indices for Case VII (with EVs only). The increment in reliability indices of Case VII compared to the base case (Case V) ranges from 2.95% to 138.21%, which indicates uneven impacts of EVs on reliability of system buses.

The results for the cases of the IEEE 33-Bus Distribution System are shown in Table 20 and Table 21. From Table 20, we can see that the number of EVs that can be penetrated at the IEEE 33-Bus Distribution System based on the proposed method is 268 cars. The equivalent load for this number of cars is 201 kW. Table 20 also shows that for Case XI (effects of EVs), the increase in EDNS compared to Case VIII (base case) is about 0.52 kW/yr for the calculated penetration level in Case II. From Table 20 we can also see that the LOLP for all the cases of the IEEE 33-Bus Distribution System are same. This happens due to the fact that the available generation at the slack bus and line capacities of the IEEE 33-Bus Distribution System are very large compared to the demand of all cases. Also, the IEEE 33-Bus Distribution System is a balance radial distribution system. Thus, failure probabilities of all the cases (LOLP) depend only on the failure probabilities of the IEEE 33-Bus Distribution System components, which is same for all the cases. However, if

EVs are penetrated in an unbalance system with limited generation and line capacities, then the LOLP for different cases will be different. Moreover, Table 20 shows that the increment in LOEE for Case IX compared to Case XI is about 31.97 kWh/yr. This indicates that the calculated penetration level of EVs in the IEEE 33-Bus Distribution System based on the proposed method is 201 kW with existing resources while the reduction in the LOEE for this penetration level is 31.97 kWh/yr.

Table 21 shows the penetration level of EVs at the buses of IEEE 33-Bus Distribution System based on the proposed method. From Table 21, we can see that the maximum number of EVs can be penetrated at bus 24 and 25 of the IEEE 33-Bus Distribution System. This happens because the maximum penetration levels at different buses are calculated based on the ratio of their existing loads. Table 21 also shows that the calculated bus reliability indices for Case IX (with EVs and DR based on proposed method) are approximately same as the base case (Case VIII). Thus, we can say that the proposed method is capable to maintain the reliability level of the system with EVs. Moreover, Table 21 shows that the calculated bus reliability indices for Case IX (considering mobility of EV loads due to drivers' behavior and preferences) are slightly different from Case X (ignoring mobility of EV loads due to drivers' behavior and preferences). This also happens due to the high available generation at the slack bus and line capacities of the IEEE 33-Bus Distribution System. Therefore, it can be concluded that the uncertain mobility of EV loads between buses due to drivers' behavior and preferences has small impacts on reliability indices of balanced radial distribution systems with high line capacities. Furthermore, Table 21 shows the bus reliability indices for Case XI (with EVs only). The increment in reliability indices of Case XI compared to the base case (Case VIII) ranges from 0.00613 kW/yr to 0.04988 kW/yr. The highest increment in EDNS happens at bus 24 of the IEEE 33-Bus Distribution System because the penetration level at bus 24 is high compared to the other buses.

From these studies, it can be deduced that the I/C loads-based DR programs are effective in calculating the maximum number of EVs that can be penetrated at power system buses with existing resources. Also, the proposed method is effective in reducing the negative impacts of EVs on the reliability of power systems. Moreover, planners can investigate the impacts of EVs on the reliability indices of power system using the proposed method. Further, the planners can determine the largest affected area of the network using the proposed method. These will be beneficial for future generation expansion planning to satisfy the increased demand resulted from EVs.

Chapter 8. Conclusions and Future Work

This dissertation has introduced two metrics to evaluate the impact of EVs on power system reliability and to provide a decision aid tool for power system operators and planners to plan for the increase of EVs' penetration. These metrics are: 1) the “extra effective available energy” of power system to accommodate the load demand of EVs (EEAE-EVs) with controlled charging in power system reliability assessment and 2) the “extra effective required generation” for EVs (EERG-EVs). Also, a method to calculate these metrics considering forced outages of the generating units, system load profile, and charging patterns of EVs is introduced. In order to calculate the EEAE-EVs, the extra hourly available generation was calculated using the sequential MC simulation method. Moreover, a load profile for EVs in a form of hourly, daily, and weekly load that depicts drivers' behavior and preferences is developed. The load profile of EVs was constructed based on data collected from several technical reports and research papers. The amount of EV loads that can be accommodated by the IEEE-RTS without adding any resources under a fully controlled charging scenario was calculated through estimating the EEAE-EVs metric. The proposed EERG-EVs concept was demonstrated on the IEEE-RTS with 330–660 MW of EV loads. The amount of extra generation needed to maintain the reliability of the IEEE-RTS versus the increase in EV loads was provided. The EERG-EVs metric is important in determining the required resources to maintain the reliability of power systems against the increase in EVs' penetration. The proposed algorithm to analyze impacts of uncertain EV movements on power system buses was developed without considering the uneven amount of EV load shifting from one bus to another bus based on their distances. Investigating the impact of this uneven load shifting can be a future research question.

This dissertation also introduced a voltage constrained-based approach to calculate the maximum hosting capacity of DSs to EVs. To determine the maximum hosting capacity of EVs in

DSs, the HEAP was calculated using the maximum loading capacity and existing load profile of DSs. The proposed method was demonstrated on the IEEE 123-node test feeder under uncontrolled and fully controlled charging scenarios through four case studies. The results showed that the proposed method can effectively determine the maximum hosting capacity of EVs in the IEEE 123-node test feeder. Also, the results showed that the maximum hosting capacity of EVs in the IEEE 123-node test feeder under fully controlled charging is much higher than the uncontrolled charging scenario. Moreover, it can be seen that the maximum hosting capacity for the selected nodes is low compared to the cases of all nodes.

Moreover, this dissertation has proposed a smart charging/discharging-based method to calculate the EMHC of power systems to EVs. In the proposed method, the charging/discharging rates are controlled based on network constraints, charging/discharging limits of smart chargers, and daily energy demand and parking durations of EVs. The parking durations are calculated based on the PDFs of arrival and departure times. The daily energy demand is calculated based on energy required to travel each mile and PDF of daily travel distances. The optimization problem to maximize the HC is formulated using linearized AC power flow and solved by linear programming solver. The EMHC is calculated for charging stations at both homes and workplaces. The proposed method was demonstrated on the modified IEEE 33-bus system as a power system. The results showed that the daily EMHC of the modified IEEE 33-bus system varied between 20-41 cars for selected nodes.

Further, this work has introduced a reliability-constrained DR based method to incorporate the load demand of EVs in composite system reliability assessment. Also, a method to build EV load profiles at power system buses is presented assuming drivers' behavior and preferences in terms of charging locations, times, and periods. A mathematical model to calculate the amount of I/C loads is developed assuming incentives, penalties, and demand-price elasticity. Furthermore, a model to

chronologically combine the load demand of EVs with the existing (system) loads at each bus and to incorporate with the I/C loads-based DR program is developed. The permissible penetration level of EVs at load buses were determined with existing resources based on the proposed method. Also, the effects of EVs on composite system reliability indices were investigated for the movements of EVs between charging stations. The potential of I/C loads-based DR programs to compensate the negative effects of EVs on system reliability was demonstrated. The effectiveness of the proposed method was demonstrated on the RBTS, IEEE-RTS, and IEEE 33-Bus Distribution System through eleven different case studies. The MC simulation was used in these case studies to calculate the reliability indices (e.g., LOLP and EDNS). The results also showed that I/C loads-based DR programs can significantly compensate the negative effects of EV penetration on systems reliability. The size of batteries for the EVs are continuously increasing, which will provide more flexibility to implement DR response for improving power system reliability. Incorporating these facts in power system planning studies to increase the penetration level of EVs will be the subject of future research.

References

- [1] “Market data: EV geographic forecasts,” Navigant Research, Boulder, CO, USA, Tech. Rep. 1Q 2019. Accessed: May 13, 2019. [Online]. Available: <https://guidehouseinsights.com/reports/market-data-ev-market-forecasts>
- [2] “Annual plug-in electric vehicle sales in North America are expected to exceed 1.1 million by 2024,” Navigant Research, Boulder, CO, USA, Newsletter. May 2015. Accessed: May 13, 2019. [Online]. Available: <https://www.greencarcongress.com/2015/05/20150527-navigant.html>
- [3] “Evaluating electric vehicle charging impacts and customer charging behaviors: Experiences from six smart grid investment grant projects,” U.S. Dept. Energy Elect. Del. Energy Rel., Washington, DC, USA, Tech. Rep., 2014. Accessed: January 11, 2018. [Online]. Available: <https://www.energy.gov/sites/prod/files/2014/12/f19/SGIG-EvaluatingEVcharging-Dec2014.pdf>
- [4] G. Pasaoglu, D. Fiorello, L. Zani, A. Martino, A. Zubaryeva, and C. Thiel, “Projections for electric vehicle load profiles in Europe based on travel survey data,” Joint Research Centre of the European Commission, Tech. Rep., 2013.
- [5] X. Wang and R. Karki, “Exploiting PHEV to augment power system reliability,” in *IEEE Transactions on Smart Grid*, vol. 8, no. 5, pp. 2100–2108, Sept. 2017.
- [6] S. Rezaee, E. Farjah, and B. Khorramdel, “Probabilistic analysis of plugin electric vehicles impact on electrical grid through homes and parking lots,” in *IEEE Transactions on Sustainable Energy*, vol. 4, pp. 1024–1033, Oct. 2013.
- [7] AEP Ohio, “A community-based approach to leading the nation in smart energy use,” US Department of Energy, Technical Report, June 2014.
- [8] Pilot evaluation report, “Electric vehicle charging station,” Energy, Xcel, Technical Report, May 2015.
- [9] W. Kuihua, N. Xinsheng, W. Jian, W. Kuizhong, and J. Shanjie, “Electric vehicle load characteristic analysis and impact of regional power grid,” in *International Conference on Electronic & Mechanical Engineering and Information Technology*, Shenyang, China, Sept. 2012, pp. 257–261.
- [10] M. Biviji, C. Ukun, G. Bassett, J. Wang, and D. Ton, “Patterns of electric vehicle charging with time of use rates: Case studies in California and Portland,” in *IEEE Power Energy Society (PES) Innovative Smart Grid Technologies Conference (ISGT)*, Washington, DC, USA, Feb. 2014, pp. 1–5.
- [11] B. Zhang and M. Kezunovic, “Impact of available electric vehicle battery power capacity on power system reliability,” in *IEEE PES General Meeting*, Vancouver, BC, July 2013, pp. 1–5.
- [12] L. Henrik and K. Willett, “Integration of renewable energy into the transport and electricity sectors through V2G,” in *Energy Policy*, vol. 36, no. 9, pp. 3578–3587, Sep. 2008.
- [13] K. Willett and J. Tomic, “Vehicle-to-grid power fundamentals: Calculating capacity and net revenue,” in *Journal of Power Sources*, vol. 144, no. 1, pp. 268–279, June 2005.
- [14] C. Camus, C. M. Silva, T. L. Farias, and J. Esteves, “Impact of plug-in hybrid electric vehicles in the Portuguese electric utility system,” in *International Conference on Power Engineering, Energy and Electrical Drives*, Lisbon, Portugal, Mar. 2009, pp. 285–290.
- [15] C. D. White and K. M. Zhang, “Using vehicle-to-grid technology for frequency regulation and peak-load reduction,” in *Journal of Power Sources*, vol. 196, no. 8, pp. 3972–3980, April 2011.
- [16] W. Kempton and T. Kubo, “Electric-drive vehicles for peak power in Japan,” in *Energy Policy*, vol. 28, no. 1, pp. 9–18, Jan. 2000.

- [17] J. Kiviluoma and P. Meibom, "Influence of wind power, plug-in electric vehicles, and heat storages on power system investments," in *Energy*, vol. 35, no. 3, pp. 1244–1255, March 2010.
- [18] K. Schneider, C. Gerkenmeyer, M. Kintner-Meyer, and R. Fletcher, "Impact assessment of plug-in hybrid vehicles on pacific northwest distribution systems," in *IEEE PES General Meeting - Conversion and Delivery of Electrical Energy in the 21st Century*, Pittsburgh, PA, 2008, pp. 1–6.
- [19] S. W. Hadley, "Impact of plug-in hybrid vehicles on the electric grid," Oak Ridge National Laboratory, Oak Ridge TN, USA, Tech. Rep. ORNL/TM-2006/554, October 2006.
- [20] L. Cheng, Y. Chang, J. Lin, and C. Singh, "Power system reliability assessment with electric vehicle integration using battery exchange mode," in *IEEE Transactions on Sustainable Energy*, vol. 4, no. 4, pp. 1034–1042, Oct. 2013.
- [21] B. Falahati, Y. Fu, Z. Darabi, and L. Wu, "Reliability assessment of power systems considering the large-scale PHEV integration," in *IEEE Vehicle Power and Propulsion Conference*, Chicago, IL, USA, Sep. 2011, pp. 1–6.
- [22] R. C. Green, L. Wang, M. Alam, and S. S. S. R. Depuru, "Evaluating the impact of plug-in hybrid electric vehicles on composite power system reliability," in *North American Power Symposium*, Boston, MA, USA, Aug. 2011, pp. 1–7.
- [23] M. Kamruzzaman and M. Benidris, "Modeling of electric vehicles as movable loads in composite system reliability assessment," in *IEEE PES General Meeting*, Portland, OR, USA, Aug. 2018, pp. 1–5.
- [24] C. Roe, E. Farantatos, J. Meisel, A. P. Meliopoulos, and T. Overbye, "Power system level impacts of PHEVs," in *Hawaii International Conference on System Sciences*, HI, USA, Jan. 2009, pp. 1–10.
- [25] S. Rahman and G. B. Shrestha, "An investigation into the impact of electric vehicle load on the electric utility distribution system," in *IEEE Transactions on Power Delivery*, vol. 8, no. 2, pp. 591–597, April 1993.
- [26] Q. Gong, S. Midlam-Mohler, V. Marano, and G. Rizzoni, "Study of PEV charging on residential distribution transformer life," in *IEEE Transactions on Smart Grid*, vol. 3, no. 1, pp. 404–412, March 2012.
- [27] F. Lanati, M. Benini, and A. Gelmini, "Impact of the penetration of electric vehicles on the Italian power system: A 2030 scenario," in *IEEE PES General Meeting*, Detroit, MI, USA, USA, July 2011, pp. 1–8.
- [28] A. D. Hilshey, P. Rezaei, P. D. H. Hines, and J. Frolik, "Electric vehicle charging: Transformer impacts and smart, decentralized solutions," in *IEEE PES General Meeting*, San Diego, CA, USA, July 2012, pp. 1–8.
- [29] M. Kamruzzaman and M. Benidris, "Effective accessible energy to accommodate load demand of electric vehicles," in *IEEE Industry Applications Society (IAS) Annual Meeting*, Portland, OR, USA, Sep. 2018, pp. 1–8.
- [30] J. Taylor, A. Maitra, M. Alexander, D. Brooks, and M. Duvall, "Evaluation of the impact of plug-in electric vehicle loading on distribution system operations," in *IEEE PES General Meeting*, Calgary, AB, Canada, July 2009, pp. 1–6.
- [31] K. Clement-Nyns, E. Haesen, and J. Driesen, "The impact of charging plug-in hybrid electric vehicles on a residential distribution grid," in *IEEE Transactions on Power Systems*, vol. 25, no. 1, pp. 371–380, Feb. 2010.
- [32] L. Pieltain Fernandez, T. Gomez San Roman, R. Cossent, C. Mateo Domingo, and P. Frias, "Assessment of the impact of plug-in electric vehicles on distribution networks," in *IEEE Transactions on Power Systems*, vol. 26, no. 1, pp. 206–213, Feb. 2011.

- [33] M. J. Rutherford and V. Yousefzadeh, "The impact of electric vehicle battery charging on distribution transformers," in Twenty-Sixth Annual IEEE Applied Power Electronics Conference and Exposition (APEC), Fort Worth, TX, USA, March 2011, pp. 396–400.
- [34] S. Shafiee, M. Fotuhi-Firuzabad, and M. Rastegar, "Investigating the impacts of plug-in hybrid electric vehicles on power distribution systems," *IEEE Transactions on Smart Grid*, vol. 4, no. 3, pp. 1351–1360, Sep. 2013.
- [35] A. Sharma, S. Shih, and D. Srinivasan, "A smart scheduling strategy for charging and discharging of electric vehicles," in *IEEE Innovative Smart Grid Technologies - Asia*, Bangkok, Thailand, Nov 2015, pp. 1–6.
- [36] J. Yu, W. Gu, and Z. Wu, "Intelligent PHEV charging and discharging strategy in smart grid," in *IEEE Fifth International conference on Advanced Computational Intelligence*, Nanjing, China, Oct. 2012, pp. 1107–1112.
- [37] H. K. Nguyen and J. B. Song, "Optimal charging and discharging for multiple PHEVs with demand side management in vehicle-to-building," in *Journal of Communications and Networks*, vol. 14, no. 6, pp. 662–671, Dec. 2012.
- [38] T. He, J. Zhu, J. Zhang, and L. Zheng, "An optimal charging/discharging strategy for smart electrical car parks," *Chinese Journal of Electrical Engineering*, vol. 4, no. 2, pp. 28–35, June 2018.
- [39] P. You, Z. Yang, M. Chow, and Y. Sun, "Optimal cooperative charging strategy for a smart charging station of electric vehicles," *IEEE Transactions on Power Systems*, vol. 31, no. 4, pp. 2946–2956, July 2016.
- [40] M. Kamruzzaman, N. Bhusal, and M. Benidris, "Determining maximum hosting capacity of electric distribution systems to electric vehicles," in *IEEE IAS Annual Meeting*, Baltimore, MD, USA, Sep. 2019, pp. 1–7.
- [41] M. Kamruzzaman and M. Benidris, "Maximum permissible load demand for electric vehicles at power system buses," in *IEEE PES General Meeting*, Atlanta, GA, USA, Aug 2019, pp. 1–5.
- [42] M. Galus and G. Andersson, "Demand management of grid connected plug-in hybrid electric vehicles (PHEV)," in *IEEE Energy 2030 conference*, Atlanta, GA, USA; 2008. pp. 1–8.
- [43] C. Wu, H. Mohsenian-Rad, and J. Huang, "Vehicle-to-aggregator interaction game," in *IEEE Transactions on Smart Grid*, vol. 3, no. 1, pp. 434–442, March 2012.
- [44] Z. Li, Q. Guo, H. Sun, Y. Wang, and S. Xin, "Emission-concerned wind-EV coordination on the transmission grid side with network constraints: concept and case study," in *IEEE Transactions on Smart Grid*, vol. 4, no. 3, pp. 1692–1704, Sept. 2013.
- [45] R. Quint, D. Kosterev, J. Undrill, J. Eto, R. Bravo, and J. Wen "Power quality requirements for electric vehicle chargers: bulk power system perspective," in *IEEE PES general meeting*, Boston, MA, USA; 2016. p. 1–5.
- [46] U.S. Department of Energy, "Summary report on EVs at scale and the U.S. electric power system," Technical report, November 2019. URL: <https://www.energy.gov/sites/prod/files/2019/12/f69/GITT%20ISATT%20EVs%20at%20Scale%20Grid%20Summary%20Report%20FINAL%20Nov2019.pdf>.
- [47] "North American Electric Reliability Corporation, NERC: Long-term reliability uncertain amid rapid changes to bulk power system," Tech. rep. (Accessed on March 2020). URL:<https://www.powermag.com/nerc-long-term-reliabilityuncertain-amid-rapid-changes-to-bulk-power-system/>.
- [48] M. Shafie-khah, E. Heydarian-Forushani, G. Osrio, F. Gil, J. Aghaei, and M. Barani, "Optimal behavior of electric vehicle parking lots as demand response aggregation agents," in *IEEE Transactions on Smart Grid*, vol. 7, no. 6, pp. 2654–2665, Nov. 2016..

- [49] L. Yao, W. Lim, and T. Tsai “A real-time charging scheme for demand response in electric vehicle parking station,” in *IEEE Transactions on Smart Grid*, vol. 8, no. 1, pp. 52–62, Jan. 2017.
- [50] Z. Yu and L. Tong, “Demand response via large scale charging of electric vehicles,” in *IEEE PES general meeting*, Boston, MA, USA, 2016. pp. 1–5.
- [51] Z. Lu, J. Qi, J. Zhang, L. He and H. Zhao, “Modelling dynamic demand response for plug-in hybrid electric vehicles based on real-time charging pricing,” *IET Generation, Transmission & Distribution*, vol. 11, no. 1, pp. 228–235, January 2017.
- [52] R. Yu, W. Zhong, S. Xie, C. Yuen, S. Gjessing and Y. Zhang, “Balancing power demand through EV mobility in vehicle-to-grid mobile energy networks,” *IEEE Transactions on Industrial Informatics*, vol. 12, no. 1, pp. 79–90, Feb. 2016.
- [53] W. Zhong, R. Yu, S. Xie, Y. Zhang and D. K. Y. Yau, “On stability and robustness of demand response in V2G mobile energy networks,” in *IEEE Transactions on Smart Grid*, vol. 9, no. 4, pp. 3203–3212, July 2018.
- [54] Z. Wang and R. Paranjape, “Evaluation of electric vehicle penetration in a residential sector under demand response considering both cost and convenience,” In *IEEE Electrical Power and Energy Conference (EPEC)*, Saskatoon, SK, Canada; 2017. pp. 1–5.
- [55] S. Shojaabadi, S. Abapour, M. Abapour and A. Nahavandi, “Optimal planning of plug-in hybrid electric vehicle charging station in distribution network considering demand response programs and uncertainties,” *IET Generation, Transmission & Distribution*, vol. 10, no. 13, pp. 3330–3340, 6 10 2016..
- [56] A. Almutairi and M. M. A. Salama, “Assessment and enhancement frameworks for system reliability performance using different PEV charging models,” *IEEE Transactions on Sustainable Energy*, vol. 9, no. 4, pp. 1969–1984, Oct. 2018.
- [57] Y. Linhao, W. Ke, and C. Xu, Tingcheng H, Mengying L. “Reliability evaluation of microgrid considering electric vehicles and demand response,” in *International conference on power system technology (POWERCON)*, Guangzhou, China; 2018. p. 1668–72.
- [58] “Electric vehicle charging station, pilot evaluation report,” Xcel Energy, Minneapolis, MN, USA, Tech. Rep., May 2015. [Online]. Available:<https://www.xcelenergy.com/staticfiles/xcel-responsive/Admin/Managed Documents & 20PDFs/CO-DSM-2014-EV-Pilot-Evaluation.pdf>
- [59] P. M. Subcommittee, “IEEE reliability test system,” *IEEE Transactions on Power Apparatus and Systems*, vol. PAS-98, no. 6, pp. 2047–2054, Nov. 1979
- [60] Z. Darabi and M. Ferdowsi, “Aggregated impact of plug-in hybrid electric vehicles on electricity demand profile,” *IEEE Transactions on Sustainable Energy*, vol. 2, no. 4, pp. 501–508, Oct. 2011.
- [61] M. Kamruzzaman, M. Benidris, and S. Elsaiah, “Effective load demand of electric vehicles in power system adequacy assessment,” in *Proc. IEEE International Conference on Probabilistic Methods Applied on Power Systems*, Jun. 2018, pp. 1–5.
- [62] J. F. Prada, “The value of reliability in power systems-pricing operating reserves,” *Energy Lab., Massachusetts Inst. Technol., Massachusetts, MA, USA*, Rep. no. MIT EL 99–005 WP, Jun. 1999.
- [63] E. Hirst and B. Kirby, “Technical and market issues for operating reserves,” *Elect. J.*, vol. 12, no. 2, pp. 36–48, Mar. 1999.
- [64] S. Sulaeman, M. Benidris, and J. Mitra, “Evaluation of wind power capacity value including effects of transmission system,” in *North American Power Symposium*, Charlotte, NC, USA, Oct. 2015, pp. 1–6.

- [65] A. Keane, M. Milligan, C. J. Dent, B. Hasche, C. D'Annunzio, K. Dragoon, H. Holttinen, N. Samaan, L. Soder and M. O'Malley, "Capacity value of wind power," *IEEE Transactions on Power Systems*, vol. 26, no. 2, pp. 564–572, May 2011.
- [66] S. Zhu, Y. Zhang, and A. A. Chowdhury, "Capacity credit of wind generation based on minimum resource adequacy procurement," *IEEE Transactions on Industry Applications*, vol. 48, no. 2, pp. 730–735, Mar. 2012.
- [67] "2001 National Household Travel Survey user's guide NHTS," U.S. Department of Transportation, Federal Highway Administration, Tech. Rep., Dec. 2004. [Online]. Available: <https://nhts.ornl.gov/2001/pub/STT.pdf>
- [68] M. F. Fotuhi, F. Aminifar, and A. Shahzadeh, "Reliability-based maintenance scheduling of generating units in restructured power systems," *Turkish J. Elect. Eng. Comput. Sci.*, vol. 22, no. 5, pp. 1147–1158, Aug. 2014.
- [69] M. Benidris, S. Elsaiah, and J. Mitra, "Composite system reliability assessment using dynamically directed particle swarm optimization," in *North American Power Symposium*, Manhattan, KS, USA, Sept. 2013, pp. 1–6.
- [70] US Department of Transportation Federal Highway Administration, "2009 National Household Travel Survey," Tech. Rep., June 2011. [Online]. Available: <https://nhts.ornl.gov/2009/pub/AddOnWorkshop8.pdf> (accessed on Feb. 11, 2019).
- [71] L. Chen, C. Y. Chung, Y. Nie, and R. Yu, "Modeling and optimization of electric vehicle charging load in a parking lot," in *IEEE PES Asia-Pacific Power and Energy Engineering Conference (APPEEC)*, Kowloon, China, Dec. 2013, pp. 1–5.
- [72] E. C. Kara, J. S. Macdonald, D. Black, M. Brges, G. Hug, and S. Kiliccote, "Estimating the benefits of electric vehicle smart charging at non-residential locations: A data-driven approach," *Applied Energy*, vol. 155, pp. 515–525, Oct. 2015.
- [73] American National Standards Institute, Inc., "American national standard for electric power systems and equipment voltage ratings (60 hertz)," Tech. Rep., June 2016. [Online]. Available: <https://www.nema.org/standards/view/American-National-Standard-for-Electric-Power-Systems-and-Equipment-Voltage-Ratings> (accessed on Feb. 11, 2019).
- [74] Electric Power Research Institute (EPRI), "Open distribution system simulation." [Online]. Available: <https://sourceforge.net/projects/electricdss/>
- [75] Distribution System Analysis Subcommittee, "IEEE 123-node test feeder," Tech. Rep., 1992. [Online]. Available: <https://site.ieee.org/pes-testfeeders/resources/> (accessed on Feb. 11, 2019).
- [76] J. Axsen, S. Goldberg, J. Bailey, G. Kamiya, B. Langman, J. Cairns, M. Wolinetz, and A. Miele, "Electrifying vehicles: insights from the Canadian plug-in electric vehicle study," Simon Fraser University, Vancouver, Canada, Tech. Rep., July 2015. [Online]. Available: https://sfustart.files.wordpress.com/2016/10/electrifying-vehicles-final-v2-8-july-10-high-res-download-rgb-no-bleeds_executivesummary.pdf, (accessed on Feb. 20, 2019).
- [77] S. Elsaiah, M. Benidris, and J. Mitra, "Analytical approach for placement and sizing of distributed generation on distribution systems," in *IET Generation, Transmission & Distribution*, vol. 8, no. 6, pp. 1039–1049, June 2014.
- [78] Z. Xu, "Forecasting electric vehicle arrival & departure time on UCSD campus using support vector machines," UC San Diego, Tech. Rep., 2017. [Online]. Available: <https://escholarship.org/uc/item/1z43n3km> (accessed on Feb. 11, 2020)
- [79] X. Luo, C. Singh, and A. D. Patton, "Power system reliability evaluation using self-organizing map," in *IEEE Power Engineering Society Winter Meeting Conference Proceedings*, vol. 2, Singapore, Jan. 2000, pp. 1103–1108.

- [80] S. Elsaiah, M. Benidris, and J. Mitra, “Reliability improvement of power distribution system through feeder reconfiguration,” in International conference on Probabilistic Methods Applied to Power Systems, Durham, UK, July 2014, pp. 1–6.
- [81] C. Zhang, Y. Xu and Z. Y. Dong, “Robustly coordinated operation of a multi-energy micro-grid in grid-connected and islanded modes under uncertainties,” in IEEE Transactions on Sustainable Energy, vol. 11, no. 2, pp. 640–651, April 2020.
- [82] National Renewable Energy Laboratory (NREL), “NREL’s PVWatts® Calculator,” accessed on Feb. 2 2018. [Online]. Available: <https://pvwatts.nrel.gov/>
- [83] US Department of Energy, “Plug-in electric vehicle handbook,” Tech. Rep., April 2017. [Online]. Available: https://afdc.energy.gov/files/u/publication/pev_consumer_handbook.pdf
- [84] Trading Economics, “United states employment rate,” Tech. Rep. [Online]. Available: <https://tradingeconomics.com/unitedstates/employment-rate> (accessed on Feb. 11, 2020).
- [85] H. Aalami, M. P. Moghaddam, and G. Yousefi, “Demand response modeling considering interruptible/curtailable loads and capacity market programs,” Applied Energy, vol. 87, no. 1, pp. 243–250, Jan. 2010.
- [86] A. Ng’uni and L. A. Tuan, “Interruptible load and demand response: Worldwide picture and the situation in Sweden,” in 38th North American Power Symposium, Carbondale, IL, USA, Sept. 2006, pp. 121–127.
- [87] F. C. Schweppe, M. C. Caramanis, R. D. Tabors, and R. E. Bohn, “Spot pricing of electricity,” Springer Science & Business Media, 2013.
- [88] P. Jazayeri, A. Schellenberg, W. D. Rosehart, J. Doudna, S. Widergren, D. Lawrence, J. Mickey, and S. Jones, “A survey of load control programs for price and system stability,” in IEEE Transactions on Power Systems, vol. 20, no. 3, pp. 1504–1509, Aug. 2005.
- [89] L. Goel, Q. Wu, and P. Wang, “Reliability enhancement of a deregulated power system considering demand response,” in IEEE Power Engineering Society General Meeting, Montreal, Que., Canada, June 2006, pp. 1–6.
- [90] M. Benidris, J. Mitra, and C. Singh, “Integrated evaluation of reliability and stability of power systems,” in IEEE Transactions on Power Systems, vol. 32, no. 5, pp. 4131–4139, Sept. 2017.
- [91] C. Singh, “Calculating the time-specific frequency of system failure,” in IEEE Transactions on Reliability, vol. R-28, no. 2, pp. 124–126, June 1979.
- [92] J. Mitra and C. Singh, “Pruning and simulation for determination of frequency and duration indices of composite power systems,” in IEEE Transactions on Power Systems, vol. 14, no. 3, pp. 899–905, Aug. 1999.
- [93] A. C. G. Melo, M. V. F. Pereira, and A. M. Leite da Silva, “A conditional probability approach to the calculation of frequency and duration indices in composite reliability evaluation,” in IEEE Transactions on Power Systems, vol. 8, no. 3, pp. 1118–1125, Aug. 1993.
- [94] M. Benidris and J. Mitra, “Reliability and sensitivity analysis of composite power systems considering voltage and reactive power constraints,” in IET Generation, Transmission & Distribution, vol. 9, no. 12, pp. 1245–1253, Aug. 2015.
- [95] D. S. Kirschen, G. Strbac, P. Cumperayot and D. de Paiva Mendes, “Factoring the elasticity of demand in electricity prices,” in IEEE Transactions on Power Systems, vol. 15, no. 2, pp. 612–617, May 2000.
- [96] NEVADA POWER COMPANY—NV Energy. (2017) Effective rates applicable to Nevada Power Company electric schedules. [Online]. Available: www.nvenergy.com/company/rates/snv/schedules

- [97] K. Chaudhari, N. K. Kandasamy, A. Krishnan, A. Ukil, and H. B. Gooi, "Agent-based aggregated behavior modeling for electric vehicle charging load," in *IEEE Transactions on Industrial Informatics*, Feb. 2019, Vol. 15, No. 2, pp. 856–68.
- [98] Z. Li, Q. Guo, H. Sun, S. Xin, and J. Wang, "A new real-time smart-charging method considering expected electric vehicle fleet connections," in *IEEE Transactions on Power Systems*, Vol. 29, No. 6, pp. 3114–3115, Nov. 2014.
- [99] T. Yang, X. Xu, Q. Guo, L. Zhang, and H. Sun, "EV charging behaviour analysis and modelling based on mobile crowdsensing data," in *IET Generation, Transmission, and Distribution*, June 2017, Vol. 11, No. 7, pp. 1683–1691.
- [100] M. Benidris, S. Elsaiah, and J. Mitra, "Applications of particle swarm optimization in composite power system reliability evaluation," *IGI Global, Handbook of Research on Swarm Intelligence in Engineering*, 2015, pp. 573–610.
- [101] M. Bhavaraju and R. Billinton, "Transmission system reliability methods," in *IEEE Transactions on Power Apparatus and Systems*, vol. PAS-91, no. 2, pp. 628–637, March 1972 .
- [102] J. Mitra and C. Singh, "Incorporating the DC load flow model in the decomposition-simulation method of multi-area reliability evaluation," in *IEEE Transactions on Power Systems*, vol. 11, no. 3, pp. 1245–1254, Aug. 1996.
- [103] C. Singh and J. Mitra, "Composite system reliability evaluation using state space pruning," in *IEEE Transactions on Power Systems*, vol. 12, no. 1, pp. 471–479, Feb. 1997
- [104] R. Billinton, and W. Li, "Reliability assessment of electric power systems using Monte Carlo methods," New York, USA, Plenum Press, 1994.
- [105] L. Salvaderi, and R. Billinton, "A comparison between two fundamentally different approaches to composite system reliability evaluation," in *IEEE Power Engineering Review*, vol. PER-5, no. 12, pp. 43–44, Dec. 1985
- [106] R. Billinton, and S. Jonnavithula, "A test system for teaching overall power system reliability assessment," in *IEEE Transactions on Power Systems*, vol. 11, no. 4, pp. 1670–1676, Nov. 1996.
- [107] "Finite math B: Chapter 4, linear programming: the simplex method," URL: <https://www.avon-schools.org/site/default.aspx?PageType=3&ModuleInstanceID=23833&ViewID=7b97f7ed-8e5e-4120-848f-a8b4987d588f&RenderLoc=0&FlexDataID=17943&PageID=6726>
- [108] M. Goemans, "Linear programming," 18.310A lecture notes, March 17, 2015, URL: <http://math.mit.edu/~goemans/18310S15/lpnotes310.pdf>
- [109] M. Kamruzzaman, X. Zhang, M. Abdelmalak, M. Benidris, and D. Shi, "A method to evaluate the maximum hosting capacity of power systems to electric vehicles," in *IEEE International Conference on Probabilistic Methods Applied to Power Systems*, Liege, Belgium, Aug. 2020, pp. 1–6.
- [110] M. Kamruzzaman and M. Benidris, "Demand response-based power system reliability enhancement," in *IEEE International Conference on Probabilistic Methods Applied to Power Systems*, Boise, ID, June 2018, pp. 1–6.
- [111] M. Kamruzzaman, and M. Benidris, "A reliability-constrained demand response-based method to increase the hosting capacity of power systems to electric vehicles," in *International Journal of Electrical Power & Energy Systems*, Volume 121, October 2020, No. 106046, pp. 1–11.
- [112] T. Mai, P. Jadun, J. Logan, C. McMillan, M. Muratori, D. Steinberg, L. Vimmerstedt, R. Jones, B. Haley, and B. Nelson, "Electrification futures study: Scenarios of electric technology adoption and power consumption for the United States," No. NREL/TP-6A20-

71500. National Renewable Energy Lab.(NREL), Golden, CO (United States), 2018.URL:
https://afdc.energy.gov/files/u/publication/electrification_futures_study.pdf
- [113] Y. Moysoglou, "Limitations of linear programming as a model of approximate computation," in Ph.D. Dissertaton, National and Kapodistrian University of Athens (EKPA). School of Sciences. Department of Informatics and Telecommunications, 2015.
- [114] W. Ogryczak, and T. Śliwiński, "On solving linear programs with the ordered weighted averaging objective," in European Journal of Operational Research, Volume 148, number 1, July 2003, pp. 80–91.